COMPOSITION–PROPERTY RELATIONSHIPS IN MULTICOMPONENT GERMANIUM–BASED POLYALKENOATE CEMENTS

by

Victoria Dickinson

Submitted in partial fulfillment of the requirements
for the degree of Master of Applied Science

at

Dalhousie University
Halifax, Nova Scotia
September 2014

to Susannah Abigail Dickinson

Table of Contents

List of Tables

List of Figures

Abstract

Vertebral compression fractures are increasingly treated through minimally invasive, rather than surgical, procedures due to the draw of improved outcomes and reduced risk of infection. Conventional clinical materials fail to balance excellent biocompatibility with appropriate mechanical properties. Glass polyalkenoate cements (GPCs) show significant potential to overcome this restraint, however they have been avoided in non–dental applications because Al^{3+} has been implicated in localized poor bone mineralisation and neurotoxicity. Aluminum–free glass polyalkenoate cements fall short of ideal clinical injectability (6 to 10 minutes) and basic mechanical property needs (compressive strength >30 MPa). The synthesis of germanium (Ge) containing glasses has ameliorated this limitation and has provided new GPCs with clinically useful characteristics. However, it is unknown whether the Ge modifications may compromise biocompatibility. This study examines 12 multicomponent glasses with varying silicon:germanium molar ratios and their contiguous polalkenoate cements. Glasses were melt-quenched (1520C, 1hr, ground to <45 μm) and subjected to thermogravimetric analysis (TGA) and x–ray diffraction (XRD), then blended with 50 wt % H_2O polyacrylic acid (2:1.5) and set in Teflon molds. Design of Mixtures (DoM) regression analyses were used to examine composition–property relationships with respect to temporal ion release and NIH 3T3 mouse fibroblast cytocompatibility of extracts derived from these glasses and cements, paying particular attention to germanium given its potential toxic characteristics. The results of this investigation have shown that cell viability remained between 92 to 124 % for the glasses, and between 94 to 105 % for all setting cements. $[Ge^{4+}]$, $[Si^{4+}]$, $[Na^{+}]$ and $[Sr^{2+}]$ ion release were detected up to 370 ppm, 12 ppm, 110 ppm and 20 ppm, respectively, for glasses and up to 200 ppm, 45 ppm, 32 ppm and 5 ppm, respectively, for cements. An optimization validation was performed based on the acquired data; this study has shown that the composition produced ($0.36ZnO_2 - 0.04SrO_2 - 0.021SiO_2 - 0.459GeO_2 - 0.0095ZrO_2 - 0.0095Na_2O - 0.101CaO$) gives equivalent characteristics to a previously developed germanium–containing composition (DG 209) with respect to ion release but possesses inferior mechanical characteristics. DG 209 is a promising GPC material for further investigation.

List of Abbreviations and Symbols Used

AANS	American Association of Neurological Surgeons
AAOS	American Academy of Orthopaedic Surgeons
ANOVA	Analysis of variance
CaP	Calcium phosphate
cDG(#)	Dal Glass germanate cements
cDM(#)	Dal Glass mixed former cements
cDS(#)	Dal Glass silicate cements
CIRA	Canadian Interventional Radiology Association
CSC	Calcium sulphate cements
CV	Cell viability
DG	Dal Glass
DI	Deionized water
DoM	Design of Mixtures
FDA	US Food and Drug Administration
gDG(#)	Dal Glass germanate glasses
gDM(#)	Dal Glass mixed former glasses
gDS(#)	Dal Glass silicate glasses
GPC	Glass polyalkenoate cement
HA	Hydroxyapatite
ICP	Inductively coupled plasma optical emission spectroscopy
ISO	International Organization for Standardization
KP	Kyphoplasty
LD_{50}	Median lethal dose
MMA	Methyl methacrylate
MPa	Megapascal
MTT	(3–(4,5–Dimethylthiazol–2–yl)–2,5–diphenyltetrazolium bromide)
PAA	Poly(acrylic acid)
P:L	Powder/liquid ratio

PMMA	Poly(methyl methacrylate)
PVA	Percutaneous vertebral augmentation
PVP	Percutaneous vertebroplasty
SIR	Society of Interventional Radiology
TCW	Tissue culture water
TGA	Thermogravimetric analysis
TSC	Trisodium citrate
VBCF	Vertebral body compression fracture
XRD	X-ray diffraction
β_i	Effects of individual χ_i
β_{ij}	Effect of two-way interactions between χ_i
β_{ijk}	Coefficients of the cubic blending of ternaries ($\chi_i\chi_j\chi_k$)
e	Residual
E_d	Dissociation energy
E_{Sun}	Sun's energy criterion
F	Ratio of the variance between groups to the variance within groups
γ_{ij}	Coefficients of the cubic blending of binaries
I	Ion dissociation energy
K	Rate constant (reciprocal time units)
p	p–value: probablility of observing results at least as extreme as observed given that the null hypothesis is true
R^2	Coefficient of determination
$R^2adj.$	Adjusted coefficient of determination
$R^2pred.$	Predicted coefficient of determination
$\mathrm{T_g}$	Glass transition temperature
$t_{1/2}$	Half life of ion dissolution
τ	Time constant (tau)
$\emptyset$	Diameter
θ	Angle between incident X-ray and scattering planes (Bragg angle)
X	Incubation time (days)
χ_i	i^{th} Compositional factors
Y	Concentration (ppm)
Y_0	Ion concentration at $X = 0$

Acknowledgements

I am grateful to my supervisor, Daniel Boyd, for the opportunity to work on this project and for his guidance throughout. I thank the members of the Boyd research group, especially Brett Dickey and Nancy Kilcup, for their support and assistance. Sincere thanks also to my committee members Robert Abraham and Mark Filiaggi for their guidance.

I extend my thanks to several kind individuals who have provided assistance and resources, and without whom this project would not have been possible: Maxine Langman (Dept. of Applied Oral Sciences), Gordon Hall (Dept. of Applied Oral Sceinces), Sharon Kehoe (ABK BioMedical, Inc.), Xiaofang Zhang (ABK BioMedical, Inc.), Mike Johnson (Dept. of Physics; thermogravimetric analysis), Robbie Sanderson (Dept. of Physics; X–ray diffraction), Darren Cole (Dept. of Biomedical Eng.), and Adrian West (Dept. of Biomedical Eng.).

Lastly, I am grateful for funding provided by the Atlantic Innovation Fund (AIF) and the Natural Sciences and Engineering Research Council (NSERC), and I thank Eleanor Seaman–Bolton, who is simultaneously NSERC CREATE: BioMedic program coordinator and a dear friend.

Halifax, August 2014

Victoria Dickinson

Chapter 1

Introduction

1.1 Anatomy of the Human Spine

The vertebral column is responsible for a triumvirate of primary functions that allow for the bipedal motion enjoyed by humans. Firstly, the vertebral column functions as a skeletal mediator that transfers loads and bending moments from the neck and torso to the pelvis. Secondly, it facilitates motion between the head, torso, and pelvis. Thirdly, it houses and guards the spinal cord. The vertebral column provides crucial support and protection while enabling a vast range of physiological motions. This juxtaposition of properties – strength and flexibility – is one best explained by a hierarchical look at the column [1].

1.1.1 The Vertebral Column

Vertebrae and intervertebral discs form the building blocks of the vertebral column. The column comprises five regions of vertebrae: cervical, thoracic, lumbar, sacral, and coccygeal, in order of superior to inferior positioning, as depicted in figure 1.1 [2]. 24 separate vertebrae populate the three superior regions – 7 cervical (C1-C7), 12 thoracic (T1-T12) and 5 lumbar (L1-L5); the inferior regions comprise fused vertebrae – 5 sacral and 4 coccygeal – to form the sacrum and the coccyx, respectively [3]. Cartilaginous intervertebral discs cushion successive vertebrae from the second cervical vertebra to the lumbosacral junction [3].

Successive vertebral regions have alternating curvatures that lend flexibility and shock absorbance to the spine. The convex curve of the cervical and lumbar vertebrae

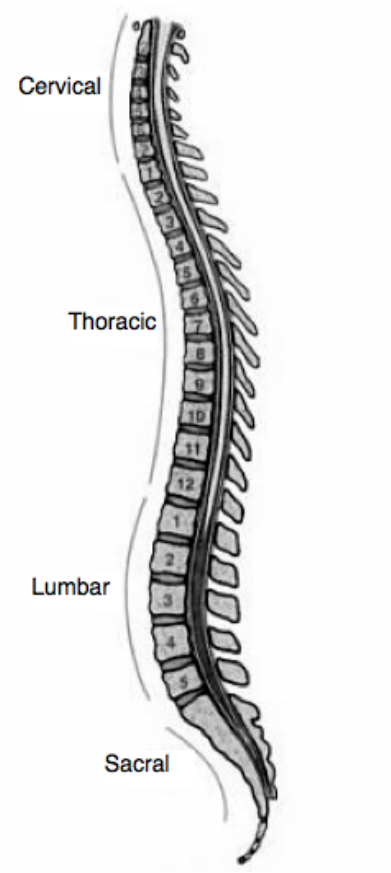

Figure 1.1: Saggital view of the human spinal column, adapted from [2].

is attributed to the uneven thickness of the intervertebral discs in these regions, while the thoracic and sacral regions form concave arcs attributable to vertebral geometry. Vertebrae and intervertebral discs increase in size from the cervical region to the lumbar region to match the increasing load in lower regions of the spine [3].

1.1.2 The Vertebral Body

Vertebrae comprise a hard cortical exterior shell (compact bone) encasing softer trabecular bone on the interior. Cortical bone provides structural rigidity while trabecular bone lends additional strength and hosts marrow to provide for blood cell production, shown in figure 1.2 [4]. The shape and thickness of cortical bone and ratio of trabecular bone depend on anatomical location and functional role [4]; together these two bone types provide appropriate support with optimized skeletal weight.

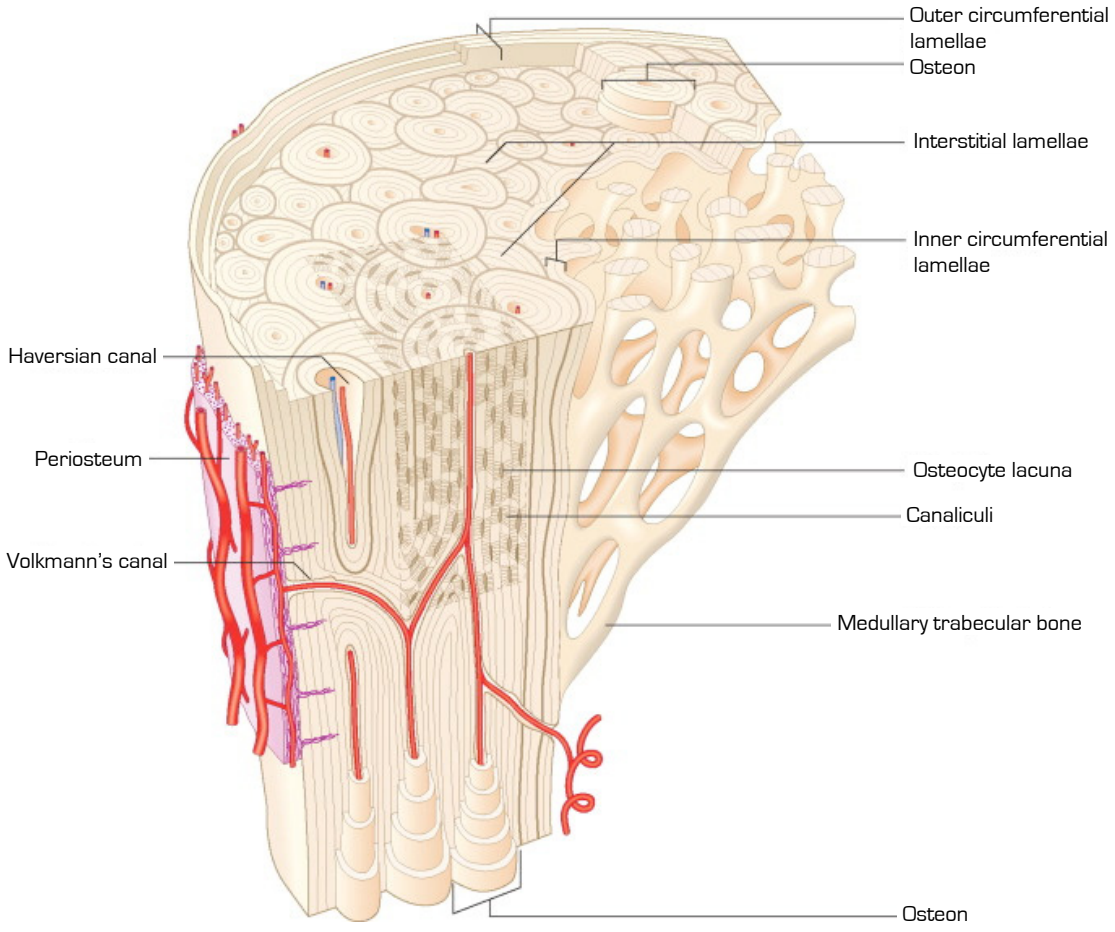

Figure 1.2: Cortical and cancellous bone, adapted from [5].

1.1.2.1 Macrostructure

Structurally, each vertebra comprises a vertebral body, vertebral arch, vertebral foramen, and processes, as depicted in figure 1.3 [4]. The processes provide mechanical support, means of articulation, and attachment sites for spinal muscles; pedicle processes, in particular, bridge the vertebral arch to the vertebral body [6, 4]. Processes of adjacent vertebrae couple to form facet joints that facilitate limited relative vertebral motion.

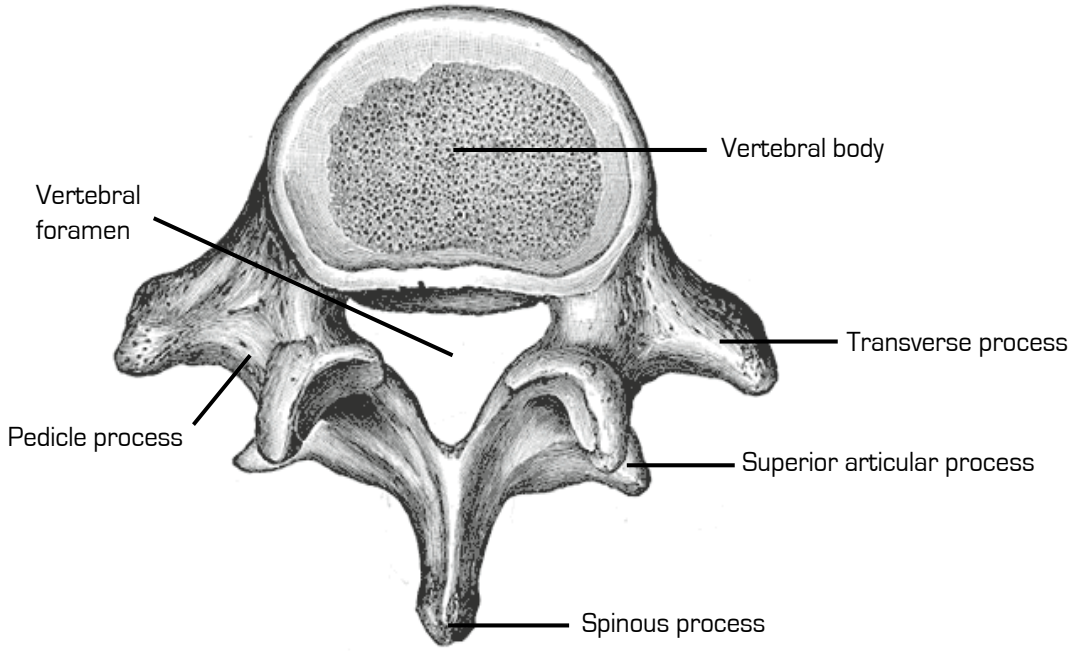

Figure 1.3: Example lumbar vertebra viewed from above, adapted from [7].

1.1.2.2 Microstructure

The osteon represents the basic structural unit of compact bone, and comprises a Haversian canal encircled by concentric layers of compact bone tissue termed lamellae. Situated between the lamellae are fluid-filled, oblong cavities known as lacunae. The lacunae are connected with one another as well as with the Haversian canals by a communication network of microscopic channels called canaliculi [4]. Cortical bone consists of a series of osteons bound together in a regular pattern while trabecular bone consists of osteons bound more loosely in a less regular pattern. Bone vasculature and innervation reside in Haversian canals comprising a linked

gridwork of vertical osteonic ducts and horizontal perforating ducts. Unlike the more rigid lamellular arrangement of osteons, the porous structure of trabeculae is responsible for the spongy nature of cancellous bone tissue, shown in figure 1.2. Trabecular bone pore size is on the order of 0.5–1 mm [8].

1.1.2.3 Nanostructure

The extracellular matrix of bone is a mineralized structure comprising 10-20% water, 60-70% mineral salts – primarily hydroxyapatite – and approximately 30% collagen [4]. Hydroxyapatite (HA) is a mineral with the formula $Ca_{10}(PO_4)_6(OH)_2$. HA imparts rigidity to bone and is the principle mode of storage of calcium and phosphorus in bone [4]. Collagen, the most abundant protein in the human body, is a fibrous, elastic structural protein that resists mechanical loads and promotes resilience [9]. The basic collagen molecule consists of three helical chains coiled around each other to form a supercoil [10]. This highly coiled structure is approximately 2 nm in diameter and is stabilized by interchain hydrogen bonds, covalent cross-linking between amino acid residues, and the tight packing of non-flexible proline residues. Collagen molecules aggregate in a staggered manner with various minor proteins and growth factors to form 500 nm diameter fibrils, which further aggregate to form strong, insoluble, mineralized fibers a few microns in diameter [10]. These mineralized fibers fall in semi-random patterns in trabecular bone, allowing for an open cell foam. In cortical bone, the mineralized collagen fibers align in highly organized sheets, forming circular osteons and a central hollow core. Figure 1.4 depicts the progression of bone anatomy from nanostructure to microstructure.

1.1.2.4 Bone Cell Types and Remodeling

Three primary cell types are found in bone: osteoblasts, osteocytes and osteoclasts [11]. Osteoblasts derive from mesenchymal precursor cells and present with cuboidal morphology upon maturation [11]. These cells are situated at the bone surface, particularly at sites where bone formation is actively occurring. Although osteoblasts are principally responsible for bone formation, they also enact bone mineralization: osteoblasts secrete collagen as well as non–collagenous proteins responsible for deposition of minerals within the bone structure [12]. Most mature osteoblasts (50–70%) undergo apoptosis, however some become dormant to function as lining

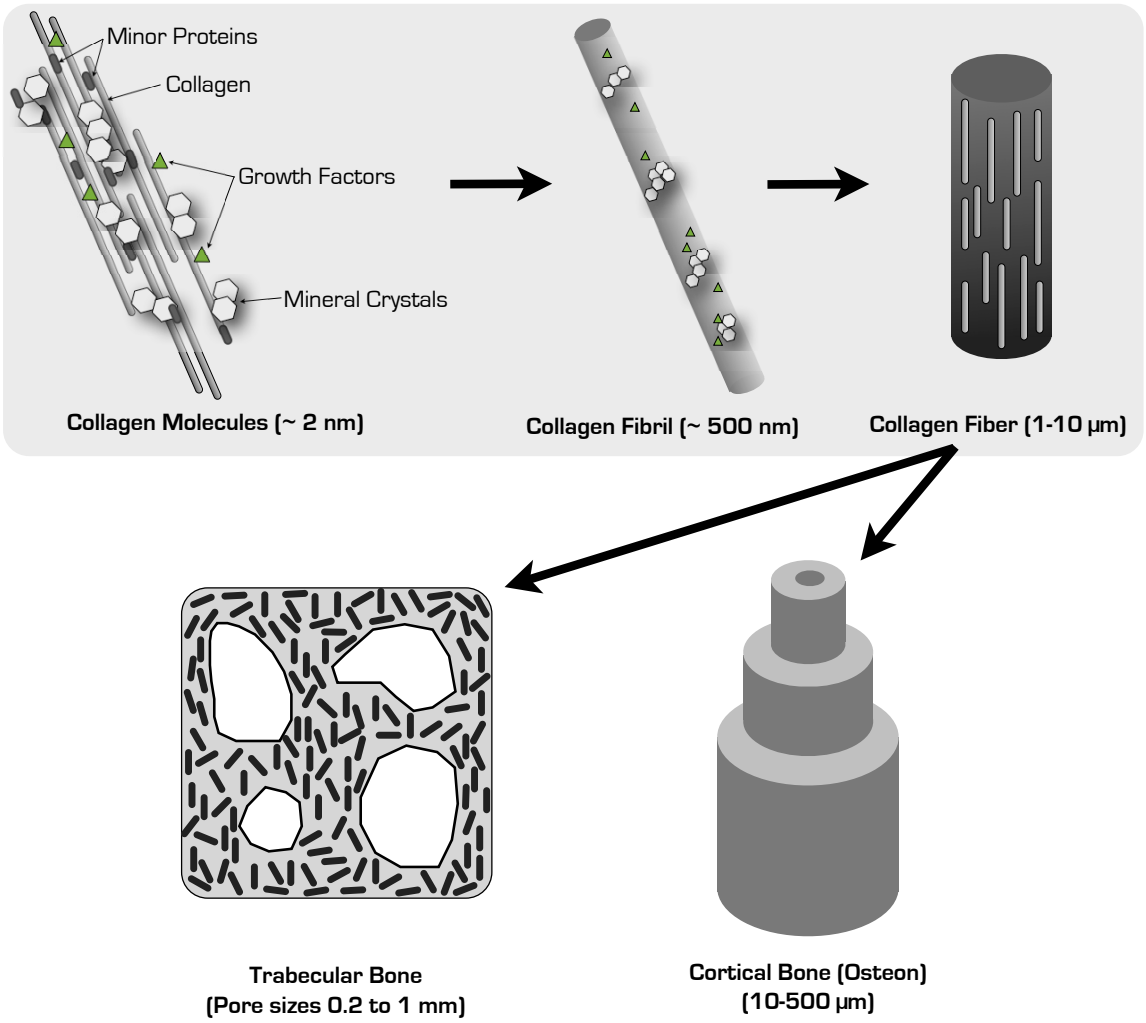

Figure 1.4: Bone tissue organization from the smallest components to whole tissues, adapted from [8].

cells within the bone matrix, while the remaining differentiate to become osteocytes [13].

The most abundant bone cells, osteocytes are non-proliferative, differentiated from osteoblasts, and form approximately 90–95% all bone cells in the adult human [11]. Osteocytes are biological mechanosensors that play a critical role in the maintenance of bone structure by signaling bone resorption and formation [14]. Due to their branched, star–shaped morphology and their distribution within the lacunae of the bone matrix, osteocytes are favourably situated for sensing mechanical signals and transducing these inputs into biological signals to regulate bone remodeling [11].

Osteoclasts are multinucleated giant cells that function to resorb bone [15]. They

derive from myeloid cells and express different morphology depending on function [11]. In the motile state, osteoclasts are flattened cells that possess lamellipodia and podosomes to facilitate migration from the bone marrow to the site of resorption [16]. In the resorptive state, these cells undergo cytoskeletal reorganization to produce a functional secretory domain and a sealing zone that separates resorptive secretions from the organelles of the cell [16].

Bone remodelling is achieved through cycles of bone resorption and formation, and functions to substitute primary (or immature) bone with secondary, more mechanically sound bone; to remove damaged bone tissue; and to maintain appropriate calcium levels [17]. The remodeling process is achieved by osteoblasts, which secrete the matrix necessary for bone formation, and multinucleated osteoclasts, which effect bone removal via pH mediated bone tissue resorption [18]. During resorption, osteoclasts anchor themselves to the bone surface and create a sealed, acidic environment to dissolve mineral content. The demineralized collagenous matrix is then resorbed through enzymes secreted by the osteoclasts, leaving a resorptive cavity into which osteoblasts migrate [11]. Osteoblasts then deposit osteoid, a collagenous organic material that composes a scaffold into which minerals begin to aggregate [11]. Osteoblasts that become trapped in the newly deposited matrix become osteocytes. It is the intrinsic properties of the mineralized collagen fibers working in concert with other minor proteins at the fundamental material level that largely provide the necessary biological signals to achieve the balance of bone resorption and formation [8]. These cellular activities maintain the structure and strength of the vertebral column at its core to resist mechanical forces and fractures.

1.2 Osteoporosis and Vertebral Body Compression Fractures

1.2.1 Pathology and Incidence

The continual cycle of bone resorption and redeposition is critical to the healthy functioning of the skeletal tissues; compromised bone remodeling often leads to osteoporosis [11]. Osteoporosis is a medical condition characterized by loss of bone tissue leading to reduced bone mass and concomitantly increased risk of orthopaedic fractures. More than 10 million people in the US, and approximately 100

million people worldwide suffer from osteoporosis [19, 20]. Bone tissue pathologically weakened by osteoporosis is susceptible to vertebral body compression fractures (VBCFs) arising from the axial compression loads transferred through the spine. Although VBCFs may be caused by compressive load trauma in isolation, they are most commonly found in patients with pre–existing osteoporosis [21]. Patients presenting clinically with VBCFs primarily complain of back pain that may or may not be localized at the vertebral fracture site [20]. Osteoporotic VBCFs are common and are accompanied by significant morbidity [22]. 700,000 cases of osteoporotic VBCFs are reported annually in the US, and 440,000 in the EU [20, 23]. One third of these present with chronic pain, leading to the hosptalization of one tenth [20, 24]. Vertebral body compression fractures can have a devastating effect on patients. Even those vertebral fractures not associated with pain cause declines in physical performance, and the effect on patients' quality of life rivals that of hip fractures [22].

1.2.2 Spinal Metastases and VBCFs

Although VBCFs are the hallmark of osteoporosis, it is important to bear in mind another prevalent cause of these spinal ailments [22]. In some cases, refractory spinal pain is secondary to damage caused by cancerous cells invading the vertebral bodies. In the U.S. alone, 1.4 million new cases of cancer are diagnosed, and 0.5 million metastasis-related deaths occur annually [25]. Metastases of the skeletal tissue are the third most prevalent secondary malignant growths, and the spinal column represents the most common skeletal site for metastatic cancers [25]. Extended lifespan due to advances in cancer treatments has influenced a concomitant increase in metastatic diseases of the spine, leading to an increase in cancer-related vertebral fractures that may result in the need for vertebral augmentation [20].

1.2.3 Treatment Options

VBCF treatment conventionally falls into three categories [20, 26, 27]:

1. conservative therapies, including lifestyle modification, physical assistive devices and pain medications;

2. therapies targeted at the underlying physiology; and

3. surgical intervention.

With respect to point 1, patients may modify their level of activity, take a period of bed rest, or pursue physical therapy to increase flexibility and strengthen the vertebral column [28]. External back-bracing and assistive devices may help to reduce strain on fractured vertebrae and promote gradual mobilization[29]. This approach is effective in some patients, however long treatment timeframes accompanied by high costs to both finances and livelihood limit the deisrability of these treatments. Narcotic analgesics may be administered to patients to reduce chronic back pain [30]. In the context of point 2, osteoporosis may be targeted with osteoporosis medication, particularly with a view to further fracture prevention [31]. Although patients benefit from pain management and improved bone health, these treatments involve long timeframes and increased opportunity for opioid dependence [30]. Metastatic cancers may be treated with interventions such as radiotherapy, hormone therapy, and cytotoxic drugs [32]. With respect to point 3, fractured vertebrae may be augmented surgically with clinical materials [27, 32]. Although surgical interventions offer long term reward with lessened long term maintenance, they carry heightened risk of infection and disruptive recovery periods [25, 20]. Each of these treatments functions to achieve pain control, strengthen vertebral bone, or both; those interventions that achieve both are surgically invasive. One contemporary intervention, percutaneous vertebroplasty, enables both pain control and bone strengthening in a minimally invasive manner.

1.3 Percutaneous Vertebroplasty

Percutaneous vertebroplasty (PVP) boasts many advantages in the treatment of VBCFs. The procedure involves the introduction of one or two cannulae through the skin into the fractured vertebra of a consciously sedated patient under the guidance of fluoroscopic imaging [33]. Bone cement is injected through the bore and into the fractured vertebral body, as depicted in 1.5. A transpedicular approach is used to avoid vascular and neural structures [21]. The cement then hardens within minutes while the patient remains still, providing internal fixation of the fracture fragments, restoring the integrity of the vertebra and alleviating back pain. Patients benefit

markedly from decreased back pain and improved quality of life shortly following the procedure, all without the rigours and interruption of invasive surgery [33]. A procedure termed balloon kyphoplasty (KP) treats pathological vertebral fractures using a similar cement injection process; however, in KP the physician inserts a balloon tamp into the fracture region and inflates it to partially restore height to the collapsed vertebra prior to cement injection [34].

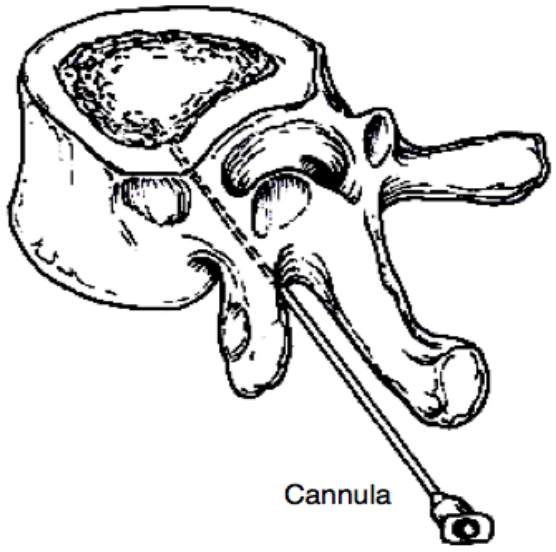

Figure 1.5: Oblique view of the transpedicular approach for delivery of an injectable bone cement in vertebroplasty, adapted from [33]

Percutaneous vertebroplasty was first introduced in France in 1984 by radiologists Galibert and Deramond [35]. The first procedure was performed using poly(methyl methacrylate) cement on a middle-aged female suffering from a painful hemangioma in one of her cervical vertebrae; the procedure achieved immediate spinal pain relief. Percutaneous vertebroplasty was later adopted as a treatment for VBCFs [36].

The safety and efficacy of percutaneous vertebroplasty has been a subject of debate in the clinical and scientific communities in recent years. A number of clinical studies have been reviewed by Lewis, who concluded that percutaneous vertebroplasty is an acceptable intervention for VBCFs, but that further blind, randomized trials are needed to truly evalute the efficacy of the procedure [34].

Two such randomized controlled studies arrived in the pages of the New England Journal of Medicine in 2009; Buchbinder *et al.* (Australia; 78 patients) and Kallmes

et al. (in connection with the Mayo Clinic; 131 patients) compared PVP to a sham procedure and to conventional treatments, respectively [37, 38]. Both discredited percutaneous vertebroplasty, citing the post-procedure similarity between groups treated using PVP and control groups. Mainstream media leapt at the opportunity and released headlines such as the following: "Percutaneous vertebroplasty exposed as ineffective" (The Medical News, 2009); "Studies find no benefit to popular spine procedure" (The Wall Street Journal, 2009) [39, 40].

Since then, other publications have opposed these controversial claims, criticizing flaws and omissions in the study methodologies and discussions [41, 42]. For example, patients in both sham and vertebroplasty procedure groups were allowed to receive the other treatment if they were dissatisfied with the pain relief outcome of their initial procedure. Only 12% of those who underwent vertebroplasty crossed over to undergo the placebo procedure, while a much greater 43% of sham control intervention patients elected to have vertebroplasty performed later on. Patient selection also hampered clinical interpretation of the Buchbinder and Kallmes studies. According to standards of practice, vertebroplasty proves most efficacious as a treatment for acute vertebral fractures [42]. Some patients in these studies, however, suffered from subacute and chronic fractures; in fact, more than half of the Mayo Clinic study patients were treated for vertebral fractures at least 6 months old [38]. Furthermore, apart from procedural trial criticisms, the author notes the absurdity of the balance of evidence: just 2 sham studies stacked against numerous previous publications and clinical trials elicited impassioned media coverage and caused the American Academy of Orthopaedic Surgeons (AAOS) to issue a strong recommendation against the use of vertebroplasty [43].

Two more recent randomized controlled trials concluded the safety and efficacy of PVP as a treatment for osteoporotic VBCFs [29, 42]. In 2011, Miller, Kallmes and Buchbinder urged that benefits of PVP derive from the placebo response, and questioned the continuing use of the procedure in clinical practice [44]. Today, however, half a decade after the Kallmes and Buchbinder studies emerged, eight high profile societies including the Society of Interventional Radiology (SIR), American Association of Neurological Surgeons (AANS) and the Canadian Interventional Radiology Association (CIRA) have expressed general consensus that, "... percutaneous

vertebral augmentation (PVA) with the use of vertebroplasty... is a safe, efficacious and durable procedure in appropriate patients with symptomatic osteoporotic and neoplastic fractures, when performed in a manner in accordance with published standards" [45].

Controversy over percutaneous vertebroplasty in the literature has been fueled in part by complications burdening the procedure, however rare. Although PVP is termed minimally invasive, it certainly carries greater risk than basic, external back-bracing interventions, for example. Cement extravasation, emboli and allergic reactions may occur acutely [46, 33]. This past year even, a report emerged on cardiac perforation caused by migrant bone cement that deposited and set in the right ventrical of the heart and in distal branches of both pulmonary arteries of a patient following vertebroplasty [47]. The procedure also carries a possible increased risk of new VBCFs in adjacent vertebrae. These complications may be linked to properties of the clinical materials used as well as physician expertise. The latter is addressed by clinical trial considerations from the Food and Drug Administration (FDA) and with continually updated quality improvement guidelines from the Society of Interventional Radiology (SIR) [48, 49]. As for the former, if the current literature were to express a consensus on PVP, it would be the unsuitability of available materials for the indication.

1.3.1 Current Clinical Materials

Conventionally, vertebroplasty bone cements have fallen into one of three material categories: ceramics (calcium sulphates and calcium phosphates), acrylic bone cements, and composite cements [50]. Many of these cements were formulated to suit different indications, then extrapolated to vertebroplasty use; as such, they are often weak in one or more categories of biocompatibility or mechanical functionality. Even cements formulated for the indication leave room for improvement.

Calcium sulphate cements (CSC) (better known as plaster of Paris) have been used for over a century in orthopaedics [34]. The material comprises calcium sulphate hemihydrate powder which produces a hydrated paste when combined with water, according to

$$CaSO_4 \cdot 0.5H_2O + 1.5H_2O \Rightarrow CaSO_4 \cdot 2H_2O[34].$$

In addition to provoking minimal inflammatory response, and inhibiting ingrowth of fibrous tissues, these cements are known to induce angiogenesis and osteogenesis [34]. Ideally, bone forms in concert with cement dissolution. Unfortunately, due to the load–bearing demands of vertebral body augmentation, CSC provide insufficient persistence as scaffolds over time, a feature attributable to their quick resorption timeframe under *in vivo* conditions [51, 52]. Specifically, these bone cements may be resorbed within weeks and fail to allow for sufficient native bone remodeling at the site of a vertebral fracture [34].

The first calcium phosphate (CaP) bone cement was invented in 1983 by Brown and Chow [53]. These cements comprise a tricalcium powder mixed with a liquid phase to produce a hydroxyapatite structure deficient in calcium and similar to the mineral phase of native bone tissue [34]. In fact, their inherent resorption allows for bone integration and remodelling. Calcium phosphate cements do not attain high curing temperatures due to their slow setting mechanism [34]. Although the low exotherm is advantageous in a clinical setting, the slow curing timeframe is insufficient for percutaneous vertebroplasty: mechanical injection through a cannula (an integral component of the procedure) combined with a slow setting reaction results in phase separation that limits their material integrity, and, ultimately, the application of CaP cements in load-bearing capacities [53].

Poly(methyl methacrylate) (PMMA) cement is a self–polymerizing acrylic bone cement. The cement is formed through free radical polymerization by mixing a powder component (comprising pre–polymerized PMMA, an inhibitor, and a radiopacifier) with a complementary liquid component (comprising methyl methacrylate (MMA) monomers, an initiator, and a stabilizer) [34]. Steric effects, which limit the flexibility of individual poly (methyl methacrylate) chains, coupled with tight chain packing leads to material stiffness under body temperature conditions, and consequently to high compressive strengths able to withstand the mechanical demands of the spine [54]. Although PMMA is generally considered safe and is used commonly today in vertebroplasty procedures (consider, for example, the brand SpinePlex® by Stryker International), it features a number of drawbacks. The polymer has a large setting exotherm, undesirable interaction with native tissues, and produces noxious fumes upon mixing in the clinic due to the volatile MMA monomers. The shrinking and

non-bonding properties of acrylic materials lead to gap formation at the bone-implant interface [55, 50]. Furthermore, PMMA is not inherently radiopaque and must be enhanced with contrast media additives such as barium sulphate ($BaSO_4$) [34].

Composite bone cements comprise a mixture of acrylate resins incorporating glass–ceramic particles and a radiopacifier [34]. Cortoss^{TM} by Orthovita (Malvern, USA) is the most prominent composite bone cement clinically used today. It claims a lower exotherm (approximately 63°C) than PMMA, produces fewer noxious fumes due to a non–volatile liquid phase and a contained delivery system, high compressive strength, and low sustained viscosity over the working period of 3.5 to 8 minutes[34]. Although composite materials show promising biocompatibility, they are susceptible to extensive leakage in native tissues prior to setting; extravasation rates up to 70% have been observed [56]. Furthermore, they are still formed of allergenic agents [57].

In considering the ideal material for vertebroplasty, Lewis cites the most desirable properties that would be characteristic of a cement optimized for vertebroplasty in his prominent bone cement review [50]. The most clinically relevant of these are listed below (adapted from [50]).

- Injectability (5 to 10 minutes of constant viscosity)
- Innate, high radiopacity
- Low curing temperature
- Mechanical properties similar to those of cancellous bone
- Adhesive to bone structures
- Non-toxic
- Low cost

Room exists for the introduction of a novel material that satisfies the competing biological and mechanical demands of vertebral body augmentation.

1.4 Glass polyalkenoate Cements

Glass polyalkenoate cements (GPCs) represent a logical progression in the evolution of orthopaedic biomaterials. Typically, they fall into one of three primary groupings:

conventional, metal re-inforced, and resin-modified [58]. The novel material concerned in this thesis belongs to the former category, so the following assertions pertain to conventional glass polyalkenoates. Conventional GPCs comprise a polymeric acid reacted with a reactive glass component, usually a fluoroaluminosilicate, in the presence of water. Typically the reactive glass is provided in powder form, and the polymeric acid is provided as an aqueous liquid. In this thesis specifically, for example, poly(acrylic acid) is matched with its own weight in water and used as the liquid phase. Poly(acrylic acid), or PAA, is a synthetic, acidic polymer of the simplest unsaturated carboxylic acid: prop-2-enoic acid (depicted in figure 1.6).

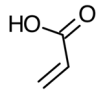

Figure 1.6: Prop-2-enoic acid

A paste forms upon mixing aqueous PAA with ground glass particles; within the paste, hydronium ions freed from PAA carboxylate functional groups etch the glass surface, resulting in the release of metal ions from the glass network [59]. These ions crosslink the entangled poly(acrylic acid) chains resulting in a set cement whose microstructure consists of reacted and unreacted glass particles embedded in a polysalt matrix, depicted in figure 1.7 [60]. After the cement sets, it undergoes further maturation, particularly in aqueous physiological environments, involving migration of less mobile, covalently bonded glass ions throughout the matrix [59]. Water, which worked at first as a reaction medium, then works to hydrate the polysalt matrix and to produce a stable gel structure at the implant site [59]. At the implant-bone interface, carboxylate groups bond favourably to calcium ions found plentifully in hydroxyapatite to yield strong interfacial bonding. From an orthopaedic materials perspective, glass polyalkenoate cements boast a number of advantageous properties, including low setting temperatures, no requirement for external setting aids due to the innate acid-base chemistry, chemical bonding to bone, working and setting times amenable to clinical use, and mechanical properties (compressive strength) comparable to those of bone. Furthermore, the properties of glass polyalkenoate cements can be tailored to suit desired indications by varying any number of factors, including glass composition, powder-liquid ratio and polymer density. This thesis

exploits the first of these, examining a range of glass compositions to establish composition-property relationships.

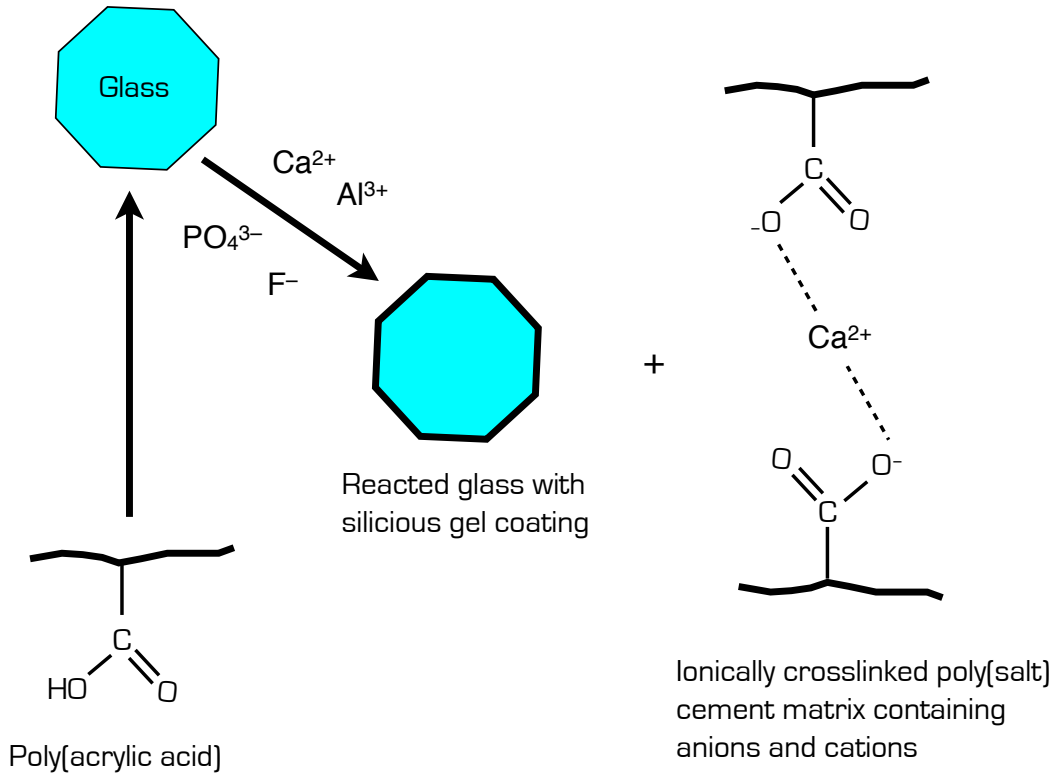

Figure 1.7: Basic schematic of the setting reaction of glass polyalkenoate cement components to form a porous framework of reacted an unreacted glass particles embedded in a polysalt matrix, adapted from [61].

1.4.1 Glass Polyalkenoate Cements as Orthopaedic Biomaterials

Wilson and Kent developed the first clinically available glass polyalkenoate cement in 1972 [62]. It comprised a calcium-fluoroaluminosilicate glass mixed with a polyalkenoic acid and was indicated for dental applications. Glass polyalkenoate cements made their orthopaedics debut in the late 1980s with the work of Jonck and Grobbelaar [63, 64]. In 1990, they reported orthopaedic use of a glass polyalkenoate cement (Ionos Medizinische Produkte GmbH & Co. Seefeld, Germany). They evaluated the cement using baboon models for hip and knee arthroplasties, and later clinically in patients for whom PMMA bone cement was contra-indicated [65]. The glass polyalkenoate cement showed effective structural and functional incorporation

into the native primate bone tissue; fibrous encapsulation was not observed, and normal bone marrow and haemopoietic cells were discovered adjacent to the cement surface. Satisfactory performance in the human trials warranted further clinical evaluation.

Babighian reports use of this same glass polyalkenoate cement in a variety of clinical otological procedures in 1992, including ossicular reconstructions and middle ear bone wall repair [66]. The report points to 95 percent anatomical post-operative satisfaction from a total of 59 procedures with post-operative follow-ups ranging from six to 18 months, and cites a number of clinical advantages offered by the glass polyalkenoate cement: biocompatibility, absence of toxicity, adhesion to bone, appropriate physical properties, and ease of shaping. The three failed procedures presented with glass polyalkenoate extrusion attributed largely to clinical overuse of the cement in bone regions with insufficient tissue cover.

The same year, Ramsden et al. released a preliminary study detailing clinical use of a polymaleinate glass polyalkenoate cement in 80 neuro-otological and skull base procedures [67]. Speed of surgery and ease of use, culminating in lowered clinical frustration, were cited as advantages offered by use of the cement. The study also indicated that patients presented with no adverse side effects following the procedures, and emphasized the value of the material for use in acoustic neuroma surgery and other skull base surgeries that necessitate opening of the cerebrospinal fluid space. Two years later, Helms and Greyer reported the use of Ionos glass polyalkenoate bone cement in 12 successful cases of endocranial space closure following translabyrinthine removal of acoustic neuromas [68]. They claimed that the availability of this cementous hard tissue provided an alternative to the former soft tissue dural closure material, with furthered risk diminishment of post-operative meningitis.

These positive reviews continued in the late 1990s when Ionos glass polyalkenoate bone cement was used to affix an electrode array in the cochleae of 240 patients (monitored post-operatively for two years): Kempf, Issing and Lenarz reported that the cement showed continued stability and no rejection reactions [69]. In 1997, another report of 343 clinical ossicular reconstruction surgeries monitored up to 2.5 years post-operatively recommended glass polyalkenoate cement for otological applications,

citing its biocompatibility, biostability, audiologic function and workability [70]. The same year, Geyer published a study on glass polyalkenoate cement in surgeries of the middle ear in a rabbit model; he reported the same advantageous features highlighted in the clinical study [71].

A 1998 publication by Maassen and Zenner showed that glass polyalkenoate cement produced better tympanoplasty type II [1] clinical outcomes than the autograft interposition alternative [72]. Kjeldsen and Grontved echoed the same positive recommendation for use of glass polyalkenoate cement in tympanopastly type II, citing less invasive surgery and lowered risk to native ossicles as benefits [73]. In 2001, Kupperman and Tange reported long-term evaluations of glass polyalkenoate cement implantation in the middle ear cavity and in the mastoid processes of 23 patients who were monitored post-operatively for over five years. The cement was not recommended as a first-choice material for these particular procedures due to significant incidences of tissue infection and cement extrusion [74].

This positive chronology of animal trials and clinical use established glass polyalkenoate cement as a promising orthopaedic materials into the mid-1990s. Some of the publications listed outrun the mid-1990s in nominal publication date; this can be explained by the time transpired from physical treatment to medical observation to literature publication, particularly for trials with large numbers of patients. While few drawbacks were reported for particular procedures, no fatal complications were observed; then, in 1994, the enthusiastic adoption of glass polyalkenoate cements in orthopaedic applications came to an end.

1.4.1.1 Barrier to Continued Use in Orthopaedics

In 1994, Renard et al. reported fatal subacute encephalopathy in two French patients following glass polyalkenoate neurotological bone augmentation [75]. Similarly, Hantson et al. reported fatal encephalopathy with seizures in two Belgian patients treated for bone defects that arose during the course of right vestibular neurectomy interventions; aluminum-containing glass polyalkenoate cement came into contact with the cerebrospinal fluid in both cases [76]. These encephalopathies were all attributed to grossly elevated aliminium levels caused by ion leaching from the glass

[1] This procedure involves surgical reparation of the tympanic membrane and the middle ear in spite of ossicle defects

polyalkenoate cement; concentrations of aluminium in the cerebrospinal fluid of these patients ranged from 63-185 mg/L, where the normal concentration in a healthy individual typically is less than 5 μg/L. The French Health General Directorate banned use of Ionos glass polyalkenoate cement in the months following the fatality report by Renard et al. [77]. Years later, Reusche et al. reported another earlier aluminium encephalopathy fatality following otoneurosurgerical bone reconstruction with Ionos cement in an Austrian patient [78]. Furthermore, beyond toxicity complications, several studies concluded that aluminum-containing glass polyalkenoate cement inhibited bone mineralization and osteoid formation in orthopaedic applications [79, 80].

In another unfortunate case, aluminium-containing glass polyalkenoate cement was used in a 1995 surgical reparation of the external ear canal of a 20 year old man [81]. The intervention resulted in complete facial nerve paralysis and heightened aluminium levels; fortunately, recovery followed resection of the cement. The paralysis was attributed to aluminium ion leaching, and the authors recommended clinical vigilance in the use of glass polyalkenoate cements near nerves.

In 1998, Baier asserted that desirable surgical results are yielded in glass polyalkenoate otoneurological intervention when the cement is handled and applied appropriately by the clinician [82]. This note is critical to the promise of glass polyalkenoate cements in orthopaedic indications; the cements concerned in the aforementioned studies would perform better with appropriate clinical handling. In addition to physician expertise, patient selection is an important criterion that bears heavily on medical outcomes. Engelbrecht strongly recommended against the use of aluminum-containing glass polyalkenoate cements for ortheopaedic applications following his study on revision arthroplasty procedures [83]. It would be easy enough for a reader of this particular study to walk away likewise condemning orthopaedic GPCs while failing to grasp more subtle implications of a biased patient selection process: in this study, patients were used for whom all other interventions were contraindicated. For example, a number of patients may have presented with renal insufficiency that could exacerbate the effect of leached aluminum discovered systemically [76]. The reality of such venturesome medical use would cause difficulty in drawing the robust, concrete conclusions required of a strong recommendation.

In the same vein of thought, Weber published a 1999 review corroborating both the excellent performance of Ionos glass polyalkenoate cement in rhinological surgeries, and its unfortunate absence on the market due to severe toxicity complications in otoneurological applications [84]. A decade later, glass polyalkenoate cement remains contra-indicated particularly for otoneurologic applications due to aluminum toxicity complications [85]. More generally, fright in the scientific and clincal communities has dampened enthusiasm over glass polyalkenoate bone cements in all other orthopaedic applications as well. Paradoxically, a material class that boasts excellent properties and performance experiences widespread shunning in the orthopaedic world. This reality highlights a critical composition-property-function challenge for the materials scientist.

1.4.1.2 Facilitating Continued Use of Glass Polyalkenoate Cements as Orthopaedic Biomaterials

Bone cements used for percutaneous vertebroplasty must be injectable for 5 to 10 minutes to enable effective fluoroscopic delivery through cannulae into affected vertrbrae, and must possess sufficient mechanical strength (>30 MPa) to withstand spinal compression [86, 87]. These clinical properties – injectability and mechanical strength – may be approximated in the laboratory using measures of working time and compressive strength, respectively. The Al^{3+} in conventional aluminosilicate GPCs forms complexes with modifier ions to slow cement working times to within the clinical window suitable for vertebroplasty [88]. Furthermore, trivalency enables Al^{3+} to bind multiple poly(acrylic acid) chains to increase crosslinking in the GPC matrix, leading to increased cement strength suitable for vertebroplasty consideration [89].

Although aluminum is integral to the working time and mechanical properties of GPCs, reconsideration of these materials for use in vertebroplasty necessitates the removal of aluminum [90]. With a progressive outlook toward orthopaedic applications, Boyd and Towler developed an aluminum-free glass polyalkenoate cement that circumvented the issue of Al^{3+} neurotoxicity [90]. The material comprised calcium-zinc-silicate glass (zinc incorporated for its antibacterial properties) combined with 50% poly(acrylic acid) with a powder:liquid ratio of 2:1.5 [90]. Later developments saw the incorporation of strontium, which has been implicated in bone regeneration and enhances radiopacity, to yield the glass phase with composition: $0.48SiO_2$–0.36ZnO–0.12CaO–0.04SrO [91, 92]. Both of these glasses failed

to satisfy compressive strength requirements, and material handling relevant to clinical applications proved particularly challenging due to rapid working times; the working time for these cements were in the range 30–60 seconds [93, 94, 91]. Positive advances made in the exclusion of aluminium were accompanied by a concomitant shortening of working time not amenable to clinical use. Compositional alternations produced varying responses: cements with working times nearing 4 minutes had meager compressive strength of approximately 20 MPa [90]. Compressive strength could be increased to 40MPa by increasing the molecular weight of the poly (acrylic acid) (PAA) component, however this alteration decreased working time to below one minute [90]. Efforts to increased compressive strength were met with decreased working time; inversely, efforts to increase working time were met with decreased compressive strength (figure 1.8). In 2008, Boyd et al. introduced trisodium citrate (TSC) to the cement ingredients during mixing, which resulted in increased compressive strength (60MPa) and extended working time (>2 minutes); however working time still fell short of injectability requirements (figure 1.8). Clarkin et al. decreased the molecule weight and ratio of PAA in 2010, Wren et al. incorporated titanium into the glass network, and in 2013 Gomes et al. incorporated magnesium, sodium and phosphorus into the glass phase; none of these adjustments yielded sufficiently extended working time at desired compressive strengths (figure 1.8) [95, 96, 97].

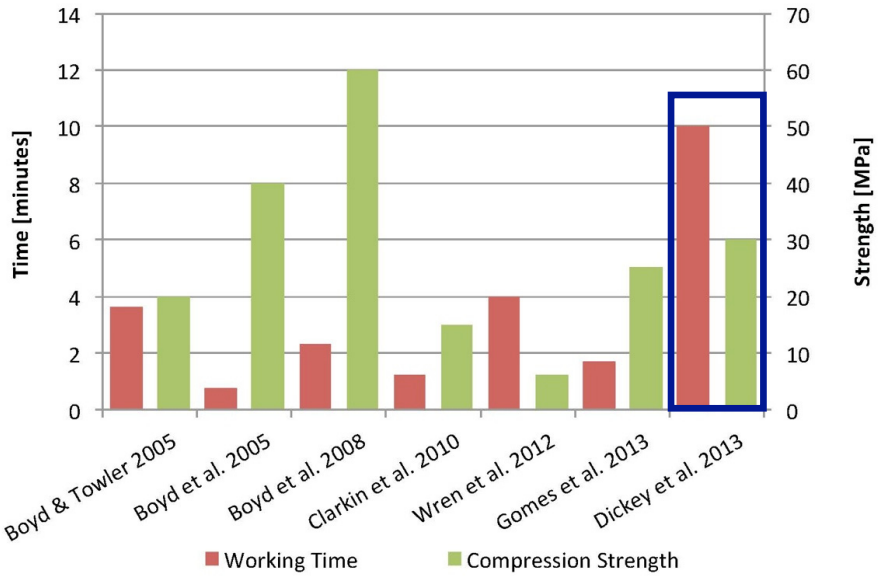

Figure 1.8: Working times and compressive strengths of aluminum–free GPCs produced over the past ten years; the blue frame denotes first instance of germanium inclusion in the glass network[87].

Recently, the calcium-zinc-strontium-silicate glass polyalkenoate developed by Boyd and Towler (0.48SiO_2-0.36ZnO-0.12CaO-0.04SrO by mole fraction) was manipulated through a series of glass component substitutions and additions to produce the Dal Glass series of GPC precursor glasses. 11 novel compositions (DG201 to DG211)[1] stem from this composition and include various substitutions of germania (GeO_2) and zirconia (ZrO_2) for silica (SiO_2) and calcia (CaO), respectively. Sodium (Na_2CO_3) charge compensates zirconia mole for mole. The development of the series through design space optimization and empirical melts is detailed in the previous work of Dickey [87]. Table 1.1 lists detailed molar compositions for glasses in this series.

[1]DG refers to "Dal Glass"

Table 1.1: Dal Glass Compositions by Molar Fraction

	Zn	Sr	Si	Ge	Zr	Na	Ca
DG 200	0.36	0.04	0.48 0	0	0	0	0.12
DG 201	0.36	0.04	0	0.447	0.0335	0.0335	0.087
DG 202	0.36	0.04	0	0.48 0	0	0	0.12
DG 203	0.36	0.04	0.215	0.215	0.05	0.05	0.07
DG 204	0.36	0.04	0.48 0	0	0.05	0.05	0.02
DG 205	0.36	0.04	0	0.38	0.05	0.05	0.12
DG 206	0.36	0.04	0.447	0	0.0335	0.0335	0.087
DG 207	0.36	0.04	0.38 0	0	0.05	0.05	0.12
DG 208	0.36	0.04	0	0.48	0.05	0.05	0.02
DG 209	0.36	0.04	0.215	0.215	0.025	0.025	0.12
DG 210	0.36	0.04	0.223	0.223	0.0335	0.0335	0.087
DG 211	0.36	0.04	0.24	0.24	0.025	0.025	0.07

Most notably, germania was a crucial component substitution [98]. Significant levels of germanium oxide were introduced into the novel glass series due to its excellent performance as a glass former. The resultant cements yielded remarkably lengthy working time and other advantageous mechanical characteristics (Table 1.2). Figure 1.8 depicts a sample cement from this series that falls within appropriate clinical windows for both working time (10 minutes) and compressive strength (30 MPa). B. Dickey has evaluated the mechanical properties and injectability of the novel glass polyalkenoate cement platform and has isolated compounds with remarkable features: extended working time leading to ease of injectability, innate radiopacity, and compression strength appropriately suited to the load-bearing indication.

Table 1.2: Radiopacity, working time, and one day incubation compression strength of Dal Glass cement compositions (standard deviations listed in parentheses) [87]

Composition	Radiopacity mm of Al	Working Time min:sec	Compression Strength MPa
DG 200	1.8 (0.4)	1:17 (0:03)	n/a
DG 201	3.1 (0.0)	5:18 (0:02)	39.52 (9.63)
DG 202	3.0 (0.0)	5:58 (0:20)	39.00 (1.96)
DG 203	2.7 (0.4)	7:05 (0:07)	n/a
DG 204	2.5 (0.0)	7:08 (0:13)	n/a
DG 205	2.8 (0.4)	4:58 (0:13)	49.22 (2.10)
DG 206	2.1 (0.4)	1:09 (0:31)	n/a
DG 207	2.3 (0.4)	0:22 (0:05)	n/a
DG 208	2.9 (0.4)	10:02 (0:09)	37.17 (4.07)
DG 209	2.6 (0.4)	5:02 (0:13)	45.16 (2.28)
DG 210	3.1 (0.0)	6:56 (0:26)	33.17 (4.06)
DG 211	2.9 (0.4)	7:54 (0:21)	n/a

Germania (GeO_2) is an inorganic oxide that, like glass polyalkenoate cements in orthopaedics, has experienced its own phases of promise and rejection. Germanium-containing dietary supplements came into vogue in Japan in the 1970s as elixirs for diseases such as cancer, and later AIDS [99]. Mounting popularity made it the target of a number of toxicological risk studies. Although a distinction needs to be made between organic and inorganic germanium, both have been implicated in health risks with a range of symptoms: weight loss, fatigue, gastrointestinal disorders, anemia, muscle weakness and kidney failure [100, 99]. So far, however, risk studies have been aimed at germanium products consumed orally or introduced dermally [101].

Interestingly, a 1997 study pointed to the inhibitory action germanium has on cancer [102]. Localized, controlled delivery of germanium at orthopaedic sites may prove beneficial as a cancer therapy, and germanium glass polyalkenoate cements have the potential to act as therapeutic delivery vehicles in that respect. Although the novel glass polyalkenoate cement is indicated primarily for augmentation of compromized vertebral bodies, potential for this second indication exists. Application of localized ion leaching from optimized bone cements to cancer therapies may stimulate a shift of interest in the treatment of cancers residing in hard tissues.

1.5 Statement of the Problem

The addition of germanium to the glass phase of glass polyalkenoate cements (GPCs) ameliorates a major limitation associated with aluminum-free GPCs [87]. Unexpectedly, germanium incorporation yields materials that are both injectable (up to 10 minutes) through vertebroplasty equipment and have significantly improved mechanical properties versus conventional aluminum-free GPCs. Such a balance of properties is not present in the literature for aluminum-free GPCs. A gap exists in continued development, however: the novel material may only proceed to clinical use with appropriate biological evaluation that ensures freedom from unacceptable risk. It remains unknown if the compositional modification (addition of germanium to the glass phase) may compromise biological performance. To begin to redress the balance, this study is the first step to analyzing the biocompatibilty of these materials, and uses a materials response and host response line of inquiry. In this work, DG glasses and their contiguous cements are prepared and analyzed for degradation byproducts and cytocompatibility to establish crucial composition–property relationships.

Chapter 2

Research Objectives, Hypotheses and Rationales

The work of this thesis is segmented into three broad experimental groupings: material synthesis and characterization, material response under simulated physiological conditions (degradation byproduct determination), and preliminary biological response evaluation (*in vitro* cell viability) of the 12 materials in the Dal Glass series and their contiguous polyalkenoate cements, reproduced below (table 2.1).

Table 2.1: Dal Glass Compositions by Molar Fraction

	Zn	Sr	Si	Ge	Zr	Na	Ca
DG 200	0.36	0.04	0.48 0	0	0	0	0.12
DG 201	0.36	0.04	0	0.447	0.0335	0.0335	0.087
DG 202	0.36	0.04	0	0.48 0	0	0	0.12
DG 203	0.36	0.04	0.215	0.215	0.05	0.05	0.07
DG 204	0.36	0.04	0.48 0	0	0.05	0.05	0.02
DG 205	0.36	0.04	0	0.38	0.05	0.05	0.12
DG 206	0.36	0.04	0.447	0	0.0335	0.0335	0.087
DG 207	0.36	0.04	0.38 0	0	0.05	0.05	0.12
DG 208	0.36	0.04	0	0.48	0.05	0.05	0.02
DG 209	0.36	0.04	0.215	0.215	0.025	0.025	0.12
DG 210	0.36	0.04	0.223	0.223	0.0335	0.0335	0.087
DG 211	0.36	0.04	0.24	0.24	0.025	0.025	0.07

The amounts of glass intermediate ZnO_2 and glass modifier SrO are held at a

fixed total mole fraction of 0.40. The author reminds the reader of the primary compositional variables within the series for the remaining 0.60 mole fraction: (1) the glass former GeO_2 replaces the glass former SiO_2 up to a mole fraction of 0.48; and (2) the glass intermediate/modifier ZrO_2/Na_2O (equimolar) replace the glass modifier CaO by up to a mole fraction of 0.10.

Following experimental work and establishment of composition–property relationships, a preliminary glass polyalkenoate cement optimization is performed. This chapter provides a broad research flow, followed by a conceptual framework for the feasibility, interest, novelty, and relevance of each experimental grouping, where appropriate [103].

2.1 Empirical Research Flow

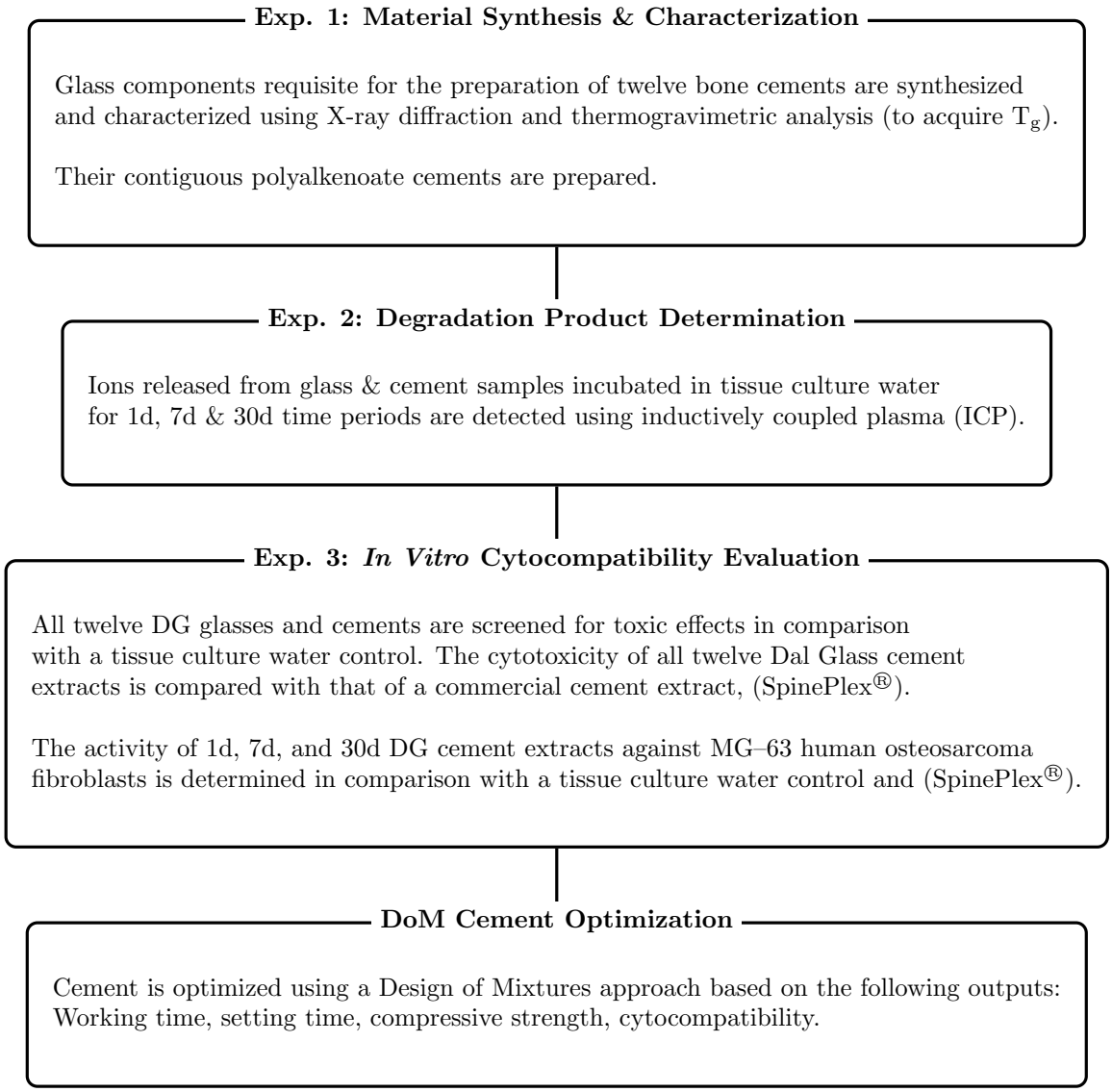

2.2 Experiment 1: DG Glass Synthesis and Characterization

2.2.1 Objective

DG glasses (n = 12) were synthesized and subsequently analyzed using X-ray diffraction (XRD) and thermogravimetric analysis (TGA) to confirm amorphous glass structure and to acquire T_g values. This screening experiment is to ensure repeatability of structural characteristics to those published in the literature [87] and to assess the effect of composition on T_g.

2.2.2 Hypothesis

With regard to the glass formers, Ge^{4+} is a lower field strength cation than Si^{4+}, implying longer Ge–O bond length and lower rotational barrier in the oxide form. Consequently, T_g values will be lower for germanium–based glasses. Furthermore, in consideration of the glass intermediates and modifiers, the exchange of equimolar ZrO_2/Na_2O for CaO in the network will not significantly impact T_g values due to the low total mole fraction of modifiers within the network.

2.2.3 Rationale

A proper understanding of composition-property-function relationships throughout the proposed work must be built upon a core understanding of material synthesis and characterization. The 12 DG glasses are characterized through x-ray diffraction (XRD) to ensure non-crystallinity, and thermal analysis to determine unique glass transition temperatures (T_g). The glass transition temperature occurs when there is enough vibrational (thermal) energy in the network to permit sufficient free volume such that sequences of atoms can diffuse toward more energetically favourable arrangements. T_g is relevant to mechanical properties of glassy materials; knowledge of the T_g allows annealing to relieve the internal stresses of the glasses, a requirement for clinical handling [104]. For the purpose of cement synthesis, annealed DG200 to DG211 glass powders are combined with a constant aqueous poly(acrylic acid) formulation to yield 12 unique glass polyalkenoate cements.

2.3 Experiment 2: Evaluation of Degradation Products from DG Glasses and DG Cements

2.3.1 Objective

To assess the levels of constituent ions released under simulated physiological conditions from glass and cement samples incubated in tissue culture water for 1d,7d and 30d time periods using inductively coupled plasma (ICP). Ion release profiles were generated for each glass constituent and cross-referenced with biocompatibility data.

2.3.2 Hypotheses

Germanium has longer cation-anion bond length than silicon, and cation-anion bond length affects glass dissolution kinetics. Assuming isostructural replacement of germanium for silicon in the glass network, germanium will be able to modulate temporal release profiles of the glass modifiers and intermediates to the effect that greater amounts of constuents will be released from germanate compositions than from silicate compositions. Furthermore, in consideration of the glass intermediates and modifiers, the exchange of equimolar ZrO_2/Na_2O for CaO in the network will not significantly impact ion release due to the low total mole fraction of modifiers within the network.

2.3.3 Rationale

Extracts will be analyzed for degradation products using inductively coupled plasma (ICP) according to international guidelines documented in ISO 10993-14 [105]. Germanium elution levels are of particular interest in this study. Cements implanted physiologically in the human body will degrade to some extent over time. Ion dissolution half–life ($t_{1/2}$) is a measure of the time required for half of the total degradable amount of a sample to degrade. This experiment will yield temporal ion release profiles under simulated physiological conditions for DG glass and cement materials. $t_{1/2}$ is a measure of kinetics, not of quantified amounts, and so this study must be augmented with consideration of total extract ion concentrations.

The DG glass series comprises a number of complex networks, each containing from 4 to 7 different glass oxides including formers, intermediates and modifiers. It is well known that binary and ternary glass systems are simpler, more straightforward

subjects for the purposes of composition–property evaluation. The DG glass series eschews ease of direct composition–property evaluation to instead embrace other benefits offered by multi–component networks. This limitation must be countered by use of more powerful analysis methods; hence, the author will carry out composition–property analysis using the design space software to which the DG glass series owes its origin: Design of Mixtures (DoM) [1]. This software will be used to determine the effect of composition on ($t_{1/2}$).

An understanding of the original glass and cement features from Experiment 1 coupled with cytocompatibility results and these degradation products data will augment understanding of composition–property relationships. In particular, the composition and structure of the novel materials will determine their ion leaching profiles to obtain degradation half–life ($t_{1/2}$) values, and effects on living cells can be correlated and studied accordingly.

2.4 Experiment 3: Evaluation of *In Vitro* Cytocompatibility for DG Glasses and DG Cements

2.4.1 Objective

This study screened all twelve Dal Glasses for toxic effects in comparison with a tissue culture water control. The cytotoxicity of all twelve Dal Glass cement extracts is also compared with that of a commercial cement extract (SpinePlex®). Subsidiarily, the activity of inorganic germanium against a specific human osteosarcoma cell line (MG–63 fibroblasts) is determined.

2.4.2 Hypotheses

- DG glass extracts will yield significantly lower NIH 3T3 mouse fibroblast cell viability than the tissue water control over all time periods due to the greater elution of ions from the glass network.

- DG cement extracts will yield significantly lower NIH 3T3 mouse fibroblast cell viability than SpinePlex® over all time periods due to the greater elution of ions from the novel cement matrices.

[1] Design Expert 8.0.4 (Stat-Ease Inc., USA)

- Germanium–containing cements will demonstrate significantly lower MG-63 human osteosarcoma cell viability than both non-germanium containing cements and SpinePlex® over all time periods.

2.4.3 Rationale

In vitro biological evaluation serves as the first stage in biocompatibility determination, and as a crucial bridge between the material synthesis and small animal trial stages. The chief aim of *in vitro* work is the identification and exclusion of biomaterials that are toxic to cells [106]. *In vitro* bioincompatibility may be evaluated using three primary cell culture assays: direct contact, agar diffusion and elution testing [107]. Elution cell culture testing and degradation product determination were proposed for this particular study. Cell culture and degradation product results cannot be extrapolated *a priori* to actual *in vivo* conditions, however they can be used to determine leaching of potentially harmful ions.

Elution testing was selected as the cell culture method of choice primarily because it allowed for extended exposure times, but also because it allowed for flexible extract conditions and further composition testing possibilities [106]. Glass and cement samples were incubated under simulated physiological conditions; these conditions only very roughly approximate those of a living body, however they did allow for standardized ion elution. 24 hour, 7 day, and 30 day extract testing produced meaningful elution profiles, and quantitative MTT assay determination of cytotoxicity. Two cell lines were employed: cytotoxicity of both glass and cement extracts were tested with standard, robust NIH 3T3 mouse fibroblast cells, and cements alone were examined for cytotoxicity in the presence of MG-63 human primary osteosarcoma cells. Cytotoxicity testing with human osteosarcoma cells enabled preliminary evaluation of the effect of the novel materials, particularly those containing germanium, on cancerous bone cells. A commercial standard (SpinePlex®, Stryker®) PMMA cement was subjected to identical preparation and testing procedures.

The prevalence of cancers of the spine associated with vertebral body compression fractures along with the potential anticancer activity of germanium compounds warrant a further study of the cell viability of cancer cells in the presence of inorganic germanium–containing cements. Elution extract testing was selected for this study

as well. Just one human osteosarcoma cell line was selected due to the small scope of this study and the function of the spine in the skeletal system, however any number of additional cell lines could be tested to evaluate the cytotoxicity of the novel cement extracts on metastatic cancers of the spine.

2.5 Nomenclature

DG molar glass compositions have been presented together as a set in the literature (Table 2.1) [87]. For the sake of later composition–property analyses, and in order to answer hypotheses effectively, the author has parsed the 12 glass compositions into three manageable streams:

1. No GeO_2 replacement of SiO_2: Dal Glass silicates (gDS)
2. Complete GeO_2 replacement of SiO_2: Dal Glass germanates (gDG)
3. GeO_2/SiO_2 is unity: Dal Glass mixed former glasses (gDM)

Table 2.2 lists these streams along with their composition adjustment information; these streams will be used for composition–property comparisons throughout the bulk of the analysis work. The compositions have been renamed to match the parsing: gDS refers to silicate glasses, gDG to germanate glasses, and gDM to mixed former glasses. The subscript g indicates glass phase composition. The subscript c will be used later on in this study to specify the contiguous glass polyalkenoate cements. Note that gDS1, for example, has the same glass modifier changes as gDG1, gDS2 as gDG2, and so on (table 2.2). Note also that the first two glasses in the silicate and germanate series contain no sodium or zirconium modification while all mixed former glasses contain some amount of sodium and zirconium (equimolarly).

2.6 Structure of the Study

Little is known about the biocompatibility of germanium–containing glasses or glass polyalkenoate cements. In order to evaluate the impact of germanium modification on degradation byproducts and biocompatibility, it is necessary to study the glass phase in isolation. Furthermore, due to physical qualities of the materials it is

Table 2.2: Three glass streams (percentages are with respect to total glass content)

Stream	Comp.	Nomenclature	Adjustments to original Zn-GPC glass
Silicate glasses (+ modifier adjustments)	DG200	gDS1	Original
	DG204	gDS2	$CaO \downarrow 10\%$, $ZrO_2 - Na_2O \uparrow 10\%$
	DG206	gDS3	$SiO_2 \downarrow 3.3\%$, $CaO \downarrow 3.3\%$, $ZrO_2 - Na_2O \uparrow 6.6\%$
	DG207	gDS4	$SiO_2 \downarrow 10\%$ $ZrO_2 - Na_2O \uparrow 10\%$
Germanate glasses (+ modifier adjustments)	DG202	gDG1	Original with complete GeO_2 replacement of SiO_2
	DG208	gDG2	$CaO \downarrow 10\%$, $ZrO_2 - Na_2O \uparrow 10\%$
	DG201	gDG3	$GeO_2 \downarrow 3.3\%$, $CaO \downarrow 3.3\%$, $ZrO_2 - Na_2O \uparrow 6.6\%$
	DG205	gDG4	$GeO_2 \downarrow 10\%$ $ZrO_2 - Na_2O \uparrow 10\%$
$GeO_2/SiO_2 = 1$ (+ modifier adjustments)	DG203	gDM1	SiO_2-$GeO_2 \downarrow 5\%$, $CaO \downarrow 5\%$, $ZrO_2 - Na_2O \uparrow 10\%$
	DG209	gDM2	SiO_2-$GeO_2 \downarrow 5\%$, $ZrO_2 - Na_2O \uparrow 5\%$
	DG210	gDM3	SiO_2-$GeO_2 \downarrow 3.4\%$, $CaO \downarrow 3.3\%$, $ZrO_2 - Na_2O \uparrow 6.7\%$
	DG211	gDM4	$CaO \downarrow 5\%$, $ZrO_2 - Na_2O \uparrow 5\%$

most prudent that powdered glass be studied using consistent mass values, and mixed cements by using consistent material geometries. This difference makes direct comparison of the materials (glass and cement) arduous and inaccessible. For the purpose of this thesis, therefore, chapter 4 focuses on the glass phases and chapter 5 on their contiguous cements.

Chapter 3

Materials and Methods

3.1 Experiment 1: DG Glass Synthesis and Characterization

3.1.1 DG Glass Preparation Method

Glasses were formed through rapid melt quenching. Analytical grade zinc oxide, strontium carbonate, silica, germania, zirconia, sodium carbonate and calcium carbonate reagents (Sigma–Aldrich) were weighed according to each composition to a precision of ± 0.001 g with a Kern and Sohn GmbH analytical balance (model ABJ 120-4M). Raw powder compositions were mixed mechanically in a blender (Twin shell dry blender, Patterson-Kelly, USA) for one hour, then dried in a 100°C vacuum oven for one hour. The mixed, dried powder was packed into 50 mL platinum crucibles (Alpha Aesar, Ward Hill, USA) and fired for one hour in a high temperature box furnace (Carbolite RHF 1600, UK) pre-heated to 1520°C. Crucibles were removed from the furnace with stainless steel tongs and their molten contents were pour quenched rapidly at room temperature into water. The resulting glass frit was retrieved and dried for 24 hours in a 100 °C vacuum oven. A planetary ball mill (Pulverisette 7, Fritsch GmbH, Germany) was used to grind the dried frit, which was then sieved through 45 μm standard test sieves (Cole-Parmer, Montreal, Canada) iteratively to yield powder of $<$45 μm particle size.

3.1.2 X-Ray Diffraction Method

A portion of each glass powder (n=1) was analyzed using x-ray diffraction to ensure non-crystallinity. Samples were tested using a Bruker AXS D8 diffractometer (Department of Physics, Dalhousie University). The system employed Cu-Kα radiation (0.5 mm wide collimated beam), a Göbel mirror, a Vantec-2000 area detector, and a copper target. Data acquisition was performed for a scattering angle (2 θ) range of 10 to 89.98 ° and required approximately 15 minutes per sample. Data containing evidence of residual crystallinity were run through a reference pattern database along with relevant composition information using a program from Crystal Impact called Match! [108]. This facilitated determination of any crystalline phases present.

3.1.3 Thermogravimetric Analysis Method

Powder samples (n=1) were analyzed for thermal characteristics (Department of Chemistry, Dalhousie University). 15-25 mg of powder were transferred to tared alumina sample pans. Measurements were conducted on a TA instruments SDT Q600 model TGA instrument in a temperature regime of 300 °C to 850 °C under an argon atmosphere with a ramp rate of 10.00 °C per minute and a sampling interval of 0.10 s/pt. Standard calibration protocols were employed. The instrument used has a temperature accuracy of approximately 1 °C at the ramp rate employed (10 °C/minute).

3.1.4 Annealing Method

Glass powders were annealed at T_g–30 °C for 3 hours in the high temperature box furnace (Carbolite RHF 1600, UK) and allowed to cool undisturbed overnight as per the literature [87].

3.2 Experiment 2: Evaluation of Degradation Products from DG Glasses and DG Cements

3.2.1 DG Cement Preparation Method

Glass polyalkenoate cements were formed by mixing annealed glass powder with a 50 % by weight aqueous solution of a 25,000 dalton poly(acrylic acid) (E7, Advanced

Healthcare Ltd., Tonbridge, UK) in a powder:liquid ratio of 2:1.5. The powder:liquid ratio was chosen according to that used in the predicate material developed by Boyd and Towler [91]. Immediately following mixing, cement pastes were spatulated into Ø6 mm x 1 mm teflon disc molds, clamped between flat aluminium plates using screw vises, and allowed to set in a 37 °C ambient temperature environment for one hour. Following setting, cement discs were removed from the molds, and transferred into 14 mL BD Falcon™ round bottom polypropylene tubes. 10 mL of sterile tissue culture water were added to each cement sample (n=3).

3.2.2 DG Glass Extract Preparation

Twelve glasses, DG 200 to DG 211, were prepared and ground to sub 45 micron powder. 0.1 g of each glass powder measured to a precision of ± 0.001 g with a Kern and Sohn GmbH analytical balance (model ABJ 120-4M) were transferred into 14 mL BD Falcon™ round bottom polypropylene tubes. The glasses were then vacuum autoclaved in a Primus General Purpose Steam Sterilizer (Primus Sterilizer Company, Inc., Omaha, NE) for 15 minutes at 121 °C. Samples of each glass were prepared in triplicate for each of three incubation time periods: 24 hours, 7 days, and 30 days. 10 mL of tissue culture water (Sigma–Aldrich, lot # RNBB6914 and RNBC1419) were added aseptically to each sterilized glass sample, and the vials were capped tightly. Sample vials were positioned upright in 16 mm Nalgene® 5970 unwire test tube racks (Thermo Scientific) and incubated at 37 °C in a Julabo SW22 Shaking Water Bath (Julabo USA, Inc., Allentown, PA) with a uniaxial agitation rate of 2 Hz. At the completion of each incubation time period, samples were removed from the water bath and extracts were decanted aseptically into 0.2 micron filter syringes within a SterilGARD® III Advance class II biological safety cabinet. Filtrates were collected in sterile 14mL polypropylene tubes, capped tightly and stored upright at 4 °C for later analysis (n=3).

3.2.3 DG Cement Extract Preparation

The extract preparation procedure for cements followed the same procedure detailed in section 3.2.2.

3.2.4 Ionic Content Analysis

1 mL of each of the glass and cement extracts (n=3) was diluted up to 7.5 mL with 2% (v/v) HNO_3. Calibration standards were prepared analytically in 2% (v/v)

HNO_3 from stock solutions of 1000 mg/L zinc, strontium, silicon, germanium, zirconium, sodium, and calcium analytical standards (Perkin Elmer Atomic Spectroscopy Standards) using serial dilution by high performance pipettes (VWR) and volumetric flasks (Table 3.1).

Table 3.1: Standard ion concentrations used for ICP analyte calibration

Standard	Concentration in ppm						
	Si^{4+}	Ge^{4+}	Na^{+}	Ca^{2+}	Sr^{2+}	Zn^{2+}	Zr^{4+}
1	0.001	0.001	0.001	0.001	0.001	0.001	0.001
2	0.01	1	0.01	0.01	0.01	0.01	0.01
3	1	5	1	1	1	1	1
4	5	10	5	5	2	5	5
5	10	100	10	10	4	10	10

The Si^{4+}, Ge^{4+}, Na^{+}, Ca^{2+}, Sr^{2+}, Zn^{2+}, and Zr^{4+} ionic concentrations of each extract were analyzed using inductively coupled plasma optical emission spectroscopy (ICPOES: Perkin Elmer Optima 8000 equipped with WinLab32 ICP software). Diluted extract concentrations were determined against empirical calibration curves determined at the emission wavelengths reported in Table 3.2 with corresponding linear correlation coefficients throughout the experiment.

Table 3.2: Emission wavelengths used for ICP measurement

Standard Analyte	Emission Wavelength (nm)	Linear correlation coefficient
Si^{4+}	251.611	0.997785 to 0.999796
Ge^{4+}	209.426	0.999851 to 0.999975
Na^{+}	589.592	0.984808 to 0.986008
Ca^{2+}	317.933	0.998741 to 0.999534
Sr^{2+}	407.771	0.999643 to 0.999681
Zn^{2+}	206.200	0.999903 to 0.999934
Zr^{4+}	343.823	0.999105 to 0.999114

3.2.5 Statistical Analysis

Ion release results are expressed as means with standard deviations of triplicate determinants. Analysis of the results was carried out by way of a two–way Anova test with Tukey confidence intervals using an overall significance level of $\alpha = 0.05$ to examine statistically significant differences across time and composition for analysis of ion release and cell viability. Statistical results are included in the appendices, and use the convention: $p > 0.05$ (ns), $p \leq 0.05(*)$, $p \leq 0.01(**)$, $p \leq 0.001(***)$,

and $p \leq 0.0001(****)$. Glasses and cements are divided into three groups according to the predominant glass former content (germanate, silicate and mixed), and ion release levels of each element are reported for each composition over all three time periods. Multiple centroid runs are utilized in DoM to provide for statistical validity of models in the absence of the conventional definition of an intercept.

3.2.6 Ion Release Profile Modeling

The mean of empirical ICP ion release values (n=3) is used to develop decay models to describe temporal release. DG glass and cement ion release profiles are described in terms of ion concentration (Y) over incubation time (X). Using Prism 6.0 (GraphPad) the time dependent functions have been fitted using a one phase decay exponential model according to:

$$Y = (Y_0 - Plateau) \times e^{-KX} + Plateau, \tag{3.1}$$

where Y is ion concentration in ppm, X is incubation time in days, Y_0 is the ion concentration at $X = 0$, $Plateau$ is ion release concentration at infinite time, and K is the rate constant, expressed in reciprocal time units. For later analysis, τ (tau) is the time constant, computed as the reciprocal of K, $t_{1/2}$ (half-life) is computed as $ln2/K$, or $\tau \times ln2$ and R^2 is the sum of the squares of the distances of the points from the best-fit of the exponential nonlinear regression. A discrete value of dissolution half–life is developed by this model for each ion examined, and goodness of fit is informed by the value of R^2, with a ratio of approximately 0.7 or greater constituting a satisfactory model.

3.3 Experiment 3: Evaluation of *In Vitro* Cytocompatibility for DG Glasses and DG Cements

The following procedures describe extract cell viability testing using the MTT assay method for NIH 3T3 mouse fibroblast cells. A subsequent testing procedure for human osteosarcoma cells was performed in a biosafety level 2 laboratory. An MG–63 osteosarcoma cell line (ATCC®:CRL-1427™) was used and required Eagle's essential

medium (ATCC-formulated, cat.# 30-2003) augmented with 10 % heat-inactivated fetal bovine serum (ATCC).

3.3.1 Cell Culture Preparation

NIH 3T3 mouse fibroblast cells were cultured in 75 cm^2 polystyrene cell culture flasks with 0.2 μm vented caps (BD FalconTM, Bedford, MA) in Dulbeccos Modified Eagles Medium (Sigma-Aldrich USA) augmented 5 % by volume with heat inactivated, sterile-filtered New Calf Serum (Sigma-Aldrich, St. Louis, MO, 011M8411). Cells were incubated at 37 °C in a 10 % CO_2 incubator (Sanyo Scientific, North America). At confluency, the media was discarded and 1.5 mL of 0.25 % trypsin EDTA solution (Sigma-Aldrich, USA, lot # 1196474) were added to the cell culture flask then left for 5 to 10 minutes to detach the cells. 8.5 mL of DMEM-5%NCS was added to the trypsin-EDTA-cell solution. 1 mL of this solution was transferred into sterile culture flasks; 19 mL of fresh media was added to each and the diluted cells were incubated at 37 °C for growth and later use. A sample of the remaining cell solution was analyzed for cell density using a Bright-line Hemocytometer (Hauser Scientific, Horsham, PA). A portion of the cell solution was diluted with DMEM-5 %NCS solution for a resultant 1x10^4 cells per mL solution in preparation for immediate use.

3.3.2 MTT Cell Viability Assay: Mouse Fibroblast Cells

NIH 3T3 mouse fibroblast cells were seeded at a density of 1×10^4 cells per mL and volume of 200 μL into 96 well plates. Cell laden culture media was used as a negative control, occupying one row of wells in each culture plate (n=12). Cell culture media in the absence of cells provided a blank control in one column of an additional 96 well plate (n=8). Seeded and blank plates were incubated at 37 °C for 24 hours. Following incubation, 20 μL of sterile tissue culture water were added to each control well, blank and negative alike, while 20 μL of sample extract were added to wells for cell viability testing. Each extract type was tested three times (n=3 extracts per condition) with a cell viability analysis of n=7 for each individual extract. The plates were incubated again for 24 hours at 37 °C. 15 mL of 5 mg/mL 3-(4, 5-dimethylthiazol-2-yl)-2,5-diphenyltetrazolium bromide (MTT) were prepared in pH 7.4, 0.01 M phosphate buffer solution (Sigma-Aldrich USA, lot # 028K8214) shielded with an aluminum foil covering, and stored at 4 °C. Following

the second 24 hour incubation of the plates, 22 μL of this MTT solution (an amount equivalent to 10% by volume of the well content) were added to each well. Samples were incubated for another 3 hours at 37 °C. Liquid contents of the plates were then blotted onto towels, and 100 μL of dimethyl sulfoxide (DMSO, Sigma-Aldrich USA, lot # 14196PMV) was added to each well of cells. Plates were shielded with aluminum foil and stirred on a rotating plate. Spectrophotometric optical density (absorption) values were read using a Bio-Tek® Synergy HT plate reader equipped with KCF™ Kineticalc for Windows (Version 3.2, Rev. # 2, BioTek Instruments, Inc.) A wavelength correction was performed at 977 and 900 nm; plates were read at 492 nm. Cell viability was calculated according to 3.2 (adapted from ISO 10993-5 [109]) in comparison with the negative control (seeded tissue culture water) which was set at 100 % cell viability:

$$\text{Cell viability } \% = 100\% \times \frac{OD_{492e}}{OD_{492c}} \tag{3.2}$$

where

OD_{492e} is the mean value of the measured optical density of experimental extract wells

OD_{492c} is the mean value of the measured optical density of negative control wells.

3.3.3 MTT Cell Viability Assay: Human Osteosarcoma Cells

An MTT assay was performed as per section 3.3.2 using MG-63 human osteosarcoma fibroblasts. Cells were exposed to two experimental cement extracts (from cDS1 and cDG1) as well as extracts from commerically available SpinePlex® and a tissue culture water control.

3.4 Design of Mixtures (DoM) Approach

3.4.1 Generation and Application of Mathematical Models

The Design of Mixtures approach for the Dal Glass series has been described in the literature [87]. Design Expert 8.0.4 software (Stat–Ease, Inc., USA) was used (employing backwards regression) to produce equations linking half–life of degradation product release and cell viability to compositional variables. (Half–life of degradation is a discrete temporal measure of ion release (n=1) from each glass and cement

composition; the means of cell viability values are used for each glass and cement composition.) Models with high R^2 and R^2adj approximately within 0.2 of each other were considered to show correlative effects. High R^2pred values were considered to show predictive, causative effects. Those models with high R^2 and R^2adj but poor R^2pred were considered to be correlative without the capability to inform conclusions on causative effects. p values (leq 0.05) and and an F–test (used to determine whether the variances of two independent samples are equal) also informed the strengths of the models. The software was then used to generate 2D and 3D response surface contour maps from the fitted regression equations to allow visualization of key composition–property relationships.

3.4.2 DG Cement Optimization

A DoM approach was used in accordance with the literature to identify potentially promising cement candidates [110, 111]. Methods for this section must be discussed when all of the data has been analyzed so that the author is in a position to identify optimized materials characteristics; consequently, the methodology for cement optimization is provided in chapter 6.

Chapter 4

Results and Discussion Part A: Composition–Property Relationships for DG Series Glasses

The objective of this section of the work was to synthesize 12 glasses and verify that they were amorphous so that the results obtained for the biological evaluation of these materials could be correlated with those published in the peer–reviewed literature.

4.1 DG Glasses: X-Ray Diffraction

X-ray diffraction results for silicate, germanate and mixed glasses are depicted in figures 4.1, 4.2 and 4.3, respectively. X-ray diffraction patterns exhibit amorphous characteristics distributed over a wide 2θ range, indicating the amorphous structure of all twelve glasses, and thereby satisfy the initial step of the first objective.

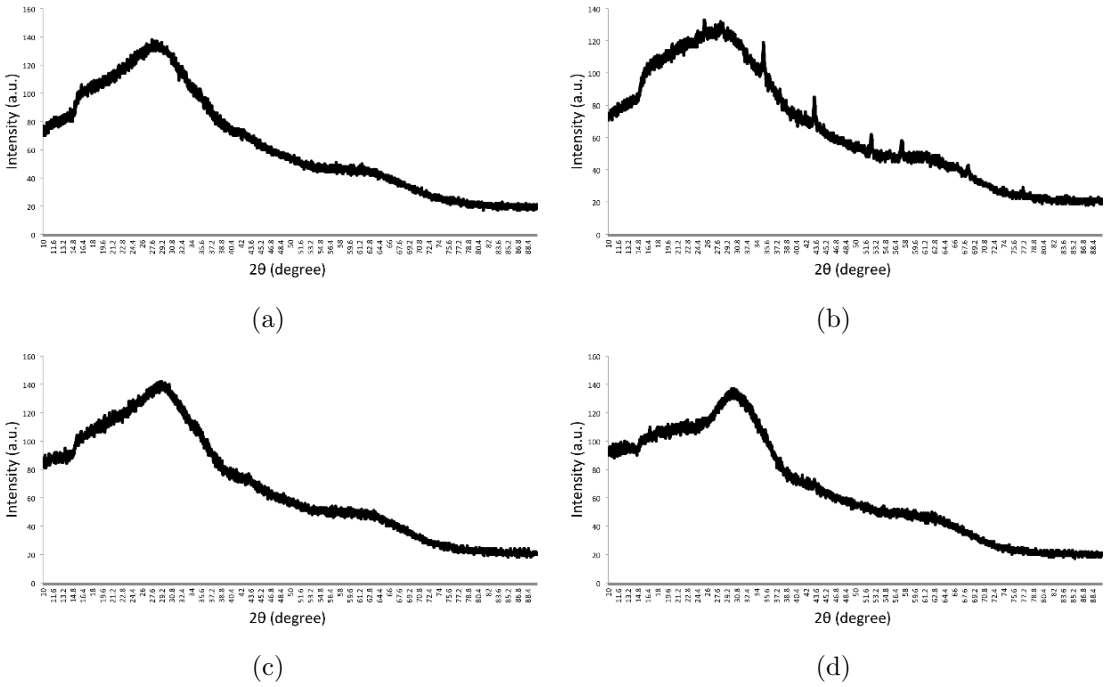

Figure 4.1: X-Ray diffraction plots for DG silicate glasses: (a) gDS1, (b) gDS2, (c) gDS3 and (d) gDS4

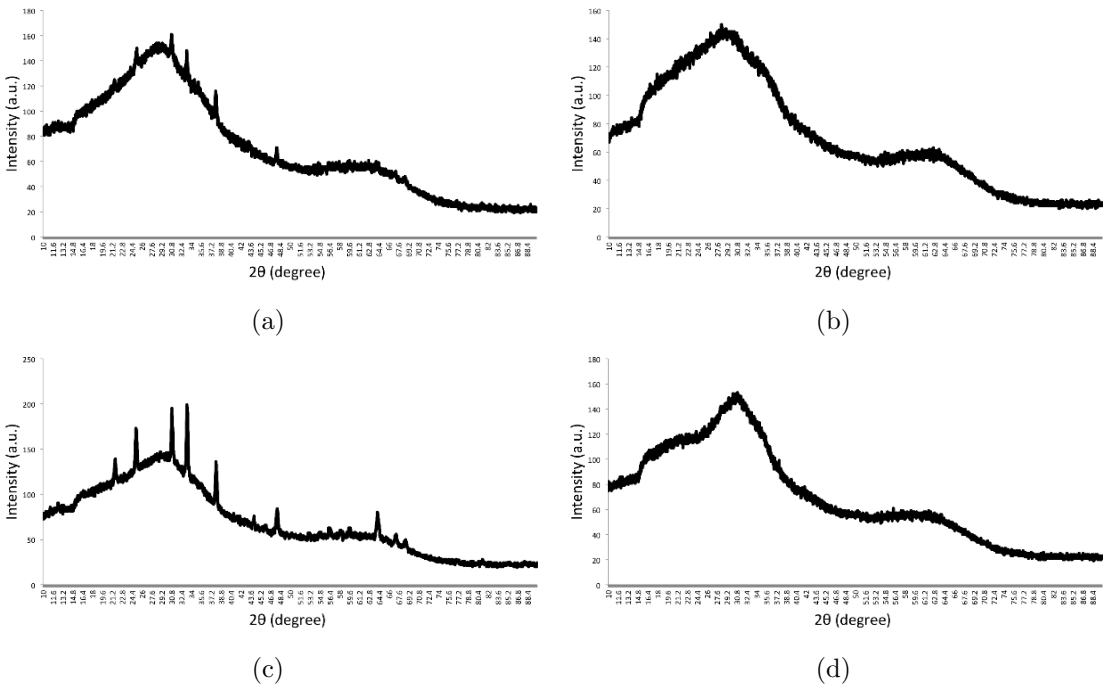

Figure 4.2: X-Ray diffraction plots for DG germanate glasses: (a) gDG1, (b) gDG2, (c) gDG3 and (d) gDG4

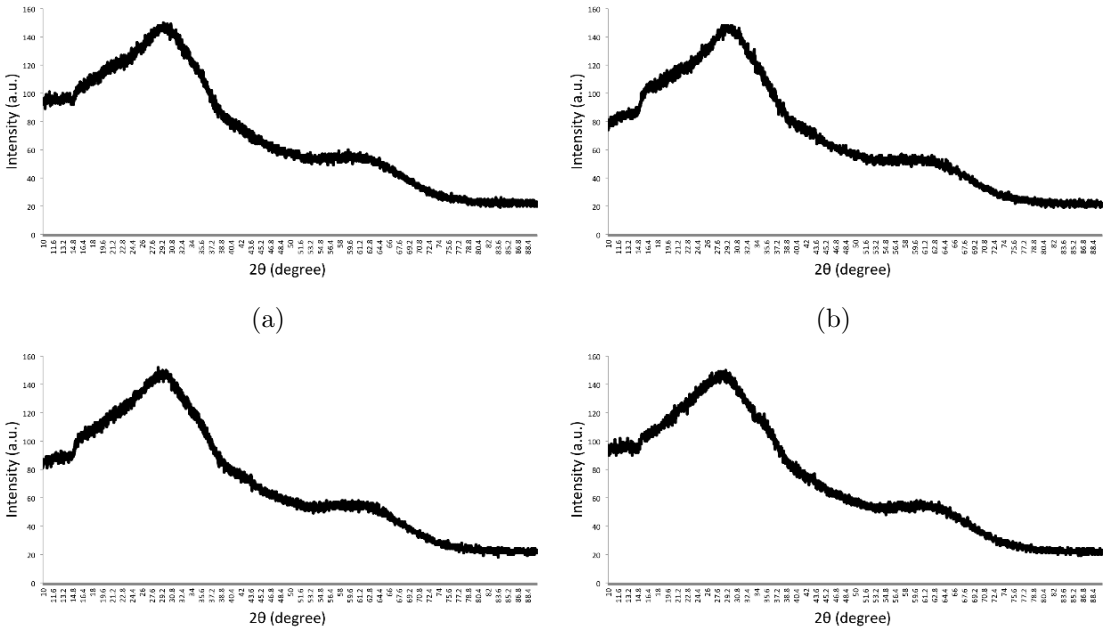

Figure 4.3: X-Ray diffraction plots for DG mixed glasses: (a) gDM1, (b) gDM2, (c) gDM3 and (d) gDM4

Glasses gDS2, gDG1 and gDG3 show artifacts of high intensity, narrower peaks indicative of residual crystallinity. The crystalline phase in both gDG1 and gDG3 was matched to zinc germanium oxide (Zn_2GeO_4), shown in figure 4.4. Peaks in gDS2 could not be identified, likely due to the low level of crystalline impurity versus the base amorphous powder. It is prudent to bear in mind these crystalline inconsistencies throughout the analysis, however results demonstrate that all glasses are principally amorphous as they have been characterized in the literature [87].

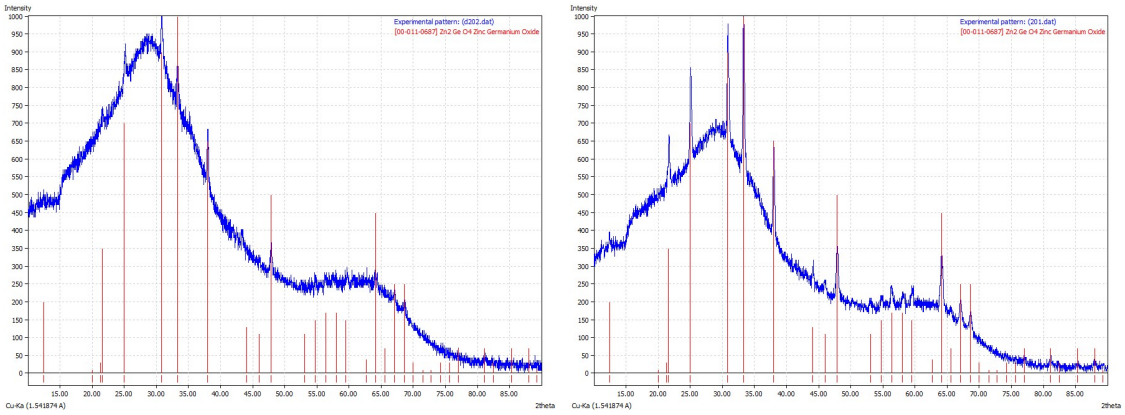

(a) (b)

Figure 4.4: Crystalline phase identification (Zn_2GeO_4) for (a) gDG1 and (b) gDG3

4.2 DG Glasses: Thermogravimetric Analysis (TGA)

Continuing from the first objective, it was hypothesized that T_g values would be lower for germanium–based glasses. Ge^{4+} is a lower field strength cation than Si^{4+}, implying longer Ge–O (germanium–oxygen) bond length and lower rotational barrier in the oxide form. Indeed, results demonstrate that the germanate glass with the highest glass transition temperature (gDG1: 881 K) has a T_g value more than 30 degrees lower than that of the silicate glass with the lowest T_g (gDS4: 917 K) (table 4.1).

Table 4.1: Glass transition temperatures (T_g) for silicate, germanate and mixed glasses

Comp.	Glass Transition Temperature		Literature value
	(deg C)	(K)	(K)
gDS1	677	950	950
gDS2	649	922	930
gDS3	648	921	918
gDS4	644	917	913
gDG1	608	881	878
gDG2	586	859	855
gDG3	591	864	866
gDG4	597	870	874
gDM1	611	884	886
gDM2	621	894	897
gDM3	616	889	885
gDM4	624	897	895

All mixed glasses (gDM series) showed intermediate glass transition temperatures between those of the germanate and silicate glass series. The silicate series demonstrates that substitution of equimolar zirconium and sodium for calcium with maintenance of silicon at 48 % (gDS1 $\rightarrow$ gDS2) results in a T_g reduction of 28 degrees. The same changes in the germante series (gDG1 $\rightarrow$ gDG2) have a similar effect, resulting in a 21 degree drop in T_g. The silicate glass with the lowest glass former content (gDS4) had the lowest T_g in its series (917 K) while the corresponding germanate glass with the lowest glass former content had an intermediate T_g for its series (870 K).

Furthermore, with respect to the glass intermediate and modifier variable, it was hypothesized that the exchange of equimolar ZrO_2/Na_2O for CaO in the glass network would not significantly impact glass transition temperature. For the germanate glasses, a comparison of gDG1 and gDG2 (for which the only compositional difference is ZrO_2/Na_2O replacement of 0.10 molar fraction of the total glass for CaO) reveals a 22 degree drop in T_g from 881 K to 859 K (table 4.1). Likewise, for the silicate glasses, a similar comparison of gDS1 and gDS2 shows a 28 degree drop in T_g from 950 K to 922 K. These data therefore falsify the glass intermediate/modifier component

of hypothesis. Together, ZrO_2 and Na_2O produce a less thermally stable network, suggesting that divalent calcium is more stably connected within the glass network than zirconium and monovalent sodium.

4.2.1 Composition & Glass Transition Temperature (T_g)

Stronger cation–anion bonds require greater structural rearrangement for crystallization to occur; theoretically, therefore, compositions with stronger oxide bonds should undergo more fascile amorphization than their counterparts with weaker oxide bonds. It is useful to consider effective theoretical bond strengths of the DG series glasses to draw out composition–thermal property relationships. To correlate bond strength with glass–formation aptitude, K Sun put forth the energy criterion: $E_{\text{Sun}} = \frac{E_d}{I}$ (kJmol^{-1}), where E_d and I represent oxide dissociation energy and coordination number, respectively. The computed weighted E_{Sun} for each DG glass composition using the E_d and I values of each oxide component are listed in table 4.2. Note two key limitations of this approximation: 1) the assumption that glass cation coordination numbers can be approximated as those of their most common crystalline counterparts; and 2) the assumption that the bond strength of a sample cation–anion bond in component bond strengths in a given glass can be approximated as a weighted sum of component bond strengths.

Table 4.2: Oxide properties of DG glass ingredients

Oxide	I	E_d (kJmole^{-1})	T_m (K)	C_p (kJmole^{-1}K^{-1})	Group
ZnO	4	601.92	2248	61.723	Intermediate oxide
SrO	8	1070.08	2733	67.333	Modifier oxide
SiO_2	4	1772.32	1999	69.844	Glassformer oxide
GeO_2	4	1801.58	1389	82.615	Glassformer oxide
ZrO_2	6	2027.3	2983	99.063	Intermediate oxide
Na_2O	6	502	1405	117.398	Modifier oxide
CaO	8	1074.26	2888	62.50	Modifier oxide

Using the composition silicate and germanate former parsing delineated earlier in table 2.2 (chapter 2), T_g was plotted against weighted cation–anion bond strength

for each silicate and germanate composition and yielded the plots in figure 4.5. Figure 4.6 displays the series together for comparison purposes.

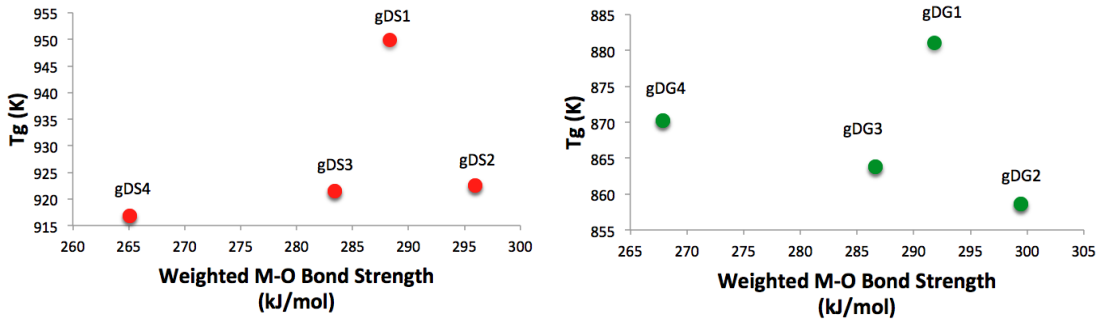

(a) (b)

Figure 4.5: Glass transition temperature versus weighted average bond strength for (a) silicate glasses and (b) germanate glasses

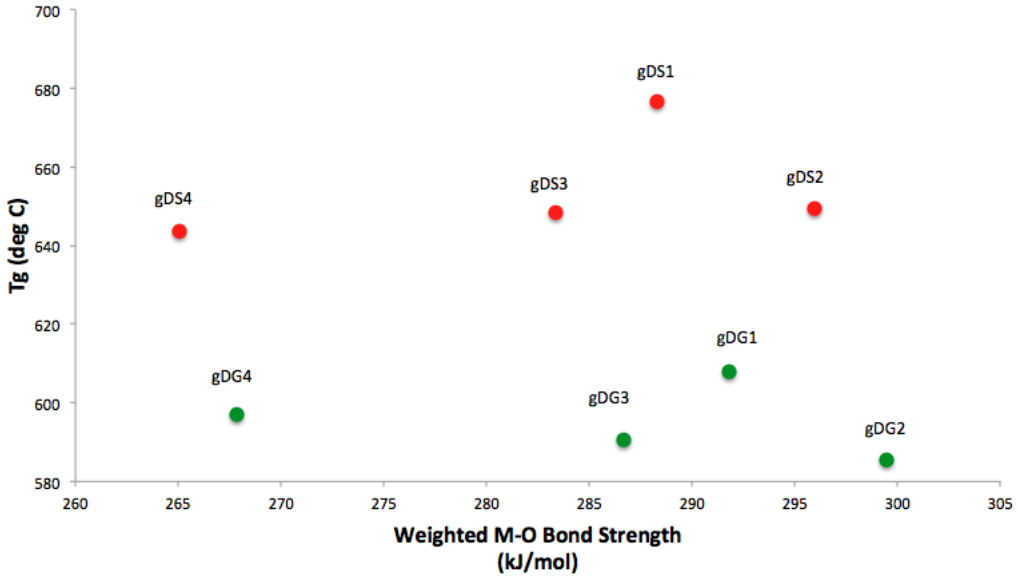

Figure 4.6: Glass transition temperature versus weighted average bond strength

The hypothesis that germanium–containing glasses have lower T_g values than their silicon–containing counterparts has been confirmed, and so the above plots (figures 4.5 and 4.6) add a layer of insight to trends within each of the glass former series. Despite key limitations, the T_g values observed do satisfy instrumental resolution levels (approximately 1 K); furthermore, data collected previously in the literature also mirror the trend observed here (table 4.1, column 4). The glass transition

temperatures of pure SiO_2 and GeO_2 are 1475 K and 980 K, respectively [112]. All complex empirical glasses (containing up to 7 different components), however, have T_g values that hover within the 850 K to 950 K range. The silicate glasses would therefore have a greater tendency to climb to higher T_g values at greater silicon loadings than the germanate glasses, for which the T_g is already closer to the pure germanate value. Theoretically this may contribute to the upward T_g trend observed for the silicate series. Conversely, the germanate series may be more susceptible to intermediate and modifier effects. The author suggests that increased germanate loading theoretically may be more strongly countered by increased network modifier destabilization to yield the downward T_g trend observed (figure 4.6) [112].

Efforts have been made in the literature to correlate the glass transition temperature of bioactive glasses with their molecular composition through predictive modeling [113]. These empirical data provide a set of information that may eventually be used to correlate the T_g of germanium–containing glass biomaterials with composition (and therefore to other clinically relevant properties) in order to model appropriate germanium loadings in bioactive implant materials.

4.3 DG Glasses: Degradation Products

The primary objective of this section was to evaluate the ion release characteristics of the DG glasses prior to them being formulated as cements, and to understand the release kinetics as a function of material composition. (The author finds it important to develop baseline composition–property relationships for the DG glass material precursors to the DG cements so that a full complement of data may augment the current literature.) Furthermore, virtually 80 % of the glass component remains unreacted within the polysalt matrix of a glass polyalkenoate cement [59]. It is important, therefore, to understand ion release from the glass component in isolation. Using a melt–quench technique and an ISO 10993–14 protocol, the modulation of release kinetics was examined for 7 constituent ions: glass former ions: Si^{4+} and Ge^{4+}; glass modifier ions: Na^{+}, Ca^{2+} and Sr^{2+}; and glass intermediate ions: Zn^{2+} and Zr^{4+}. Due to the large number of oxides comprising the glass networks, this section parses results and discussion by ion type (glass former ions, modifier ions and intermediate ions).

With respect to the glass former substitution, it was hypothesized that germanium would be able to modulate temporal release profiles of the glass modifiers and intermediates to the effect that greater amounts of constituents would be released from germanate compositions than from silicate compositions. Concerning glass intermediate and modifier substitutions, it was hypothesized that replacement of calcium with sodium and zirconium would not significantly impact ion release due to the low total mole fraction of modifiers within the network.

Only four ions were released from the glasses in quantities greater than 10 ppm: Si^{4+} (maximum 12 ppm), Ge^{4+} (maximum 370 ppm), Na^{+} (maximum 110 ppm) and Sr^{2+} (maximum 20 ppm) [1]. Elaborated data for the other three ions are included in appendix C (figures C.1, C.2 and C.3) for completeness: Ca^{2+} (maximum 7 ppm), Zn^{2+} (maximum 1.1 ppm) and Zr^{4+} (amounts not detectable).

4.3.1 Release and $t_{1/2}$ of Glass Formers from DG Glasses (Si^{4+} and Ge^{4+})

The Si^{4+} ion release levels for each silicon containing glass composition (after incubation at 1, 7 and 30 days) are shown in figure 4.7.

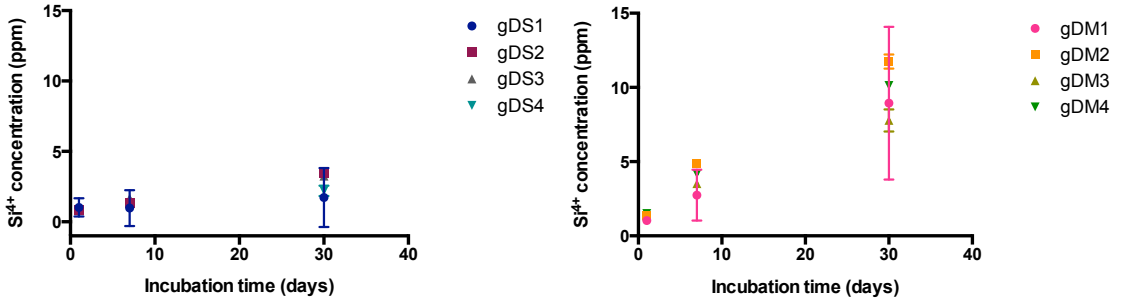

(a) (b)

Figure 4.7: The Si^{4+} ion release levels of 8 DG glasses with time dependency: (a) silicate glasses and (b) mixed glasses over 1, 7 and 30 day incubation periods.

Silicate only glasses (gDS1, 2, 3 and 4) demonstrated Si^{4+} release levels ranging from 0.6ppm (±0.1ppm) at 1 day to 3.5 ppm (±0.1ppm) at 30 days. This highest release value was recorded for gDS2, a glass with equivalent silicon content to the original (gDS1: 48 % SiO_2) yet reduced calcium content and increased sodium

[1] A table listing all DG glass degradation byproduct maxima is listed in appendix A: Degradation Product Maxima

and zirconium content. All glasses containing sodium and zirconium (gDS2, gDS3 and gDS4) show tighter standard deviations for Si^{4+} ion release than their original counterpart (gDS1), which was never augmented with sodium and zirconium. Glass gDS1 also exhibited the highest 1 day release, but the lowest 30 day release.

Mixed former glasses (gDM1, 2, 3 and 4), for which the SiO_2/GeO_2 ratio is unity, demonstrated greater Si^{4+} ion release over all time periods (figure 4.7 (b)) than glasses containing only silicate former. Silicon release ranged from 1.0 ppm ($\pm$0.2ppm) at 1 day to 11.7 ppm ($\pm$0.5ppm) at 30 days of incubation time. All mixed former glasses contain sodium and zirconium, and much less SiO_2 than their silicate counterparts containing no germanium. The highest Si^{4+} ion release resulted from gDM2, the only mixed former glass with maintained calcium content, reduced glass former content, and increased sodium and zirconium content. By contrast, the silicate glass with maintained calcium content (gDS4), greatly increased sodium and zirconium content (+10%), and greatly reduced former content (+10%) demonstrated less than one quarter of the Si^{4+} ion release from this highest releasing mixed glass, even despite containing 16.5% (of total glass content) more SiO_2.

Glasses in each stream are statistically similar to each other at all time periods (refer to appendix B) with two exceptions: 1) gDS1 and gDS2 differ significantly from each other at the 30 day timepoint; and 2) gDM2 and gDM3[2] differ from each other also at the 30 day timepoint. Statistical analysis across time periods, however, demonstrates that Si^{4+} ion release increases significantly over time for each composition with very few exceptions (exceptions include Si^{4+} release over all time periods for gDS1, the silicate glass that contains no zirconium and sodium, as well as Si^{4+} release from gDS4 between at the 7 and 30 day extract timepoints).

Degradation half–life data (table 4.3) and concentration data indicate that inclusion of germanium in the glass network increased the duration of silicon ion release. Furthermore, comparison of the $t_{1/2}$ for gDS1 with those for gDS2, gDS3 and gDS4 demonstrates that addition of sodium and zirconium to the glass network slow degradation kinetics.

[2]Both glass former contents (germanium and silicon) and zirconium/sodium content are greater for gDM3 while calcium content is reduced for gDM3 versus gDM2

Table 4.3: Best fit parameters for nonlinear one phase association model formed from Si^{4+} release over 1, 7 and 30 day incubation periods

DG Glass	$t_{1/2}$ (days)	τ (days)	Y_{max} (ppm)	R^2
Nonlinear fit of Si^{4+} *release from DG silicate glasses*				
gDS1	0.4885	0.7047	1.351	0.01532
gDS2	10.44	15.06	4.011	0.8972
gDS3	6.215	8.966	3.344	0.9202
gDS4	6.897	9.950	2.293	0.8022
Nonlinear fit of Si^{4+} *release from DG mix glasses*				
gDM1	22.63	32.65	14.86	0.6317
gDM2	10.66	15.38	13.67	0.9911
gDM3	8.499	12.26	8.486	0.9608
gDM4	10.37	14.96	11.68	0.9832

The Ge^{4+} ion release levels for each germanium containing glass composition (after incubation at 1, 7 and 30 days) are shown in figure 4.8.

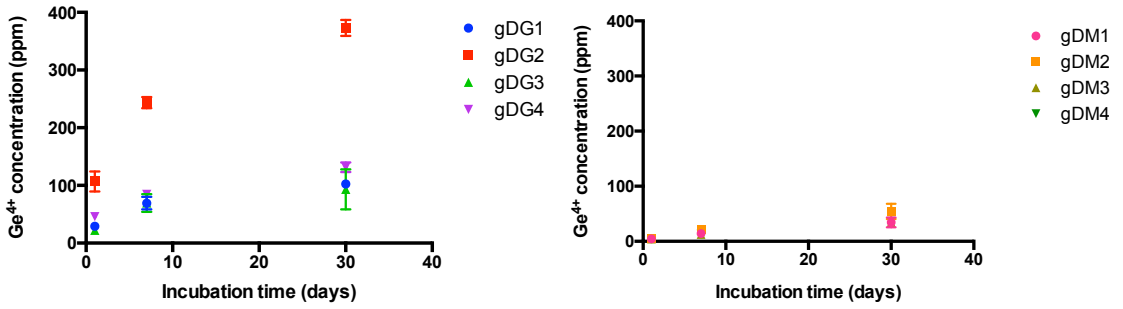

(a) (b)

Figure 4.8: The Ge^{4+} ion release levels of 8 DG glasses with time dependency: (a) germanate glasses and (b) mixed glasses over 1, 7 and 30 day incubation periods.

The greatest germanium ion release was observed for the germanate glass with the highest Ge molar fraction coupled with Zr/Na substitution (gDG2) (4.8). Predictably mixed former glasses demonstrated significant yet lower Ge ion concentration values than germanium former glasses.

Table 4.4: Best fit parameters for nonlinear one phase association model formed from Ge^{4+} release over 1, 7 and 30 day incubation periods

DG Glass	$t_{1/2}$ (days)	τ (days)	Y_{max} (ppm)	R^2
Nonlinear fit of Ge^{4+} *release from DG germanate glasses*				
gDG1	3.620	5.222	100.9	0.9060
gDG2	3.855	5.562	368.0	0.9170
gDG3	3.228	4.656	92.45	0.7235
gDG4	3.544	5.113	127.9	0.7995
Nonlinear fit of Ge^{4+} *release from DG mix glasses*				
gDM1	10.48	15.12	39.84	0.8434
gDM2	11.81	17.04	65.66	0.9031
gDM3	13.52	19.51	43.27	0.9772
gDM4	15.01	21.65	48.81	0.9861

Ion release kinetics can be modeled as degradation profiles produced from discrete empirical measurements of extract ion concentrations at sequential timepoints. Half–life of ion dissolution may be interpolated (or extrapolated) from empirical degradation profiles, and is a quantifiable measure that can be used to relate composition to degradation kinetics so that the effects of DG glass oxide substitutions may be understood.

Degradation half–life data (table 4.4) and concentration data indicate that inclusion of silicon in the glass network increased the duration of germanium ion release. Furthermore, comparison of the $t_{1/2}$ for gDG1 with those for gDS2, gDS3 and gDS4 demonstrates that addition of sodium and zirconium to the glass network has little effect on Ge degradation kinetics, unlike the observation for silicate glasses. This suggests that Ge takes on more adaptable coordination roles within the glass network. Zirconium is found to exhibit octahedral coordination ($[ZrO_6]^{2-}$) within the glass network [114]. Although germanium prefers a native tetrahedral orientation, evidence shows that Ge may access its d orbitals to exhibit six–coordinate octahedral tendency; silicon, a smaller element, has no such capability [115].

Silicon is implicated in increasing bone density and general health; the low levels released from the glass phase are by no means concerning [116]. Greater levels of germanium ions were released, however. Germanium lies adjacent to arsenic in the periodic table; naturally, this is cause for concern and bears investigation. Significant levels of germanium are released from the glass phase (up to greater than 350 ppm). The literature's general unfamiliarilty with germanium incorporation in

biomaterials pushes us to seek other baselines for material safety: one such resource is an LD_{50} measure, or the median lethal dose required to kill half the members of a tested population. GeO_2 has a LD_{50} of 1250 mg/kg delivered orally to mice, while the equivalent value for As_2O_3 is 14.6 mg/kg [117, 118]. According to this metric, germanium has much lower apparent toxicity than anticipated from its position in the periodic table. Levels of germanium release may become concerning if ions migrate and collect systemically, particularly following vertebroplasty of multiple vertebra in the same individual over a short period of time. As such, temporal glass former ion degradation profiles bear investigation (figures 4.9 and 4.10).

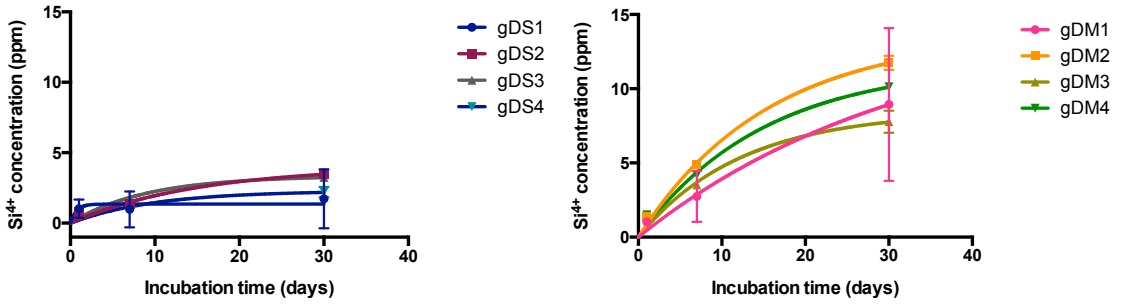

(a) (b)

Figure 4.9: The Si^{4+} ion release profiles of 8 DG glasses with time dependency: (a) silicate glasses and (b) mixed glasses over 1, 7 and 30 day incubation periods.

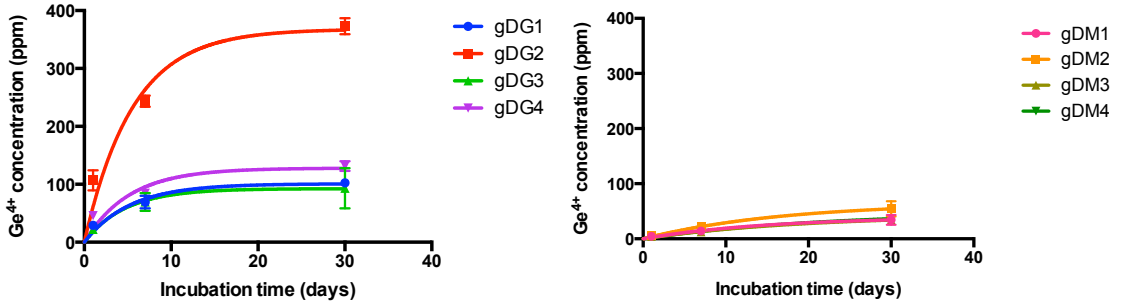

(a) (b)

Figure 4.10: The Ge^{4+} ion release profiles of 8 DG glasses with time dependency: (a) germanate glasses and (b) mixed glasses over 1, 7 and 30 day incubation periods.

In order to more quantitavely correlate composition with degradation behaviour, regression analyses were conducted. The regression models presented in table 4.3.1 are a useful tool to help correlate composition with half–life of silicon and germanium

release. Negative coefficients indicate diminished release, while positive coefficients indicate extended $t_{1/2}$ to the extent indicated by the relative magnitudes of the coefficients. Significant model coefficient terms were determined automatically because a backward regression method was used as described in section 3.4.1 (page 41).

Table 4.5: Regression models in terms of L–pseudo components and summarized ANOVA for glass former ion half–life release

Response	Regression Model	Summarized ANOVA				
		R^2	R^2 adj.	R^2 pred.	p value	F
Si^{4+} release $t_{1/2}$	+3.62*Si – 4.05*Ge +34.93*Zr/Na – 6.15*Ca + 64.81*Si*Ge	0.7409	0.5929	0.2569	0.0318	5
Ge^{4+} release $t_{1/2}$	– 0.020*Si + 4.58*Ge – 0.53*Zr/Na + 0.58*Ca + 73.97 *Si*Ge	0.9912	0.9862	0.9798	<0.0001	198.1

Both models produce significant fits, evidenced by significant p values as well as high and similar R^2 and adjusted R^2 values; however, only the Ge^{4+} model has predictive capabilities, as evidenced by a high predicted R^2 value. Germanium dissolution conforms to a robust, highly theoretically predictive degradation model with an adequate precision value of 34[3], while the model for silicon dissolution fails to reach a satisfactory value of predictive capability and possesses a lower adequate precision value of 6. The author is uncertain what causes the varying precision levels and degradation plateaus for the two glass formers considering germanium is considered to be isomorphic with silicon in the glass network [87]. It is possible that the one–phase decay germanium model owes its greater robustness to a more straightforward dissolution mechanism. Silicon–containing bioglasses are known to establish a siliceous layer instigated by the breaking of Si–O–Si bonds and the collection of Si–OH functionals at the surface of a glass bulk [119]. It is possible for silicon moeities to leave the bulk material then redeposit at the surface of the bulk.

[3]values of adequate precision appear here only in the text and not within the tables summarizing regression modeling

Although extract testing was performed temporally, it provides only an approximation of empirical kinetics extrapolated from three discrete timepoints. The involvement of a siliceous layer complicates dissolution kinetics and may also contribute to the near zero–sum release quantities observed (far less Si^{4+} is released than Ge^{4+}). It has not been established whether or not germanium moieties form a similar gel layer at implant surfaces, a fact owing to the lack of germanium investigation in the bioglass literature. The more robust germanium model suggests that Ge^{4+} dissolution is less complex kinetically than Si^{4+} dissolution; germanium likely leaches from the glass bulk with less net re–interaction at the bulk surface than is observed for silicon until a concentration gradient forces equilibrium and results in a release plateau.

Regardless of degradation mechanism, regression modeling clearly exposes the most influential factors on Si^{4+} and Ge^{4+} release (table 4.3.1). Both Si^{4+} and Ge^{4+} $t_{1/2}$ increase most notably with increased silicon and germanium (together) in the glass network. Increased Zr/Na has the second greatest impact on Si^{4+} $t_{1/2}$, yet a slightly negative impact on Ge^{4+} $t_{1/2}$. Other factors produce minimal coefficients (table 4.3.1). These influences are represented visually on the contour plots presented in figures 4.11, 4.12, 4.13 and 4.14. The plots in all four figures are confined to within the design space where (A) SiO_2 0–0.48 mole fraction, (B) GeO_2 0–0.48 mole fraction, (C) ZrO_2/Na_2O 0–0.10 mole fraction, and CaO is fixed at 0.12 mole fraction.

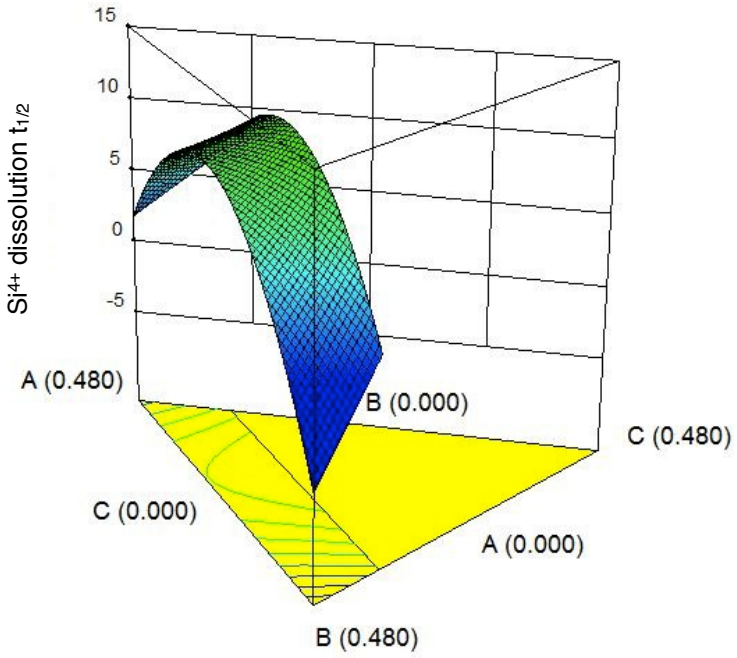

Figure 4.11: 3D contour plot showing the effect of varying glass composition within the confines of the design space and the resultant half–life of Si^{4+} dissolution.

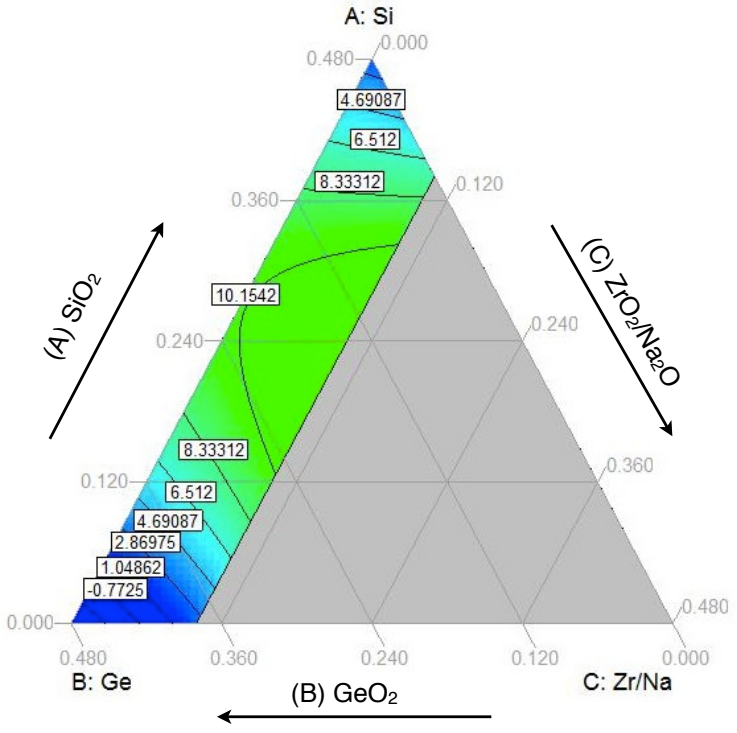

Figure 4.12: 2D contour plots showing the effect of varying glass composition within the confines of the design space and the resultant half–life of Si^{4+} dissolution.

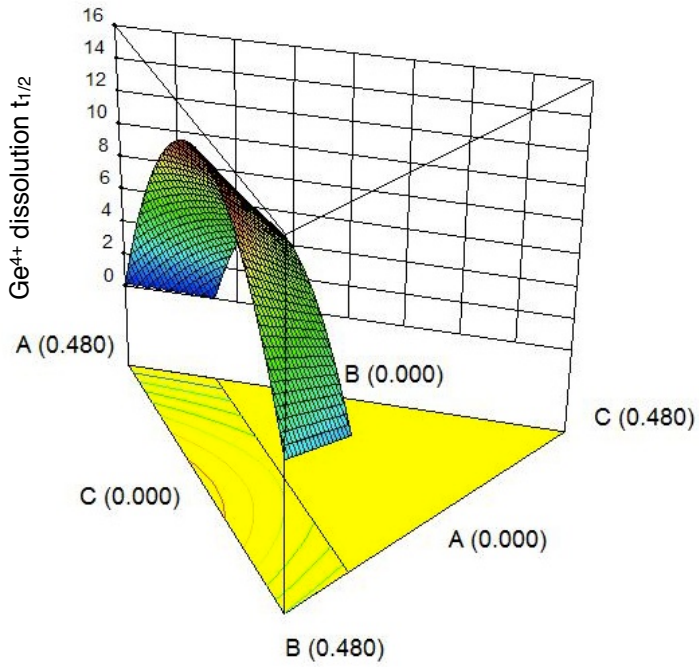

Figure 4.13: 3D contour plot showing the effect of varying glass composition within the confines of the design space and the resultant half–life of Ge^{4+} dissolution.

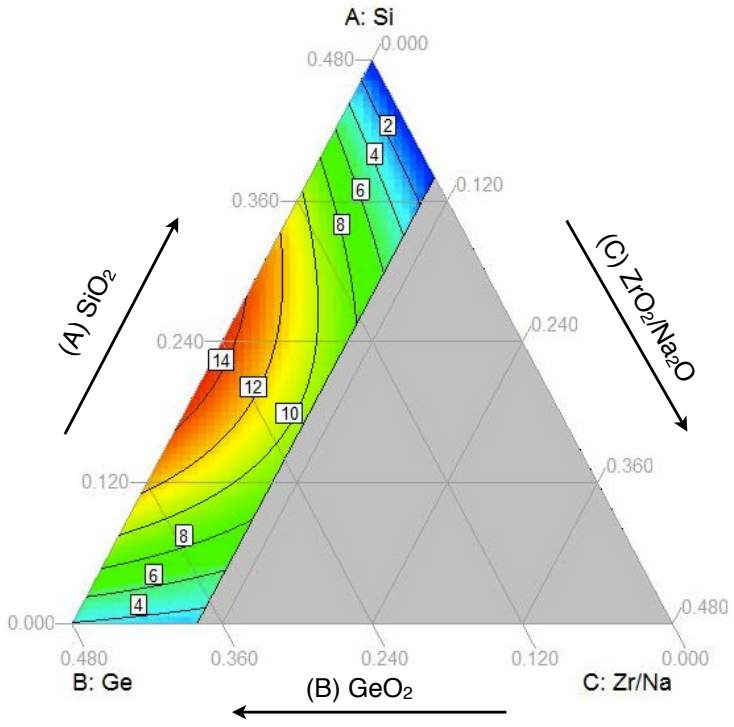

Figure 4.14: 2D contour plot showing the effect of varying glass composition within the confines of the design space and the resultant half–life of Ge^{4+} dissolution.

4.3.2 Release and $t_{1/2}$ of Glass Modifiers from DG Glasses (Na^+, Ca^{2+}, and Sr^{2+})

Statistical analyses between compositions and over time for remaining glass ions are included in appendix B due to spatial constraints. Virtually no calcium was detected in the glass extracts, and so this section details sodium and strontium release.

The Na^+ ion release levels for each sodium containing glass composition (after incubation at 1, 7 and 30 days) are shown in figure 4.15.

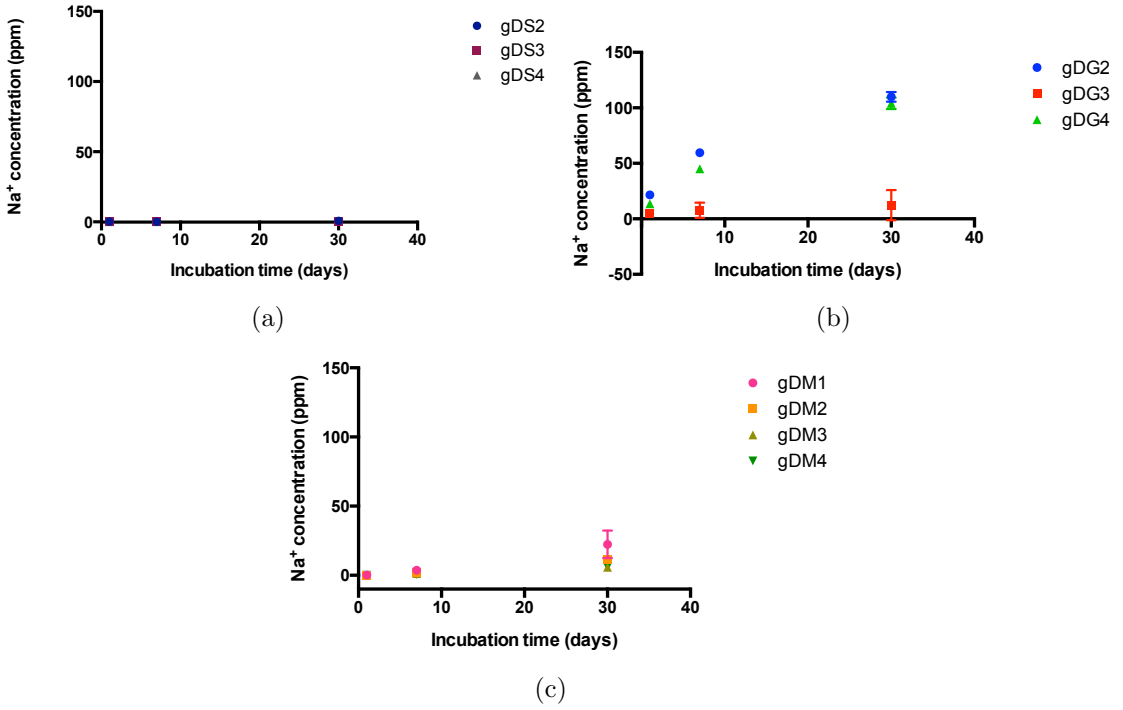

Figure 4.15: The Na^+ ion release levels of DG glasses with time dependency: (a) silicate glasses, (b) germanate glasses, and (c) mixed former glasses over 1, 7 and 30 day incubation periods.

Degradation half–life data (table 4.6) and concentration data (figure 4.15) together indicate that sodium leaches out of silicate glasses indefinitely with a very long half–life of degradation and low elution rate; none of the silicate compositions reached an emipirical plateau for sodium release. These results are limited by the timeframe examined (up to 30 days).

Quantified half–life of ion dissolution may be garnered from empirical degradation profiles to relate composition to degradation kinetics, which can be isolated to understand the effects of DG glass oxide substitutions on ion release. Sodium

degradation was modeled using an exponential one phase decay to produce the $t_{1/2}$ values listed in table 4.6.

Table 4.6: Best fit parameters for nonlinear one phase association model formed from Na^+ release over 1, 7 and 30 day incubation periods

DG Glass	$t_{1/2}$ (days)	τ (days)	Y_{max} (ppm)	R^2
Nonlinear fit of Na^+ *release from DG silicate glasses*				
gDS2	59.84	86.33	2.402	0.6325
gDS3	51881	74849	626.5	0.9034
gDS4	16970	24482	314.2	0.7939
Nonlinear fit of Na^+ *release from DG germinate glasses*				
gDG2	6.044	8.720	113.0	0.9686
gDG3	3.489	5.033	11.89	0.1192
gDG4	9.646	13.92	117.5	0.9877
Nonlinear fit of Na^+ *release from DG mix glasses*				
gDM1	11062	15959	11717	0.8039
gDM2	141784	204551	77646	0.9877
gDM3	61945	89367	17301	0.9849
gDM4	41415	59749	11513	0.9520

Considering the low levels of sodium addition to the glass, data show that significant amounts of Na^+ are released empirically from the germanate glass networks: germanate networks released large amounts of sodium (up to 117.5 ppm) with short $t_{1/2}$ of degradation (up to just less than 10 days). Inclusion of both sodium and germanium in the glass networks together, however, increased the duration of germanium ion release indefinitely. Regression models suggest that lower levels of Na^+ release occur from silicate and mixed former glasses theoretically over time periods extending far beyond those tested in this study.

The Sr^{2+} ion release levels for all DG glasses (after incubation at 1, 7 and 30 days) are shown in figure 4.16. Levels of strontium release for silicate glasses were negligable (maximum 2.1 ppm). Statistical errors were significant for germanate compositions, and so $t_{1/2}$ could not be modeled for these ions using a one–phase decay model.

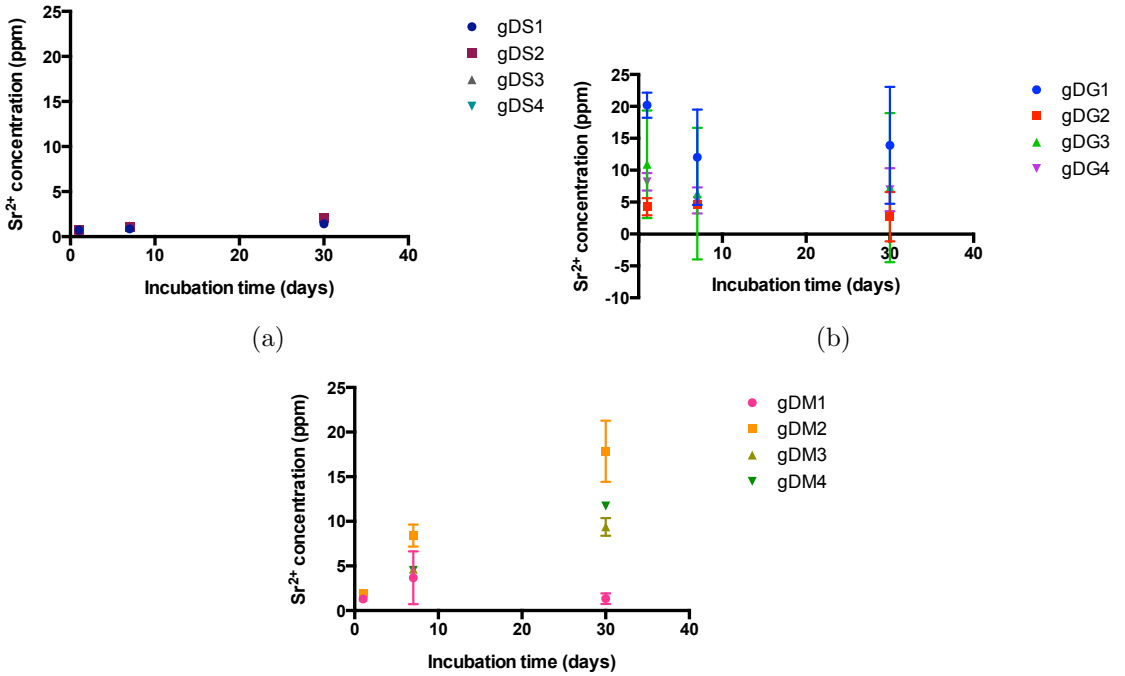

Figure 4.16: The Sr^{2+} ion release levels of DG cements with time dependency: (a) silicate glasses, (b) germanate glasses, and (c) mixed former glasses over 1, 7 and 30 day incubation periods.

Degradation data (table 4.7) and concentration data (figure 4.16) together indicate that mixed former glasses produced one phase exponential decay models for $t_{1/2}$ with good modeling certainly (R^2). Silicate former glasses failed to produce robust models, likely due to extremely low strontium elution rates, and Sr^{2+} degradation kinetics for germanate former glasses could not be modeled.

Table 4.7: Best fit parameters for nonlinear one phase association model formed from Sr^{2+} release over 1, 7 and 30 day incubation periods

DG Glass	$t_{1/2}$ (days)	τ (days)	Y_{max} (ppm)	R^2
Nonlinear fit of Sr^{2+} *release from DG silicate glasses*				
gDS1	0.6889	0.9939	1.147	0.3355
gDS2	5.236	7.554	2.094	0.6787
gDS3	4.363	6.294	2.051	0.7661
gDS4	4.822	6.957	1.702	0.5698
Nonlinear fit of Sr^{2+} *release from DG germinate glasses*				
gDG1, gDG2, gDG3, gDG4	NA (do not converge)			
Nonlinear fit of Sr^{2+} *release from DG mix glasses*				
gDM1	0.8666	1.250	2.491	0.09601
gDM2	8.463	12.21	19.52	0.9337
gDM3	7.366	10.63	9.938	0.9640
gDM4	12.32	17.78	14.36	0.9878

Modeled Na^+ and Sr^{2+} ion release profiles are depicted in figures 4.17 and 4.18, respectively. (The strontium release profile from germanate glasses could not be modeled and so does not appear delineated in figure 4.18.)

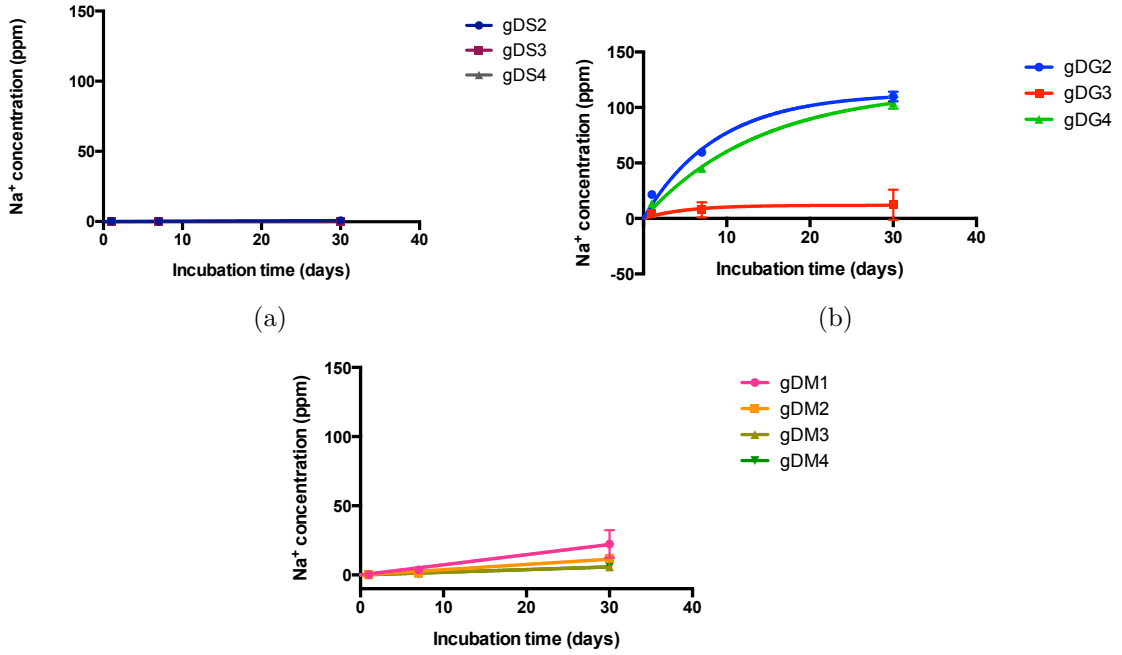

Figure 4.17: The Na^+ ion release profiles of DG glasses with time dependency: (a) silicate glasses and (b) mixed glasses over 1, 7 and 30 day incubation periods.

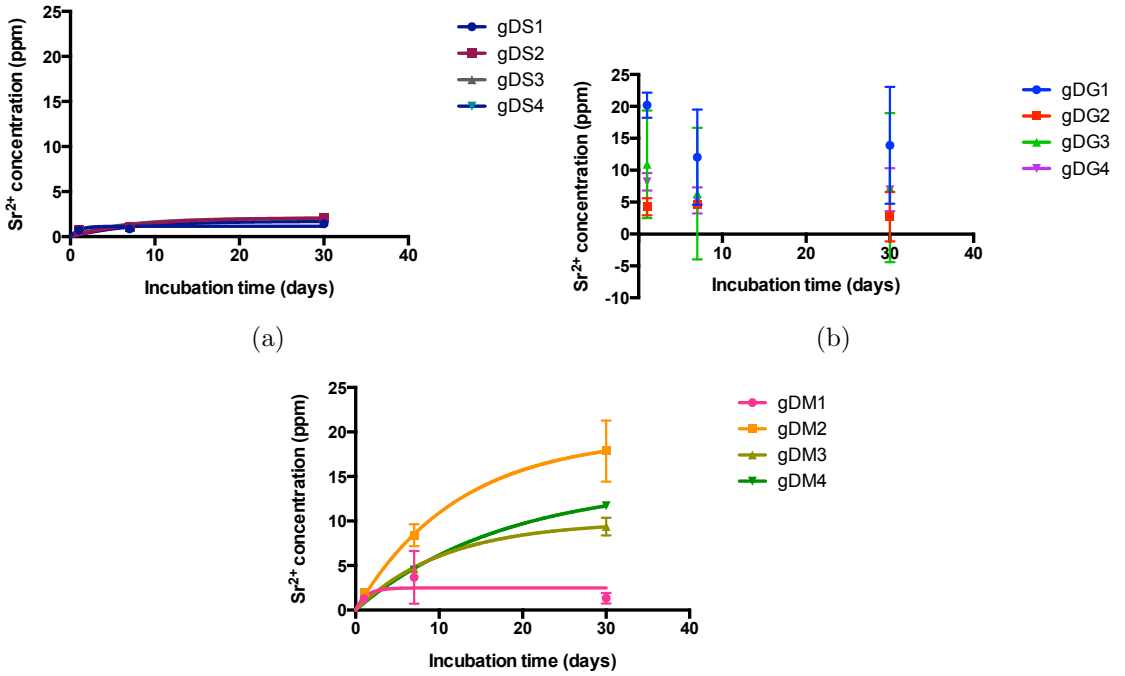

Figure 4.18: The Sr^{2+} ion release profiles of DG glasses with time dependency: (a) silicate glasses and (b) mixed glasses over 1, 7 and 30 day incubation periods.

DoM was used to model half–life of ion release for sodium and strontium (where possible) to determine the effect of compositional factors on their degradation kinetics (table 4.8). Half–life of Ca^{2+} release data have been modeled and displayed along with these to demonstrate that degradation levels also must be considered in the analysis. Although $t_{1/2}$ may be modeled with adequate certainty, the model fails to indicate the negligable ion dissolution levels that preclude calcium from a thorough analysis.

Furthermore, $t_{1/2}$ of strontium release produces a model with an R^2 value of precisely 1, along with very high adjusted and predicted R^2 values, a minute p–value, and an exceedingly high F ratio. These model statistics are unrealistic, and coupled with ion release level data (4.18) preclude this ion also from further $t_{1/2}$ analysis. Strontium is radiopaque and has been implicated in bone regeneration [95]. Although negligible levels of strontium ion release were observed in this study, strontium still constitutes a useful component of the glass network as a radiopacifier.

Sodium $t_{1/2}$ of release from DG glasses produces the only glass modifier model

Table 4.8: Regression models in terms of L–pseudo components and summarized ANOVA for glass modifier ion half–life of release

$t_{1/2}$ Response	Regression Model	Summarized ANOVA				
		R^2	R^2 adj.	R^2 pred.	p	F
Na^+ release	– 3.794E+5*Si – 3.926E+5*Ge – 8.645E+6*Zr/Na +1.853E+6*Ca + 2.183E+5 *Si*Ge +1.266E+7*Si*Zr/Na +1.259E+7*Ge*Zr/Na	0.8893	0.7565	– 0.0916	0.0272	6.7
Ca^{2+} release	+30.95*Si – 43.12*Ge + 0.84*Zr/Na +8.38*Ca – 37.57 *Si2 +71.46*Ge2	0.9784	0.9425	0.6135	0.0105	27.24
Sr^{2+} release	+ 23.13*Si – 176.66*Ge – 80.69*Zr/Na +100.33*Ca + 464.05 *Si*Ge – 250.60*Si*Ca + 490.57*Zr/Na*Ca	1	0.9999	0.9941	0.0065	13762

worth investigating further. The Na^+ model is robust and has realistic R^2 values, however with a negative predicted R^2, it fails to offer even a modicum of predictive certainty. The greatest independent compositional factor on sodium release is calcium content (table 4.8). Tilocca postulates that monovalent sodium cations can be accommodated easily in calcium network sites within the glass bulk due to the smaller ionic radius of sodium, depicted in figure 4.19 [120].

This observation suggests that increased calcium inclusion in the network facilitates rather than hinders the migration of sodium through the temporary replacement of calcium ions with sodium ions [120]. The combination of calcium together with sodium in the glass network should therefore lead to a greater dissolution and concentrations of sodium ions found in glass extracts over time. The $t_{1/2}$ model for sodium release suggests that this is the case.

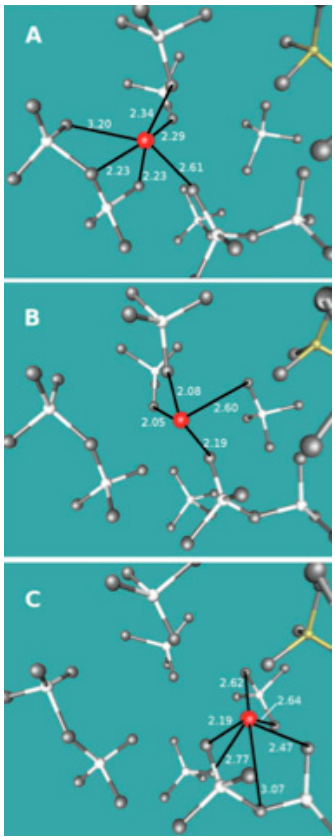

Figure 4.19: Migration of Na^+ in the glass network as facilitated by Ca^{2+}, from [120]. Sodium, silicon, phosphorus and oxygen atoms are colored red, white, yellow and gray, respectively.

Quadratic compositional factors have the greatest impact on sodium release, however (table 4.8). The combination of silicon with Zr/Na and germanium with Zr/Na produce comparable and high magnitudes of Na^+ $t_{1/2}$ of release with the coefficients $+1.266E+7$ and $+1.259E+7$, respectively. Interestingly, however, silicon, germanium and Zr/Na together produce shorter $t_{1/2}$ values of Na^+ release with the coefficients $-3.794E+5$, $-3.926E+5$ and $-8.645E+6$, respectively.

4.3.3 Release and $t_{1/2}$ of Glass Intermediates from DG Glasses (Zn^{2+} and Zr^{4+})

Zirconium level in the glass extracts fell below the instrumental detection limit, and the greatest amount of zinc released was found to be less than 1.5ppm (refer to Appendix A: Degradation Product Maxima). Studies have shown that low levels of Zn^{2+} released in a cell culture medium can induce osteoblast proliferation, and that

cytotoxicity is only observed at high release values (>400 μm) [97]. Levels discovered in this study for DG glass extracts were negligable in this respect, however. The author acknowledges that the absence of these ions within the DG glass extracts does not exempt them from involvement in the degradation kinetics of the glass networks. Some findings related to glass formers and modifier contents in glass extracts (sections 4.3.1 and 4.3.2, respectively) indicate some of the influences of intermediates on ion leaching facilitatation and arrestment.

* * *

The hypothesis that germanium modulates temporal ion release is confirmed when considering all glass degradation data together: it is clear that germanium modulates temporal release profiles for those ions released in non-negligable quantities (Si^{4+}, Ge^{4+}, Na^{+} and Sr^{2+}). The effect is best visualized by comparing release profiles for silicate, germanate, and mixed glasses side by side; degradation levels are consistently higher (and their $t_{1/2}$ values more accurately modeled) for germanate glasses and mixed former glasses than for their silicate glass counterparts.

On the other hand, data contradict the hypothesis pertaining to the effect of glass modifiers and intermediates. Replacement of calcium with sodium and zirconium leads to increased release of all constituent ions from the glass networks and cement matrices, likely the result of destabilization of the glass network through ion migration. It is difficult to elucidate the effect of sodium apart from zirconium (a limitation of this study), however the author notes that zirconium does not leave the glass network in measureable quantities. Both glass formers (silicon and germanium) are found in measureable quantities within the glass extracts. In addition to the octahedral coordination of zirconium ($[ZrO_6]^{2-}$) in glass networks, and evidence suggests that zirconium is capable of slowing degradation rates in low pH environments [121, 114]. The author believes it is likely, therefore, that zirconium interrupts the tetrahedral bonding characteristic of both sodium and germanium to establish new bonding angles in the glass network. The effects of this altered geometry would be twofold at minimum: (1) zirconium itself would be firmly bonded within the network; and (2) native glass formers would be susceptible to disruption of their coordination spheres, leading to less stability in the network and, consequently, greater dissolution levels. The degradation levels and profiles observed in this study corroborate this theory.

4.3.4 Summary of Composition–$t_{1/2}$ Relationships: DG Glasses

The following summarize compositional influences on the $t_{1/2}$ of DG glass ions:

- Germanium (Ge^{4+}) is released in large quantities (up to 370 ppm at 30 days). Increased silicon in concert with germanium (quadratically) has the greatest and only notable impact on extending germanium dissolution kinetics.

- Silicon (Si^{4+}) is released in much more modest quantities (up to 12 ppm at 30 days). Increased silicon in concert with germanium (quadratically) has the greatest impact on extending silicon dissolution kinetics; the independent compositional factor of increased zirconium/sodium content also increases $t_{1/2}$ of silicon dissolution.

- Sodium is released indefinitely from silicate and mixed former glasses, but those networks containing germanium–only formers exhibit high levels of controlled Na^{+} release over empirical time periods. The independent compositional factor with the greatest impact on the increase of sodium release $t_{1/2}$ is increased calcium content; quadratic factors of silicon combined with Zr/Na and germanaium combined with Zr/Na have the greatest overall impact on $t_{1/2}$ of extending sodium release.

- Glass former ion release data were modeled much more readily than modifier and intermediate release using one phase exponential decay, likely due to insignificant levels of ion release for the latter.

The utility of these composition–$t_{1/2}$ relationships lies in manipulation of the glass network to release or withold ions such that clinical handling properties are improved. The most tangible of these is the working time of a cement, which is associated closely with kinetics of ionic migration and dissolution. Although the utility may only truly be applied when the contiguous cements are examined, understanding of composition–property relationships for the glass phase helps guide further polyalkenoate cement development.

4.4 DG Glasses: MTT Cell Viability Assay – Mouse Fibroblast Cells

In order to complete the preliminary biological assessment of the DG glass, cell viability assays were utilized to cross reference material composition with cytotoxic response. The objective of this section of the study was to screen all twelve DG glasses for toxic effects against NIH 3T3 mouse fibroblast cells in comparison with a tissue culture water control to complete the first step in material biocompatibilty assessement.

It was hypothesized that glass extracts would yield significantly lower NIH 3T3 mouse fibroblast cell viability than a tissue culture water control over all time periods due to the greater elution of ions from the glass network.

Results falsify this hypothesis: NIH 3T3 mouse fibroblast cells exposed to 1, 7 and 30 day glass extracts had cell viabilities in the range 92 to 124 % compared to the tissue culture water (TCW) control (figure 4.20).

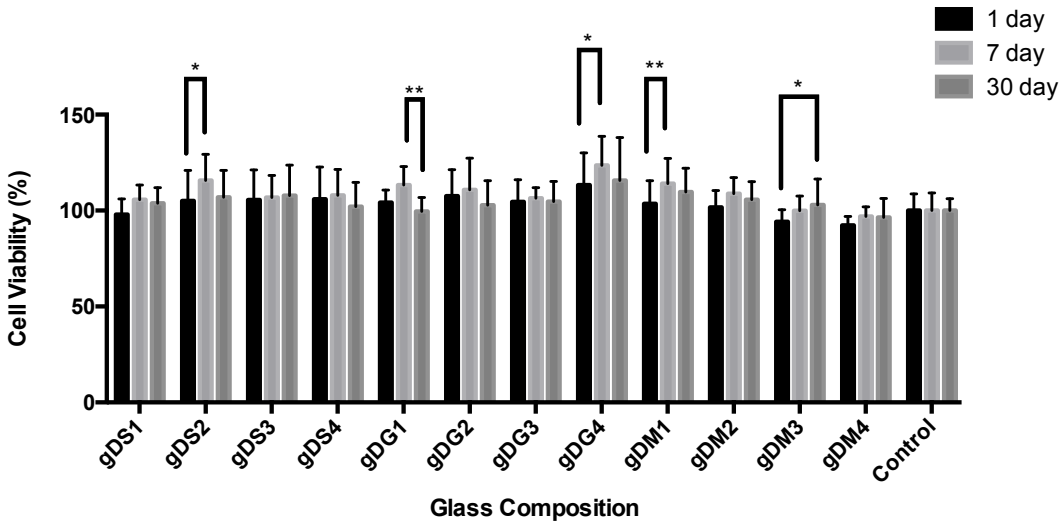

Figure 4.20: Cell viabilities of glass and control extracts over all time periods

Statistical analysis demonstrates little variation for each extract between timepoints (figure 4.20), and no variation between silicate extracts (figure 4.21 a), save for that between gDS2 with TCW at the 7 day extract timepoint. Introduction of germanium to the glass network yields greater variation in cell viability between compositions at each timepoint (figure 4.21 b and c).

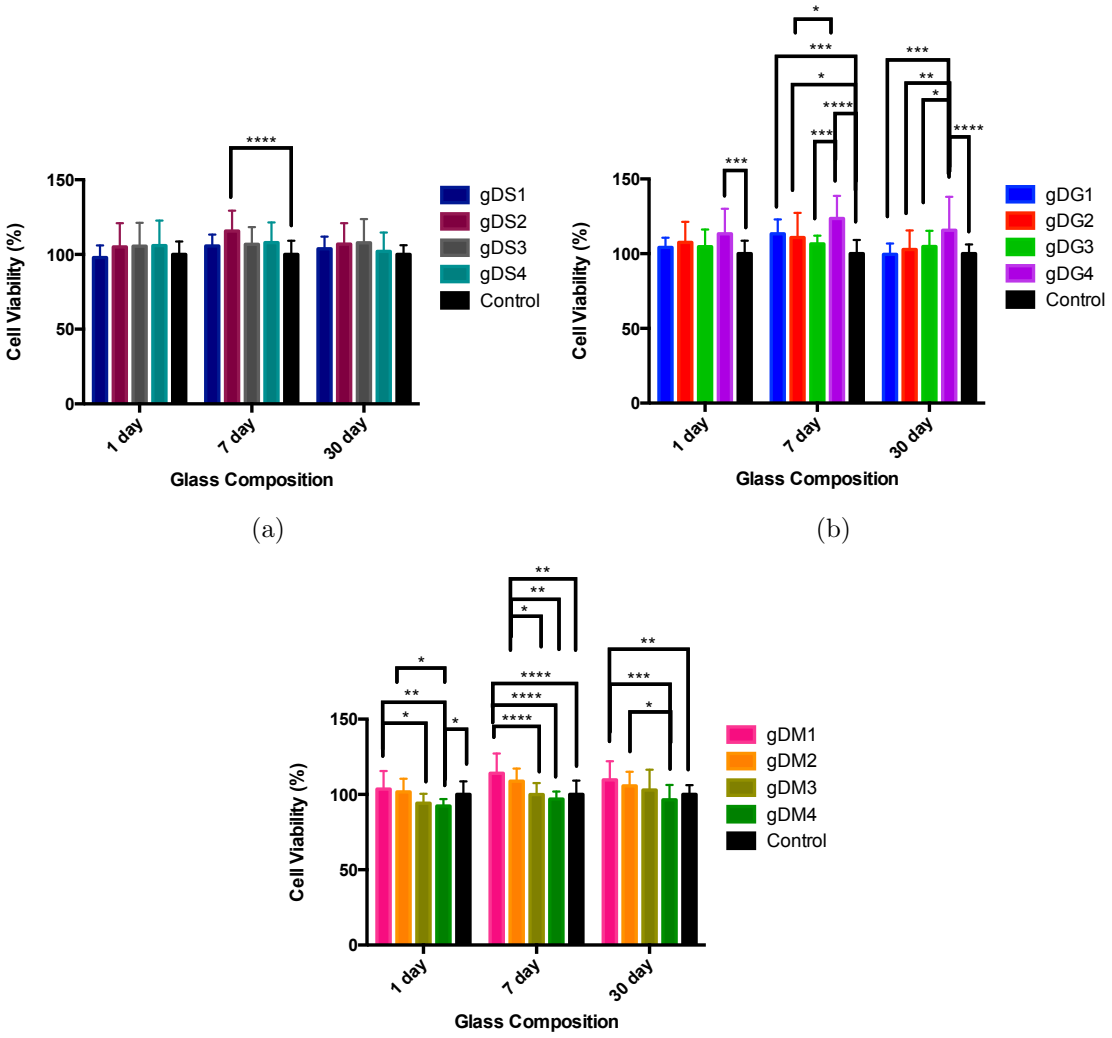

Figure 4.21: Cell viabilities of silicate, germanate and mixed former glass extracts with statistical differences at each timepoint

All cell viability values satisfy the lower limit of the safety window set by international standards (70 %); however, cell viability values exceeding 100 % are of some concern to the author [109]. Increased cell viabilities may be due to malfunctions within the regulation of the cell cycle leading to uncontrolled proliferation. Cells that sense low concentrations of toxic substances sometimes demonstrate increased enzymatic activity at an early exposure stage in an effort to compensate for the hostile conditions of the toxic environment; these cells will not be viable at increased toxic concentrations [122]. As such, the data bear further analysis to determine the relationship between composition and cell viability so that key factors influencing

heightened cell viability may be isolated.

4.4.1 Composition & Cell Viability

A Design of Mixtures (DoM) approach was selected so that analysis of the data aligns with constraints of the original experimental design to allow for more meaningful data interpretation. The author reiterates that ZnO_2 and SrO are maintained at constant mole fraction (0.36 and 0.04, respectively) in all glass networks of this study, and so effects arising due to the variation of the remaining five glass oxides are explored using the design of mixtures approach: SiO_2, GeO_2, ZrO_2 and Na_2O (together, equimolarly), and CaO.

1, 7 and 30 day glass extract cell viability results were modeled quadratically. As listed in table 4.9, R^2 and adjusted R^2 values are reasonably high and within range of each other for all three models with suitable values of adequate precision (8.957, 8.084 and 8.618, respectively). Although these models accomodate the empirical data well, their predictive capabilities are poor and suffer increasingly at greater extract timepoints.

Table 4.9: Regression models in terms of L–pseudo components and summarized ANOVA for cell viability of NIH 3T3 fibroblasts exposed to glass extracts

Response	Regression Model	Summarized ANOVA				
		R^2	R^2 adj.	R^2 pred.	p	F
1 day CV	+93.84*Si +98.55*Ge +153.15*Zr/Na +122.22*Ca – 53.44*Si*Ge	0.8249	0.7248	0.5757	0.0087	8.24
7 day CV	+ 47.52*Si + 39.65*Ge + 447.45*Zr/Na + 372.92*Ca + 116.04*Ge*Ca – 2081.81*Zr/Na*Ca	0.8257	0.6805	0.0477	0.0282	5.69
30 day CV	+ 86.14*Si +53.60*Ge + 215.51*Zr/Na + 194.55*Ca + 149.60*Ge*Zr/Na + 150.41*Ge*Ca – 787.68*Zr/Na*Ca	0.8644	0.7016	– 1.0263	0.0436	5.31

At the 1 day extract timepoint, regression model coefficients demonstrate that all glass compositional factors have a positive effect on cell viability %, save for the deleterious effect incurred when combining SiO_2 and GeO_2 together in the glass network (table 4.9). Individually, both SiO_2 and GeO_2 have the same effect on increasing cell viability. Cell viability is impacted most strongly by the inclusion of modifiers and intermediates: equimolar ZrO_2 and Na_2O inclusion has the greatest effect, followed closely by CaO inclusion. At the 7 day extract timepoint, the positive effects of independent SiO_2 and GeO_2 inclusion on cell viability remain on par with each other, but less important than other compositional factors. The combination of ZrO_2, Na_2O and CaO emerges as the greatest compositional factor, and has a strongly negative impact on cell viability. At the 30 day extract timepoint, the combination of ZrO_2, Na_2O and CaO together maintain a strongly negative impact on cell viability while all other compositional factors work to increase cell viability. Interestingly, when considered independently, all compositional factors have a positive effect on cell viabililty over all time periods.

2D and 3D contour plots depict these effects visually. Due to the large number of constituent glass oxides and variation in compositional levels, two sets of plots are depicted: in the first set (figures 4.22 and 4.23) calcium oxide (CaO) content is held at a fixed molar fraction of 0.12; in the second set (figures 4.24 and 4.25), the molar fraction of ZrO_2 and Na_2O (equimolar) is held at a fixed value of 0.10.

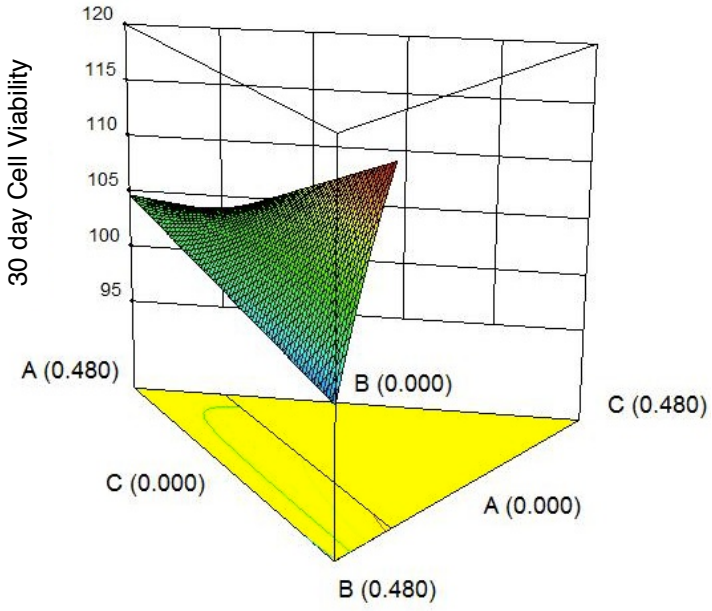

Figure 4.22: 3D contour plot showing the effect of varying glass composition within the confines of the design space and the resultant 30 day glass extract cell viability.

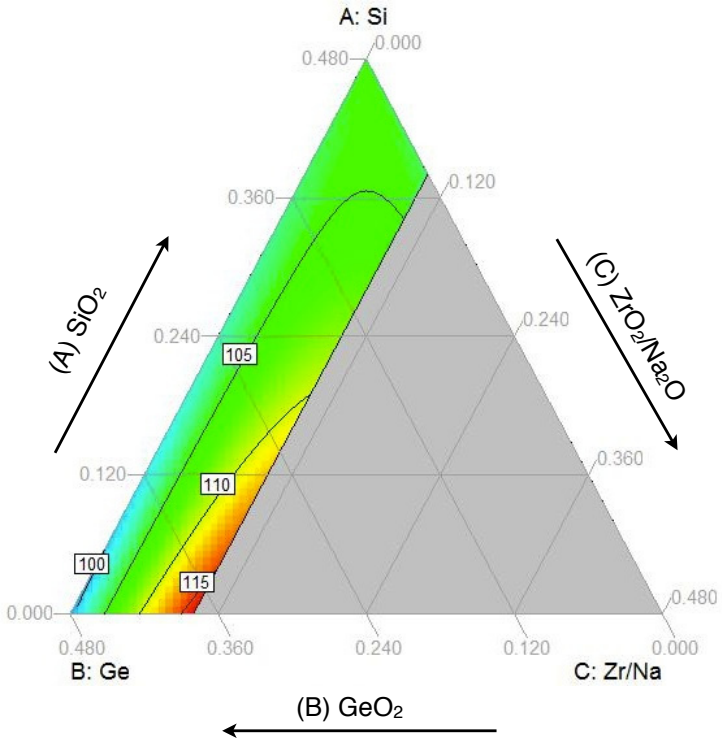

Figure 4.23: 2D contour plot showing the effect of varying glass composition within the confines of the design space and the resultant 30 day glass extract cell viability.

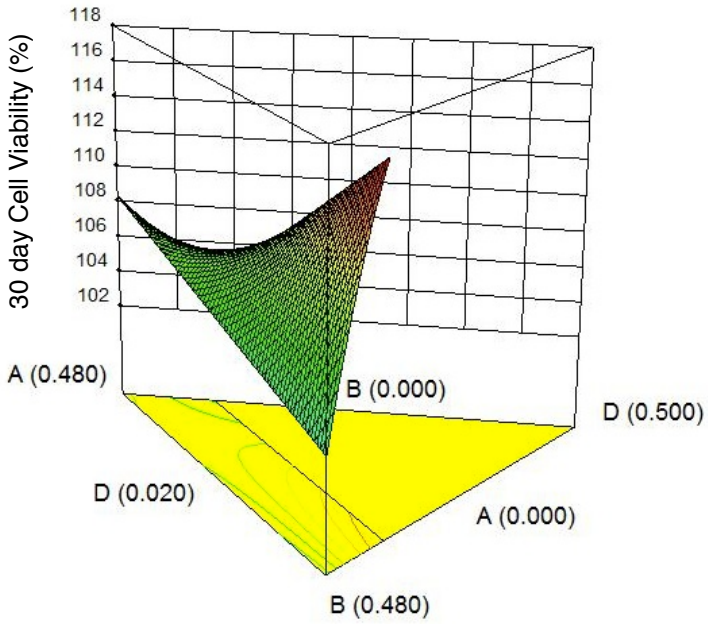

Figure 4.24: 3D contour plot showing the effect of varying glass composition within the confines of the design space and the resultant 30 day glass extract cell viability.

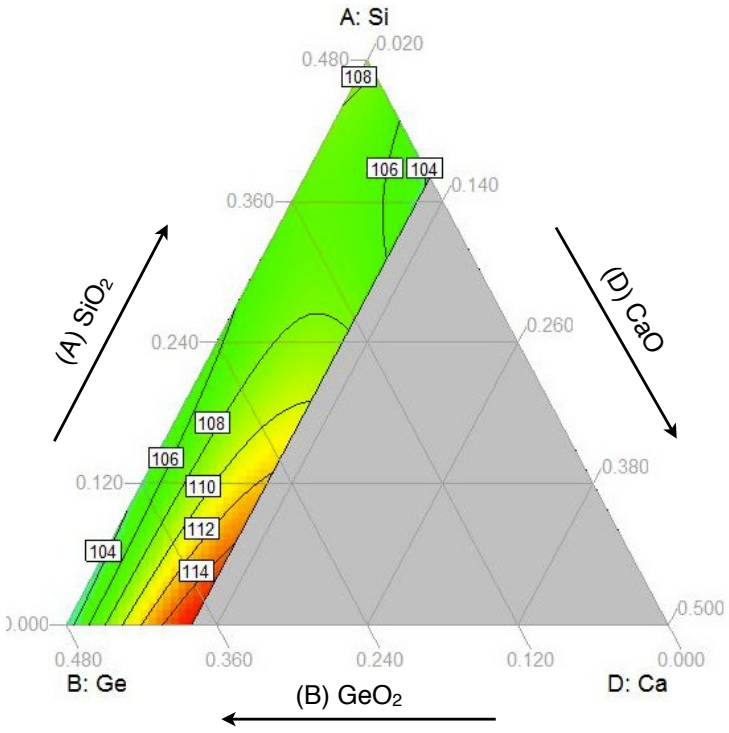

Figure 4.25: 2D contour plot showing the effect of varying glass composition within the confines of the design space and the resultant 30 day glass extract cell viability.

Both sets have similar visual appearance because the ZrO_2/Na_2O and CaO have similar effects on cell viability. Analysis shows that glass former inclusion alone – and particularly germanium inclusion – within the extract do not impact cell viability as strongly as was hypothesized in comparison to their modifier ion counterparts. Increased inclusion of modifiers (Na_2O and CaO) and intermediates (ZrO_2) in the glass network may lead to reduction of cell viability levels to reasonable levels more similar to the TCW control (set at 100 % cell viability), thereby offering a possible compositional solution toward reducing cell viabilities too far above the 100 % level. The reader must be careful to note that these regression models only point to compositional variables of the original glass melt. For example, arguing that increased extract levels of Ca^{2+} positively affect cell viability forms a weakened conclusion because it presupposes that increased calcium content in the glass melt must go hand in hand with increased extract calcium dissolution. Judgments on ionic effects can only be made when equipped with the contiguous degradation products dataset explored later in this chapter. Furthermore, effects are only modeled adequately within the predetermined parameters of the design of mixtures approach; effects outside the extreme values of the empirical dataset may not align with the models produced.

4.4.2 Limitations of MTT Assay as an Indicator of Cytocompatibility

MTT assay is one accessible tool the biomaterial scientist may employ to survey material cytocompatibility. The influence of the wealth of coded genetic information and fluctuating environmental conditions within the extracellular milieu of a living organism far eclipses the predictive capability of the MTT assay [123]. Although measures are employed to emulate physiological conditions loosely (37 °C, 5 % CO_2 environment), isolated culture flask MTT experiments extrapolate cell health indirectly from a measure of colorimetric density following reduction of tetrazolium dye by the mitochondrial dehydrogenase of live, viable cells [122]. The author argues that MTT assay is not a measure of broader cytocompatibility, but only of cell viability in comparison with a reference extract. Coupled with degradation product information, MTT assay results collected in this study are useful for determining the

effect of released ions on cell viability. Further limitations bear mentioning: tetrazolium salts are not impervious to reduction via processes other than mitochondrial dehydrogenation, however the impact of this reality on results of the study should be ruled out by the use of controls: media with cells and media without cells.

4.4.3 Summary of Composition–Cell Viability Relationships: DG Glasses

- High DG glass cell viabilities (those significantly exceeding 100 %) are concering due to the potential for leached ions stimulating mutagenic activity *in vitro*. Cell viability levels range from 92 to 124 %; germanium glasses in particular had a propensity toward high cell viability values.

- At 30 day DG glass extract testing, the greatest overall impact on cell viability is increased Zr/Na in concert with Ca (quadratically). These compositional factors work together to decrease cell viability significantly.

- At 30 day DG glass extract testing, increased Zr/Na has the greatest impact on increasing cell viability, followed by increased Ca, then by both increased Ge in concert with Zr/Na (quadratically) and increased Ge in concert with Ca (quadratically).

Chapter 5

Results and Discussion Part B: Composition–Property Relationships for DG Series Cements

As detailed in section 3.2.1 (page 36), the 12 DG glass phases discussed in chapter 4 were combined with an aqueous polymeric (PAA) phase to compose the hydrated polysalt GPCs discussed in this section.

5.1 DG Cements: Degradation Products

The primary objective of this section was to evaluate the ion release characteristics of the DG cements and to understand their release kinetics as a function of material composition. Using an ISO 10993–14 based protocol, the modulation of release kinetics was examined for 7 constituent ions: glass former ions: Si^{4+} and Ge^{4+}; glass modifier ions: Na^{+}, Ca^{2+} and Sr^{2+}; and glass intermediate ions: Zn^{2+} and Zr^{4+}.

With respect to the glass former substitution within the cement matrix, it was hypothesized that germanium would be able to modulate temporal release profiles of the glass modifiers and intermediates to the effect that greater amounts of constituents would be released from germanate cement compositions than from silicate cement compositions. Although germanium takes on a tetrahedral coordination in amorphous networks, d orbitals enable it to adopt octahedral coordination, a bonding modality

unamenable to silicon under ordinary conditions. This capability for additional coordination values may allow germanium to alter bonding angles within the glass phase of the polysalt matrix. Altered bond angles would lessen the uniformity of a tetrahedral network, leading to more fascile ion migration. With regard to glass intermediate and modifier substitutions, it was hypothesized that replacement of calcium with sodium and zirconium would destabilize the network and lead to increased release of all constituent ions from the cement matrix.

Only three ions were released from the DG cements in quantities exceeding 10 ppm: Si^{4+} (45 ppm), Ge^{4+} (200 ppm), and Na^{+} (32 ppm)[1]. Elaborated data for the other four ions analyzed are included in appendix C (figures C.4, C.5, C.6 and C.7) for completeness.

5.1.1 Release and $t_{1/2}$ of Glass Formers from DG Cements (Si^{4+} and Ge^{4+})

Figure 5.1 displays Si^{4+} ion release after incubation at 1, 7 and 30 days; ions are released up to 48 ppm after 30 day cement specimen incubation.

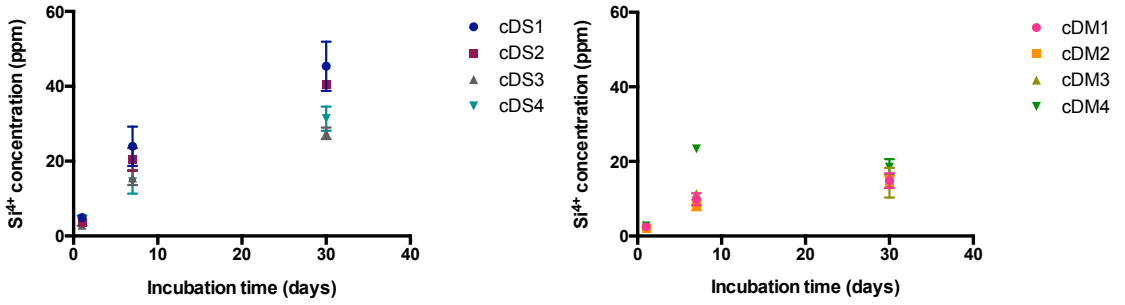

(a) (b)

Figure 5.1: The Si^{4+} ion release levels of 8 DG cements with time dependency: (a) silicate cements and (b) mixed former cements over 1, 7 and 30 day incubation periods.

All data were sufficiently modeled as one phase linear decay processes (table 5.1). Degradation half–life data indicate that inclusion of germanium in the glass phase decreased the half–life and extent of Si^{4+} ion release. $t_{1/2}$ of silicon released did not differ significantly with the addition of Zr/Na to the glass phase, as noted by a comparison of cDS1 and cDS2.

[1]A table listing all DG cement degradation byproduct maxima is listed in appendix A: Degradation Product Maxima

Table 5.1: Best fit parameters for nonlinear one phase association model formed from Si^{4+} release over 1, 7 and 30 day incubation periods

DG Cement	$t_{1/2}$ (days)	τ (days)	Y_{max} (ppm)	R^2
Nonlinear fit of Si^{4+} *release from DG silicate cements*				
cDS1	6.907	9.965	47.69	0.9452
cDS2	7.623	11.00	43.41	0.9903
cDS3	6.183	8.921	28.43	0.9865
cDS4	8.552	12.34	34.32	0.9567
Nonlinear fit of Si^{4+} *release from DG mix cements*				
cDM1	4.418	6.374	14.96	0.9458
cDM2	5.822	8.399	14.93	0.9572
cDM3	3.276	4.726	14.42	0.8732
cDM4	1.987	2.866	21.14	0.8342

The Ge^{4+} ion release levels for each germanium containing cement composition are shown in figure 5.2.

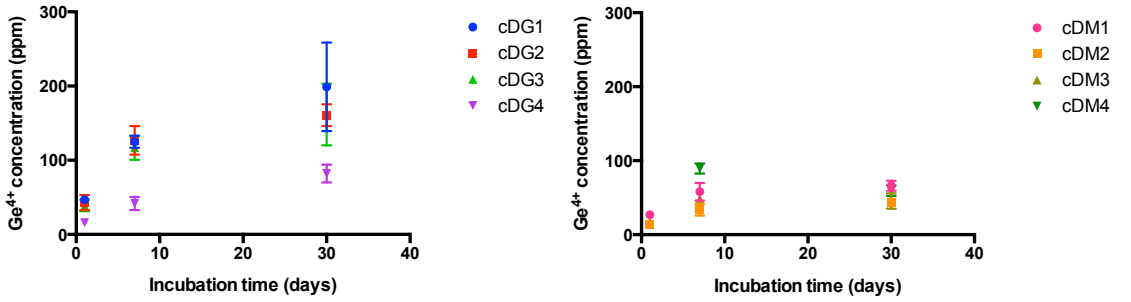

(a) (b)

Figure 5.2: The Ge^{4+} ion release levels of 8 DG cements with time dependency: (a) germanate cements and (b) mixed former cements over 1, 7 and 30 day incubation periods.

DG cement germanium (Ge^{4+}) ion dissolution were modeled according to a one phase exponential decay model (parameters listed in table 5.2). Inclusion of silicon in the glass phase significantly decreased the half–life and extent of Ge^{4+} ion release, likely owing to the halved levels of germanium oxide in the melt for mixed former cement precursor glasses.

Table 5.2: Best fit parameters for nonlinear one phase association model formed from Ge^{4+} release over 1, 7 and 30 day incubation periods

DG Cement	$t_{1/2}$ (days)	τ (days)	Y_{max} (ppm)	R^2
Nonlinear fit of Ge^{4+} *release from DG germanate cements*				
cDG1	4.466	6.442	198.9	0.7995
cDG2	2.723	3.928	158.4	0.9306
cDG3	3.424	4.939	160.3	0.8369
cDG4	6.731	9.711	85.65	0.9091
Nonlinear fit of Ge^{4+} *release from DG mix cements*				
cDM1	1.317	1.901	63.15	0.8403
cDM2	2.253	3.250	41.63	0.8050
cDM3	1.432	2.066	47.62	0.8442
cDM4	1.365	1.969	74.10	0.7226

Addition of ZrO_2/Na_2O to the glass phase (cDG1 $\rightarrow$ cDG2) yields a halved $t_{1/2}$ of Ge^{4+} release (table 5.2), although statistical analysis (included in appendix B) reveals that this difference is not statistically significant. The greatest significant factor in reducing Ge^{4+} release was reduction of GeO_2 content in the original glass composition (cDG1 $\rightarrow$ cDG4). Half–life of release was greater for Si^{4+} ions than for Ge^{4+} ions. Localized, controlled delivery of Ge^{4+} at orthopaedic sites may prove beneficial as a cancer therapy [102]. From a utility perspective, it is possible for the longer half–life of Ge^{4+} to be exploited for ion delivery over time in such indications.

Half–lives of Si^{4+} and Ge^{4+} dissolution were collected from the ion release profiles (figures 5.3 and 5.4.

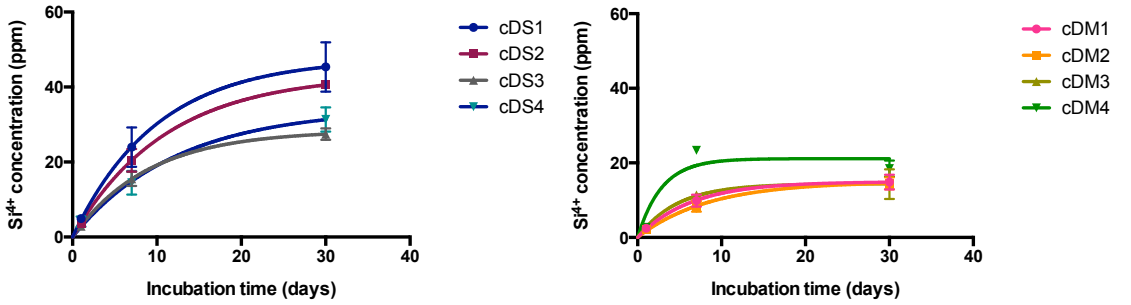

(a) (b)

Figure 5.3: The Si^{4+} ion release profiles of 8 DG cements with time dependency: (a) silicate cements and (b) mixed cements over 1, 7 and 30 day incubation periods.

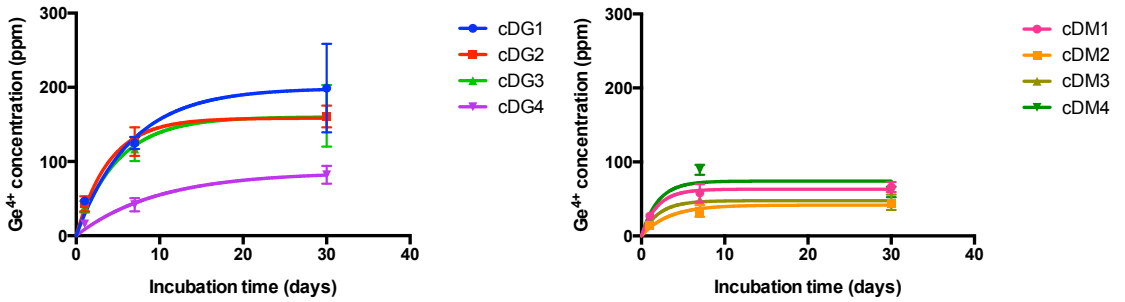

(a) (b)

Figure 5.4: The Ge^{4+} ion release profiles of 8 DG cements with time dependency: (a) germanate cements and (b) mixed cements over 1, 7 and 30 day incubation periods.

Si^{4+} and Ge^{4+} dissolution $t_{1/2}$ were modeled using linear and linear & square models, repsectively, that produced reasonable R^2 and adjusted R^2 values (table 5.3) with suitable values of adequate precision (12.088 and 15.246, respectively). Both models have suitable predictive capability. Release plateaus occur well under the 30 day elution timepoint.

Addition of unlike glass formers increases the rate at which both Si^{4+} and Ge^{4+} leach out of the cements. All compositional factors increased Si^{4+} half–life of dissolution except for GeO_2 inclusion; likewise, addition of all glass oxides to the network increases Ge^{4+} half–life of dissolution while SiO_2 inclusion expedites Ge^{4+} dissolution. The effect is more prominent in the case of Ge^{4+}, however. Although linear increases in germanate content increase half–life of Ge^{4+} release, the squaring of germanate content appears to shorten half–life greatly.

Table 5.3: Regression models in terms of L–pseudo components and summarized ANOVA for former ion half–life release from Dal Glass cements

Response	Regression Model	Summarized ANOVA				
		R^2	R^2 adj.	R^2 pred.	p	F
Si^{4+} release $t_{1/2}$	+6.72*Si, - 2.64*Ge +9.41*Zr/Na + 9.38*Ca	0.9064	0.8713	0.7873	0.0002	25.82
Ge^{4+} release $t_{1/2}$	– 17.17*Si, + 14.09*Ge +6.86*Zr/Na + 12.56*Ca + 18.37*Si^2 – 14.63*Ge^2	0.9514	0.9109	0.6082	0.0007	23.49

Figures 5.5 and 5.6 display 2D and 3D contour plots that depict these effects visually; the contour plots were selected to vary CaO while leaving ZrO_2/Na_2O at a fixed molar fraction because CaO had greater impact on half–life than ZrO_2 and Na_2O and is therefore more useful visually. Both plots are confined to within the design space where (A) SiO_2 0–0.48 mol. fraction, (B) GeO_2 0–0.48 mol. fraction, (D) CaO 0.02–0.12 mol. fraction, and ZrO_2/Na_2O is fixed at 0.10 mol. fraction.

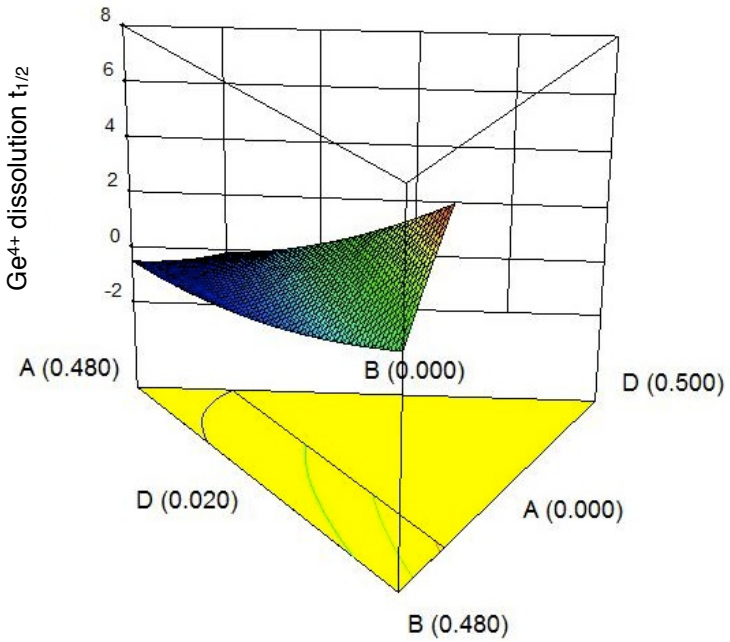

Figure 5.5: 3D contour plot showing the effect of varying glass composition within the confines of the design space and the resultant half–life of Ge^{4+} dissolution.

It is possible that the greater release half–life of Si^{4+} compared to Ge^{4+} is due to the formation of a silicate gel layer at the cement–solution interface and slows the loss of SiO_2 into the water as a solute, yet facilitates Ge^{4+} dissolution [119]. This assertion is supported by the fact that greater SiO_2 in the glass network leads to decreased Ge^{4+} dissolution half–life but increased Si^{4+} dissolution half–life. This phenomenon may lead to a more robust bulk, owing to a greater siliceous gel layer within the glass phases at the GPC surface; decreased rate of Si^{4+} release may lead to enhanced opportunity for maintenance of a silicious gel layer temporally [124].

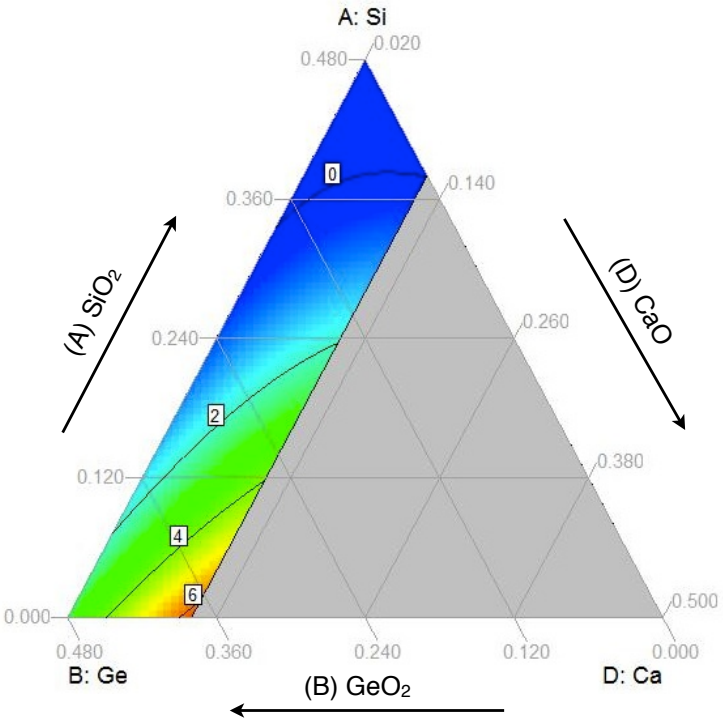

Figure 5.6: 2D contour plot showing the effect of varying glass composition within the confines of the design space and the resultant half–life of Ge^{4+} dissolution.

5.1.2 Release and $t_{1/2}$ of Glass Modifiers from DG Cements (Na^+, Ca^{2+}, and Sr^{2+})

Statistical analyses between compositions and over time for remaining ions are included in appendix B. Virtually no calcium nor strontium was detected in the glass extracts, so these ions are not discussed further.

Table 5.4: Best fit parameters for nonlinear one phase association model formed from Na^+ release over 1, 7 and 30 day incubation periods

DG Cement	$t_{1/2}$ (days)	τ (days)	Y_{max} (ppm)	R^2
Nonlinear fit of Na^+ *release from DG silicate cements*				
cDS2	0.6132	0.8847	31.09	0.6629
cDS3	7.177	10.35	7.122	0.9940
cDS4	4.613	6.656	14.81	0.8305
Nonlinear fit of Na^+ *release from DG germinate cements*				
cDG2	6.128	8.840	14.32	0.9103
cDG3	9.686	13.97	21.73	0.9160
cDG4	18.80	27.13	25.41	0.9475
Nonlinear fit of Na^+ *release from DG mix cements*				
cDM1	8.226	11.87	15.97	0.9331
cDM2	16.10	23.22	15.69	0.9768
cDM3	6.289	9.073	11.73	0.8955
cDM4	2.294	3.310	9.510	0.8025

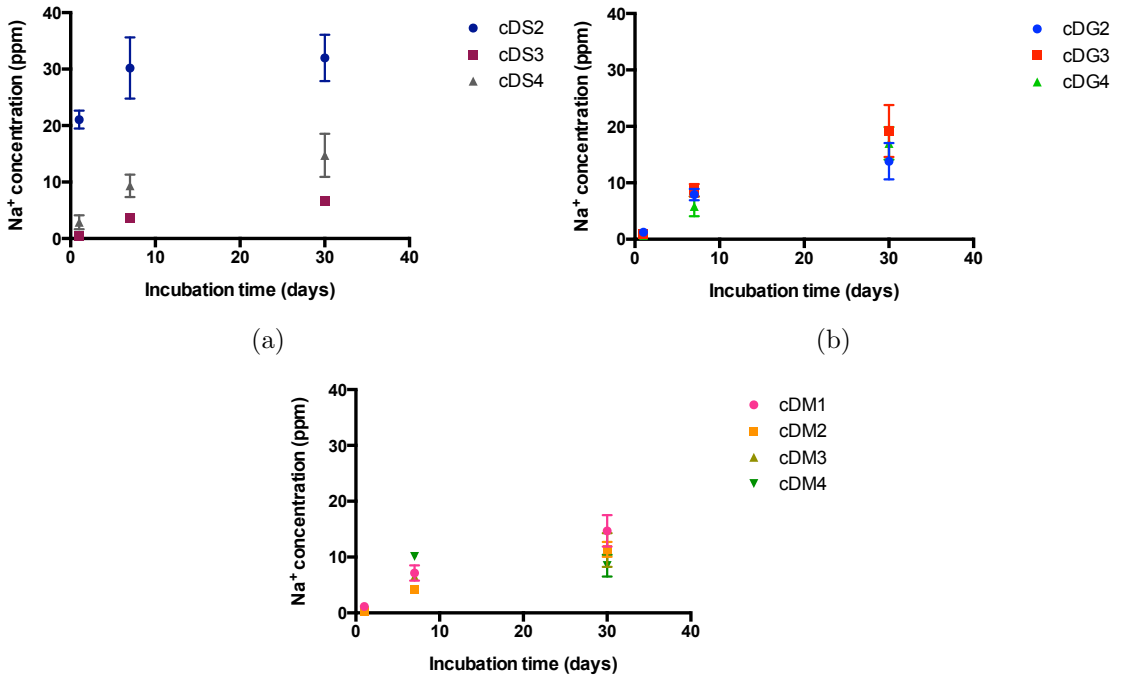

Figure 5.7: The Na^+ ion release levels of DG cements with time dependency: (a) silicate cements, (b) germanate cements, and (c) mixed former cements over 1, 7 and 30 day incubation periods.

Sodium and calcium half–life of release produced suitable models (table 5.5).

Virtually no calcium is released from any of the 12 cements, and so the practical importance of regression modeling in this case is questionable at best and is not developed further. Strontium half–life of release could not be modeled.

Table 5.5: Regression models in terms of L–pseudo components and summarized ANOVA for modifier ion half–life release from Dal Glass cements

Response	Regression Model	Summarized ANOVA				
		R^2	R^2 adj.	R^2 pred.	p	F
Na^+ release $t_{1/2}$	– 34.68*Si – 50.28*Ge – 756.51*Zr/Na +238.09*Ca + 1122.71*Si*Zr/Na – 82.75*Si*Ca +1243.96*Ge*Zr/Na	0.9537	0.8981	0.4475	0.0034	17.15
Ca^{2+} release $t_{1/2}$	+2.127E+5*Si – 3.887E+5*Ge +1.659E+6*Zr/Na +1.659E+6*Ca – 3.251E+6 *Si*Zr/Na – 3.251E+6*Si*Ca	0.8597	0.7428	– 0.8967	0.0153	7.35
Sr^{2+} release $t_{1/2}$	(insignificant model)					

Increased silicon in concert with Zr/Na as well as increased germanium in concert with Zr/Na both elicit increased Na^+ release $t_{1/2}$ most effectively. Reduction in Na^+ release $t_{1/2}$ is achieved through increased Zr/Na. Both Na+ and Ca^{2+} ion release from DG cements produced significant models aligning with one phase exponential decay. The sodium release model was superior, owing to higher R^2, adjusted R^2, values, a lower p–value and greater predictive capacity (attested by R^2). Due to the minimal release of Ca^{2+}, practical implications for modeling this ion are minimal.

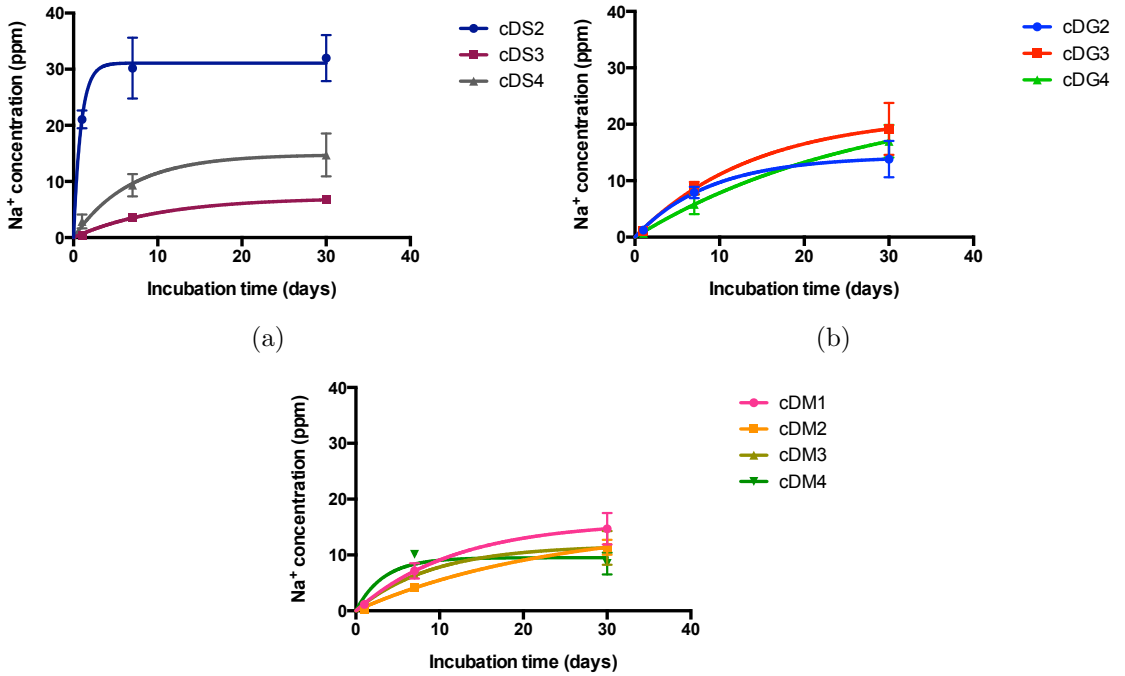

Figure 5.8: The Na^+ ion release profiles of DG cements with time dependency: (a) silicate cements and (b) mixed cements over 1, 7 and 30 day incubation periods.

It is clear from figure 5.8 that sodium undergoes a burst release from the non–setting cement (cDS2). When this cement is excluded from analysis, silicate and germanate cements see roughly equivalent levels of sodium release levels. According to the half–life of release model for sodium, calcium is the only independent compositional factor to positively influence sodium release (table 5.5). Sodium ions are more mobile and spatially less hindered than calcium ions, and can easily be accommodated in calcium bonding sites within the glass network. In this manner, sodium can use both its native bonding sites and those provided by calcium for migrating within the bulk [120]. In compositions with mixed sodium and calcium modification, therefore, sodium ions may temporarily displace calcium ions and migrate more freely than in glasses containing only sodium modification sites. Migration, of course, should lead to higher dissolution from the bulk, and may likely be the cause of the higher extract sodium concentrations observed.

Greater, selective Na^+ migration from the cement bulk alters ion exchange at the GPC surface. Dealkalization of the glass phase at the GPC surface is effected

through the replacement of Na^+ ions with hydronium ions, leading next to expansion of the siliceous gel layer characteristic of silicon–containing glasses [124, 125]. From a utility standpoint, an enhanced siliceous gel layer may produce a surface chemistry that is more resilient to bulk degradation. Mechanical properties of the bulk material, therefore, may be better protected and preserved in aqueous environments when calcium and sodium are added together to the glass phase.

5.1.3 Release and $t_{1/2}$ of Glass Intermediates from DG Cements (Zn^{2+} and Zr^{4+})

Zinc was not released from the cements in any appreciable quantities, save for its relatively high release (c. 60 ppm) from the non–setting cement (cDS2) by 30 days. Interestingly, however, and as was the case for strontium release, the two cements that contain neither sodium nor zirconium (cDS1, cDG1) were amenable to one phase decay modeling even at very low zinc release levels. Incubated cements saw virtually no zirconium dissolution, and only those cements with mixed silicate/germanate former content could be modeled with any precision so they are excluded from this work.

5.1.4 Composition & Germanium (Ge^{4+}) Ion Release: DG Cements

Germanium is released at the highest levels of all compositional moieties from both glasses and cements in this study. Although germanium–containing cements demonstrated cell viabilities similar to controls even at the 30 day time period, concerns still remain over the toxicity of inorganic germanium, particularly as it accumulates over time in living tissues; furthermore, germanium oxide is an expensive compound. Because germanium incorporation in the glass phase has yielded unprecedented, improved mechanical properties in GPCs to date, it would be beneficial for the materials scientist to maximize the impact of germanium in the network while limiting its content and dissolution. To that end, Ge^{4+} concentration at the greatest elution timepoint (30 days) is modeled so that compositional factors affecting Ge^{4+} dissolution may be isolated.

Analysis of the effect of composition on Ge^{4+} release at the 30 days of cement specimen incubation produced a predictive quadratic model with an adequate precision value of 29.722 (table 5.6).

Table 5.6: Regression models in terms of L–pseudo components and summarized ANOVA for Ge^{4+} release from Dal Glass cements at the 30 day incubation timepoint

Response	Regression Model	Summarized ANOVA				
		R^2	R^2 adj.	R^2 pred.	p	F
30d Ge^{4+} release	– 108.27*Si + 203.79*Ge + 506.8*Zr/Na – 2428.04*Ca – 185.28*Si*Ge + 3536.84*Si*Ca – 654.33*Ge*Zr/Na + 3152.02*Ge*Ca	0.9948	0.9858	0.9115	0.0002	110.15

These results are depicted visually in figures 5.9 and 5.10 as 3D and 2D contour maps. These plots are confined to within the design space where (A) SiO_2 0–0.48 mol. fraction, (B) GeO_2 0–0.48 mol. fraction, (D) CaO 0.02–0.12 mol. fraction, and ZrO_2/Na_2O is fixed at 0.10 mol. fraction. The largest positive contributors to Ge^{4+} dissolution result from increased silicon and calcium (together) and increased germanium and zirconium/sodium (together) while calcium alone works to decrease Ge^{4+} dissolution. According to predictions of the model, greater calcium loading in the glass network should arrest germanium dissolution from the DG cement matrix to its lowest levels.

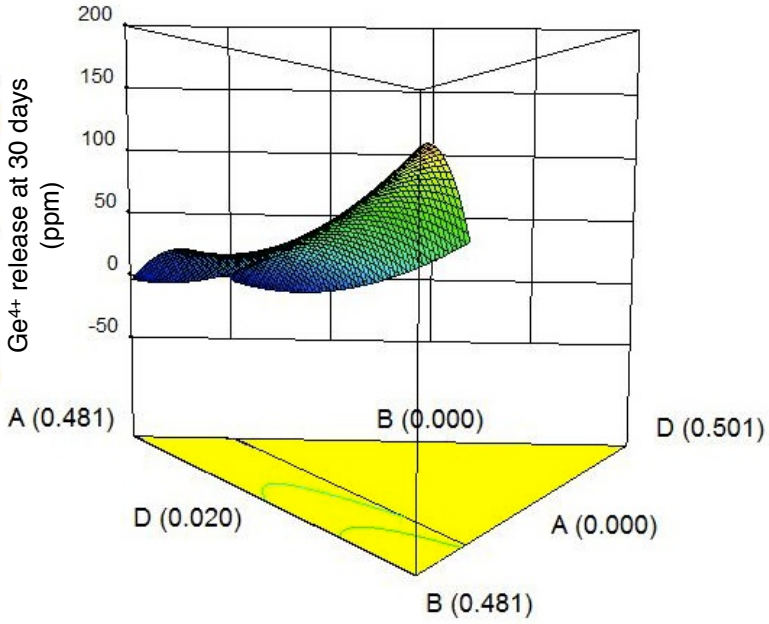

Figure 5.9: 3D contour plot showing the effect of varying glass composition within the confines of the design space and the resultant 30 day cement extract [Ge^{4+}].

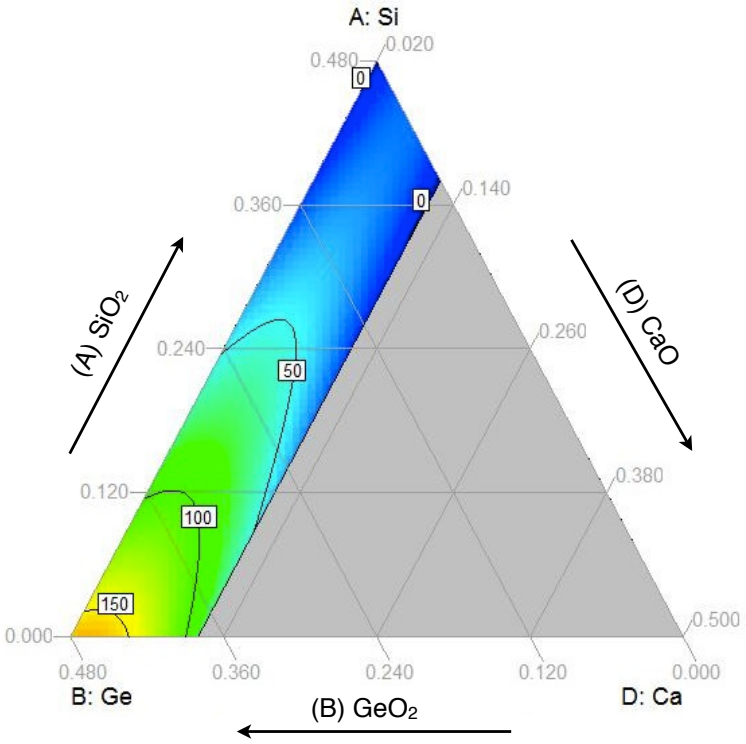

Figure 5.10: 2D contour plot showing the effect of varying glass composition within the confines of the design space and the resultant 30 day cement extract [Ge^{4+}].

5.1.5 Summary of Composition–$t_{1/2}$ Relationships: DG Cements

The following summarize compositional influences on the $t_{1/2}$ of ions within DG cements:

- Germanium (Ge^{4+}) is released from DG cements up to 200 ppm after 30 days incubation. Addition of silicon to the glass phase of the cement matrix has the greatest impact on reduction of Ge^{4+} release $t_{1/2}$. Increased calcium increases $t_{1/2}$ of Ge^{4+} release.

- Silicon (Si^{4+}) is released from DG cements up to 45 ppm after 30 days incubation. Si^{4+} release $t_{1/2}$ is most effectively (and equally) increased by the addition of Zr/Na and calcium to the glass phase of the DG cement matrix.

- Sodium (Na^{+}) is released from DG cements up to 32 ppm after 30 days incubation. Increased silicon in concert with Zr/Na as well as increased germanium in concert with Zr/Na both elicit increased Na^{+} release $t_{1/2}$ most effectively. Reduction in Na^{+} release $t_{1/2}$ is achieved through increased Zr/Na.

- Glass former ion release data were modeled much more readily for the DG cements than modifier and intermediate release using one phase exponential decay, likely due to insignificant levels of ion release for the latter.

- Zinc, zirconium, and calcium and strontium were not released from the cements.

The utility of these composition–$t_{1/2}$ relationships lies in manipulation of the glass phase within the DG cement matrix to release or withold ions in order to optimize clinical handling properties. Degradation half–life can be correlated with the availability of an ion type to effect changes within the hydrated polysalt matrix. Extended temporal availability for bond formation and bond breaking could lead firstly to extended working times, and secondly to a more robust, more highly crosslinked matrix once cement maturation is achieved.

The hypothesis that germanium would be able to modulate temporal release profiles of the glass modifiers and intermediates to the effect that greater amounts of constituents would be released from germanate cement compositions than from

silicate cement compositions was falsified for calcium, zirconium and zinc (these ions were not released from DG cements) and confirmed in the case of the sodium. For sodium leaching, however, silicon elicits an extension in Na^+ $t_{1/2}$ and concentration nearly to the degree that germanium does. With regard to glass intermediate and modifier substitutions, it was hypothesized that replacement of calcium with sodium and zirconium would destabilize the network and lead to increased release of all constituent ions from the cement matrix. For both Ge^{4+} and Si^{4+} dissolution, replacement of calcium with Zr/Na resulted in reduction of silicate and germanate ions released. This hypothesis is therefore falsified. The effects of glass oxides on ion dissolution seen more clearly in chapter 4 (when the DG glass phase is examined alone) appear to be muted by the involvement of poly(acrylic acid) in the mechanisms of glass polyalkenoate formation and equilibriation.

5.2 DG Cements: MTT Cell Viability Assay – Mouse Fibroblast Cells

The objective of this section of the study was to screen all twelve DG cements for toxic effects in comparison with a tissue culture water control and a commercial cement extract (SpinePlex®) in accordance with ISO 10993–5. Subsidiarily, the activity of inorganic germanium against a specific human osteosarcoma cell line (MG–63 fibroblasts) was to be determined.

It was hypothesized that cement extracts would yield lower NIH 3T3 mouse fibroblast cell viability than SpinePlex® over all time periods due to the greater elution of ions from the novel cement matrices.

NIH 3T3 mouse fibroblast cells exposed to 1, 7 and 30 day cement extracts had cell viabilities in the range 45 to 105 % compared to the tissue culture water (TCW) control (figure 5.11).

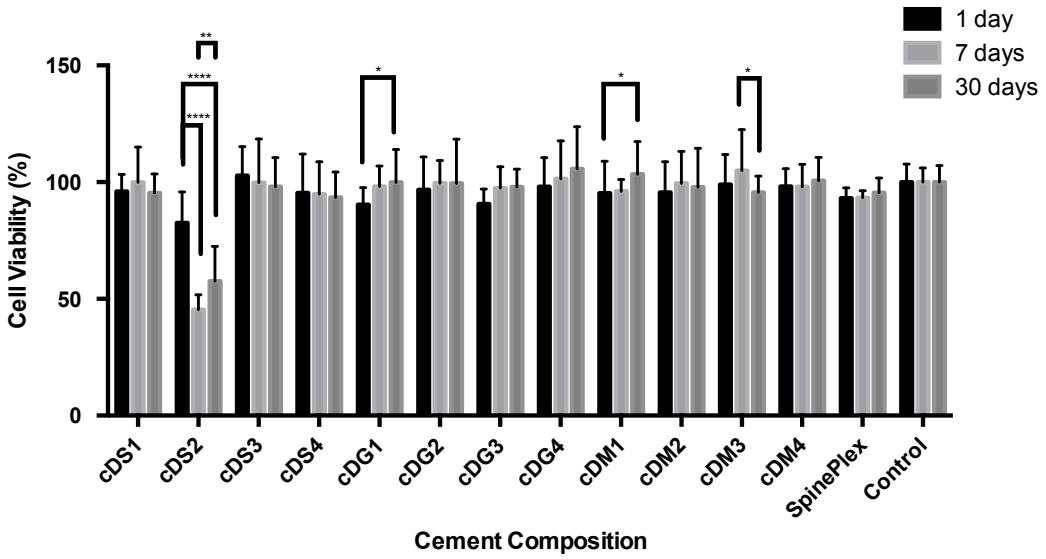

Figure 5.11: Cell viabilities of cement and control extracts over all time periods

One cement (cDS2) did not set as a hydrolytically stable mass after preparation; extracts from this cement showed cytotoxic effects at all time periods. With the exception of this extract, cell viabilities for the remaining 11 cement extracts were in the range 92 to 105%. Statistical analysis demonstrates little variation for each extract between timepoints (figure 5.11), with the exception of cDS2, and little variation between silicate, germanate and mixed extracts (figure 5.12), again with the exception of cDS2. All statistical variations depicted in figure 5.12 (a) result from cDS2. The reader should bear in mind the same limitations of the MTT assay method explored in the previous chapter.

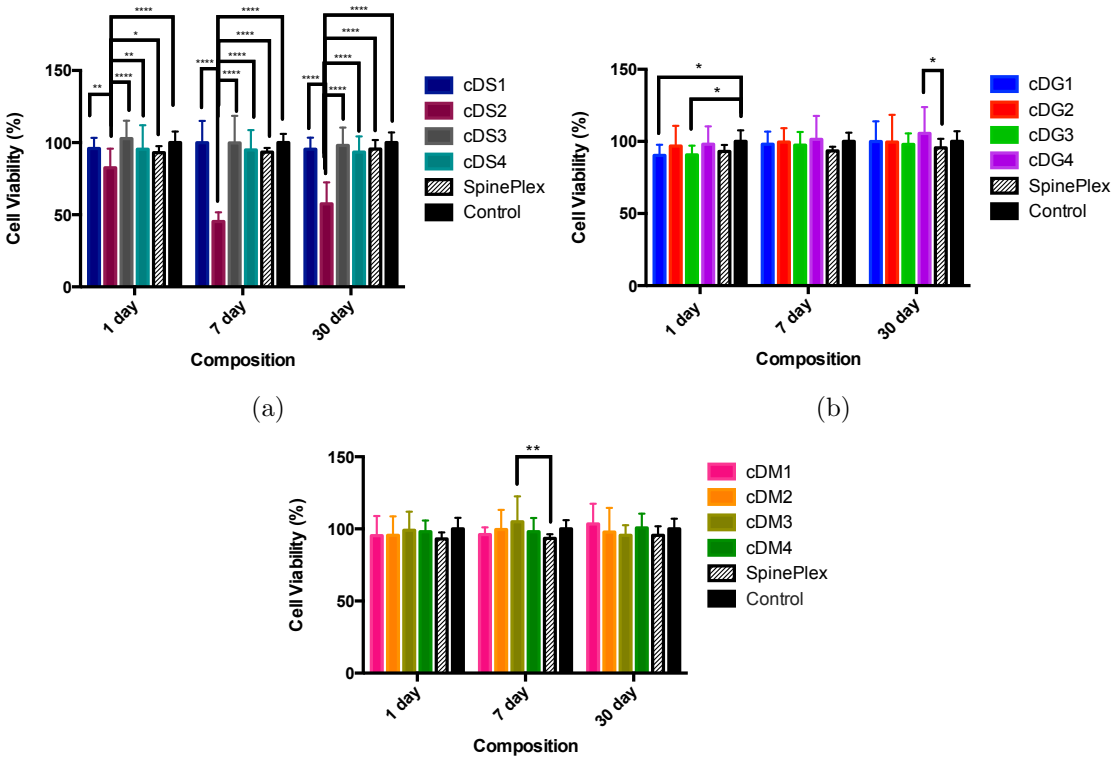

Figure 5.12: Cell viabilities of silicate, germanate and mixed former cement extracts with statistical differences at each timepoint

Results falsify the hypothesis. The only cement that produced significantly lowered cell viability (cDS2) contained no germanium.

5.2.1 Composition & Cell Viability: DG Cements

As was done for glass extract cell viability results, cement extract results were modeled using a Design of Mixtures (DoM) approach. The reader should bear in mind study limitations outlined in section 4.4.1. 1 and 7 day extract results produced insignificant models; 30 day extract cell viability was modeled quadratically with reasonable R^2 and adjusted R^2 values (table 5.7) with a suitable value of adequate precision (7.671). Although this model accommodates the empirical data, it has no predictive capability.

Table 5.7: Regression models in terms of L–pseudo components and summarized ANOVA for cell viability of NIH 3T3 fibroblasts exposed to cement extracts

Response	Regression Model	Summarized ANOVA				
		R^2	R^2 adj.	R^2 pred.	p	F
1 day CV		(insignificant model)				
7 day CV		(insignificant model)				
30 day CV	+55.59*Si +101.76*Ge +111.27*Zr/Na +101.19*Ca + 242.10*Si*Ca	0.7503	0.6077	– 1.2261	0.0282	5.26

At the 30 day extract timepoint, all compositional factors have a positive impact on cell viability. The greatest impact arises from the combination of SiO_2 and CaO. 2D and 3D contour plots depict these effects visually (figures 5.13 and 5.14). These plots are confined to within the design space where (A) SiO_2 0–0.48 mol. fraction, (B) GeO_2 0–0.48 mol. fraction, (D) CaO 0.02–0.12 mol. fraction, and ZrO_2/Na_2O is fixed at 0.10 mol. fraction.

Overall, with the exception of specimen cDS2, cell viability of cement extracts is promisingly similar to commercial and tissue culture water controls. Great variations in composition, therefore, lead to markedly different mechanical properties, all without impacting cell viability levels in any significant capacity [87].

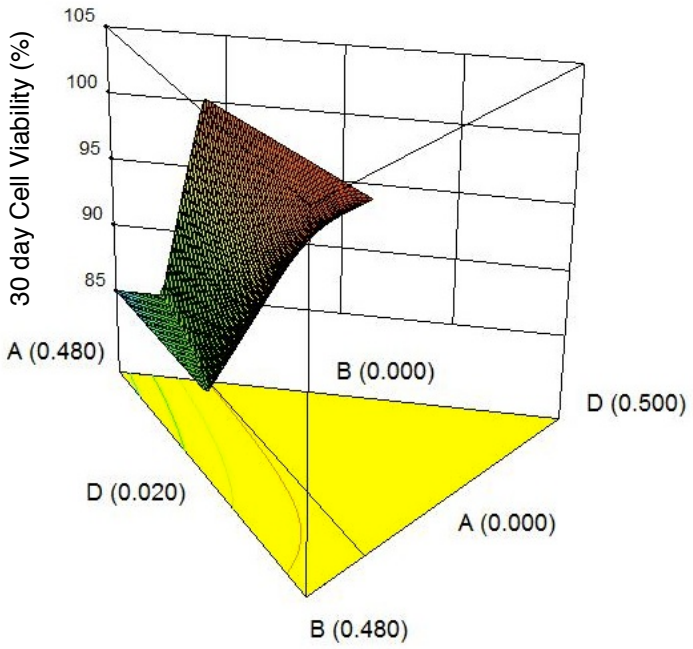

Figure 5.13: 3D contour plot showing the effect of varying glass composition within the confines of the design space and the resultant 30 day cement extract cell viability.

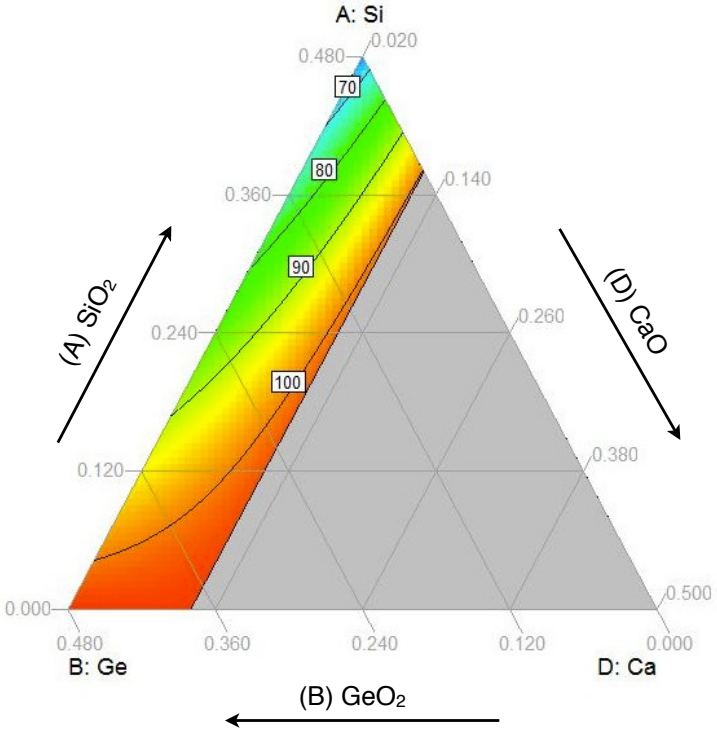

Figure 5.14: 2D contour plot showing the effect of varying glass composition within the confines of the design space and the resultant 30 day cement extract cell viability.

5.3 DG Cements: MTT Cell Viability Assay – Human Osteosarcoma Cells

It was hypothesized that germanium–containing cements would demonstrate significantly lower MG-63 human osteosarcoma cell viability than both non-germanium containing cements and SpinePlex® over all time periods.

Results obtained in this study falsify the hypothesis. Neither the silicate (cDS1) nor germanate (cDG1) cement extracts were cytotoxic to human osteosarcoma MG–63 cells as measured by MTT assay. Results did not deviate statistically from controls (figure 5.15).

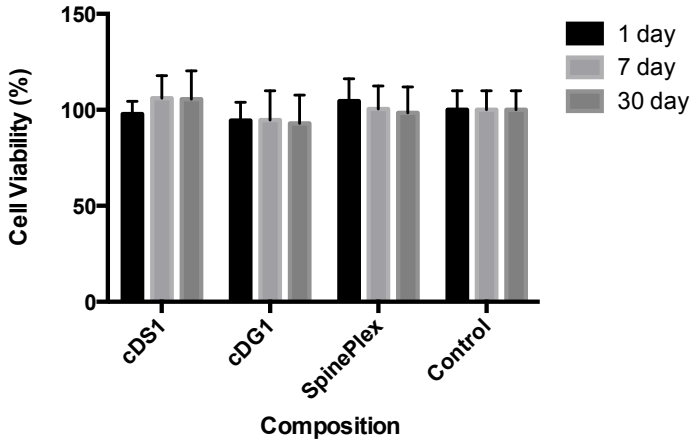

Figure 5.15: Cell viabilities of MG–63 osteosarcoma cells exposed to silicate (cDS1) and germanate (cDG1) cements and controls

When considered along with high cell viability achieved in previous NIH 3T3 MTT assays, these results are not surprising because MG–63 fibroblasts are robust cells that multiplied more rapidly than the NIH 3T3s.

This preliminary study suggests that sufficient anticancer activity from the Dal Glass GPCs would require the inclusion of more aggressive molecules rather than the base germanium oxide alone. The role of germanium for vertebroplasty therefore appears to be limited to the advantageous effects it has on clinical handling and mechanical properties, and not as an anti-cancer agent. On this topic, the effects of methotrexate inclusion in the GPC network is currently under investigation by another group member.

5.3.1 Summary of Composition–Cell Viability Relationships: DG Cements

- NIH 3T3 cell viability levels range from 94 to 105 %, with the exception of cDS2 (a DG cement that did not set as a hydrolytically stable mass and yielded cell viabilities below 50 %).
- 30 day extract composition–cell viability relationships were the only correlations that could be modeled for DG cements. At 30 day DG cement extract testing, increased Si in concert with Ca has the greatest impact on increased NIH 3T3 cell viability.
- Neither individual compositional factors nor combinations of compositional factors contribute to decreased NIH 3T3 cell viability in the presence of DG cements.
- No compositions–cell viability relationships could be drawn for cement extract interactions with MG–63 human osteosarcoma fibroblasts.

Chapter 6

Preliminary DoM Optimization

From the DG series cements analyzed, DG209 (here termed cDM2) has been identified in the literature as having the most appropriate combination of handling characteristics and mechanical properties for the indication of vertebroplasty. Given the potential issues raised in this research regarding increased cell viability (beyond 100%) for materials comprising high levels of germanium release, the following section is designed to benchmark the germanium release from DG209 with respect to cements formulated for minimal germanium release and maximal germanium release permitted by this system. Minimum and maximum germanium release systems will be simply identified and evaluated using response surface methodologies as outlined in appendix D.

6.1 Design of Mixtures (DoM) Objective and Rationale

DG209 provides a cement with a working time of 5 minutes, a setting time of 14 minutes, and a compressive strength of 45 MPa, satisfying basic handling and mechanical requirements for injectable bone cements for vertebroplasty. Using Design of Mixtures (DoM) mechanical and biological responses of DG cement candidates were modeled and traced back to compositions of optimized cements. The objective of this component of the study is to mathematically derive formulations of DG cements which provide for minimal and maximal germanium release, and to empirically

validate the characteristics of each such that the characteristics of DG209 can be benchmarked accordingly.

Full details on the modeling of cement parameters for optimization studies are provided in appendix D.

6.2 Optimization for *Maximized* Ge^{4+} Release

Table 6.1 lists various cement optimization criteria and their respective weighings, and table 6.2 lists the most desirable glass composition output for each criteria set.

Table 6.1: Optimization Criteria

Criteria set	Working time	Setting time	30d Extract [GeO_2]
1	In range: 360-602 seconds *****	In range: 900-1200 seconds ***	Maximize ***
2	In range: 360-602 seconds and target: 360 seconds *****	In range: 900-1200 seconds ***	Maximize ***
3	In range: 360-602 seconds and target: 360 seconds *****	In range: 900-1200 seconds and target: 900 seconds ***	Maximize ***
4	In range: 360-602 seconds and target: 450 seconds *****	In range: 900-1200 seconds and target: 900 seconds ***	Maximize ***
5	In range: 360-602 seconds *****	In range: 900-1200 seconds and target: 900 seconds ***	Maximize ***

The author favours criteria set 5 (table 6.1). Ideally, the cement should be workable for 6 to 10 minutes. This time window is crucial, so it has been afforded a high weighing (*****). The ideal cement should set within 15 to 20 minutes, and preferably closer to 15 minutes [87]. This criterion is less crucial, however, particularly if the targeted 15 minutes is factored into the calculation, so it is given a medium weighing (***). It would be ideal for the cement to release maximum levels of the potential therapeutic ion (GeO_2), particularly considering that ICP results showed that the levels of release are not excessive. This criterion is weighed at medium importance (***). Criteria set five satisfies these conditions with appropriate weighings, and results in a reasonable desirability factor (0.948) (table 6.2).

Table 6.2: Glass Composition Outputs

Criteria set	SiO_2	GeO_2	ZrO_2/Na_2O	CaO	Desirability
1	0	0.480	0.001	0.119	1.00
2	0.012	0.468	0.017	0.103	0.974
3	0.057	0.381	0.047	0.115	0.863
4	0.130	0.350	0.029	0.091	0.809
5	0.021	0.459	0.019	0.101	0.948

The predicted optimized glass therefore has the following nominal composition:

$$0.36ZnO_2-0.04SrO_2-0.021SiO_2-0.459GeO_2-0.0095ZrO_2-0.0095Na_2O-0.101CaO$$

6.3 Optimization for *Minimized* Ge^{4+} Release

All criteria have been maintained from the maximized Ge^{4+} release optimization with the exception of 30 day extract Ge^{4+} concentration, which has been minimized for the purposes of this low release optimization. Table 6.3 lists these optimization criteria and their respective weighings, and table 6.3 lists the most desirable glass composition output for this criteria set.

Table 6.3: Optimization Criteria

Working time	Setting time	30d Extract [GeO_2]
In range: 360-602 seconds	In range: 900-1200 seconds and target: 900 seconds	Minimize
*****	***	***

Table 6.4: Glass Composition Output

SiO_2	GeO_2	ZrO_2/Na_2O	CaO	Desirability
0.318	0.162	0.032	0.088	0.914

The predicted optimized glass therefore has the following nominal composition:

$$0.36ZnO_2-0.04SrO_2-0.318SiO_2-0.162GeO_2-0.016ZrO_2-0.016Na_2O-0.088CaO$$

6.4 Empirical Validation

Both glasses optimized for minimum and maximum Ge^{4+} release were synthesized according to the method in section 3.1.1 (page 35) and combined with PAA as detailed in section 3.2.1 (page 36) to compose their contiguous cements. 1 day cement extracts were prepared according to the method in section 3.2.2 (page 37). The cements were analyzed for compressive strength, working time, and setting time according to the methods detailed by Dickey [87], while their extracts underwent 1 day [Ge^{4+}] determination according the method in section 3.2.4 (page 37). The glass optimized for minimum Ge^{4+} ion release produced a cement with undesirable mechanical properties (table 6.5). The Ge^{4+} ion release level for this cement was higher than that of the other maximized cement, likely owing to a slow setting time that neared two hours (table 6.5).

Table 6.5: Empirical Performance of Optimized Cements

Response	Minimized Ge^{4+} release	Maximized Ge^{4+} release
Compressive strength	17 MPa (± 3 MPa)	39 MPa (± 2 MPa)
Working time (min:sec)	3:48 (± 0:13)	5:47 (± 0:23)
Setting time (min:sec)	113:45 (± 5:36)	14:44 (± 0:34)
Ge4+ release (30 day)	44 ppm (± 3 ppm)	38 ppm (± 5 ppm)

This result likely occurred because compressive strength could not be modeled for DoM optimization. A comparison of cements prepared from the two optimized glasses with the precedent DG cements (table 6.6) reveals that the glass optimized for maximum Ge^{4+} ion release produced a cement with suitable mechanical properties and ion release levels comparable to cDM2[1], a composition with similar molar germanium content (figure D.1). This cement is a potential candidate for further analysis.

[1]The compositions cDM2 is referred to as DG209 in the literature

Table 6.6: Working time, setting time, one day incubation compression strength and 30 day extract germanium concentration of Dal Glass and optimized cement compositions (standard deviations listed in parentheses) [87]

Comp.	Working Time min:sec	Setting Time min:sec	Compressive Strength MPa	$[Ge^{4+}]$ ppm
cDS1	1:17 (0:03)	2:05 (0:02)	n/a	n/a
cDS2	7:08 (0:13)	DID NOT SET	n/a	n/a
cDS3	1:09 (0:31)	3:16 (0:06)	n/a	n/a
cDS4	0:22 (0:05)	1:03 (0:12)	n/a	n/a
cDG1	5:58 (0:20)	16:06 (1:30)	39.00 (1.96)	199 (60)
cDG2	10:02 (0:09)	35:55 (2:11)	37.17 (4.07)	161 (15)
cDG3	5:18 (0:02)	13:58 (0:31)	39.52 (9.63)	162 (42)
cDG4	4:58 (0:13)	14:07 (1:41)	49.22 (2.10)	82 (12)
cDM1	7:05 (0:07)	104:19 (0:25)	n/a	66 (7)
cDM2	**5:02 (0:13)**	**14:13 (2:11)**	**45.16 (2.28)**	**43 (4)**
cDM3	6:56 (0:26)	36:05 (2:38)	33.17 (4.06)	45 (10)
cDM4	7:54 (0:21)	75:23 (4:43)	n/a	59 (7)
MIN Ge^{4+}	3:48 (0:13)	113:45 (5:36)	16.93 (2.82)	44 (3)
MAX Ge^{4+}	**5:47 (0:23)**	**14:44 (0:34)**	**39.36 (2.34)**	**38 (5)**

Having benchmarked the ion release characteristics of DG209 relative to the minimum and maximum concentrations of germanium released from the "optimized cements" in this section, it is clear that DG209 provides for a release of germanium equivalent to that formulation which was optimized for minimal germanium release. The cell viability of DG209 is not significantly different to the tissue culture water control. Whilst there are instrinsic limiatations with cell culture, the ion release and cell culture data further support the advancement of DG209 for additional studies.

6.5 Further Cement Optimization Considerations

This optimization study was conducted prior to the analysis of MG-63 human osteosarcoma cell viability in the presence of DG cements (section 5.3). Although

the cell viability study is only preliminary, it supports reasoning to explore anti–cancer alternatives that may be incorporated into the GPC network. The impact of germanium inclusion remains critically relevant to material characteristics separate from cancer therapy considerations. Germanium is capable of placing cement working times and setting times within clincally relevant ranges [87], and the germanium–containing DG cements have been positively screened for cell viability (section 5.2).

Other factors must be considered to better optimize the material. Firstly, it has been established that cell viability extract testing cannot be extrapolated *a prioi* to *in vivo* scenarios (section 2.4.3, page 32). Median lethal dose (LD_{50}) has already been considered (section 4.3, page 50), but bioaccumulation remains undiscussed. Approximately 2 grams of vertebroplasty cement are injected into a vertebra during a representative PVP procedure. In the worst possible degradation case (complete dissolution of the implant with an infinitessimally small $t_{1/2}$, maximal germanium dioxide loading (100% Ge_2, amorphous) and a P:L ratio of 2:15), a representative quantity of cement would release 1.14 grams of germanium dioxide in a representative 75 kg adult human. This release would correspond to a physiological dose of 15.2 mg/kg, well below the the LD_{50}[2] value of 1250 mg/kg [117]. A representative, maximal DG glass loading (48 mole–% GeO_2) would lead to just greater than half of this dose in any optimized composition considering germanium has the greatest molar mass of all 7 DG glass oxides.

Although calculated values for worst possible scenarios fall below median lethal dosage values, multiple vertebral fracture augmentations over a short period of time could lead to undesirable physiological accumulation of inorganic germanium. Unfortunately, the literature is scant and unclear on permissable inorganic germanium levels and bioaccumulation in humans. The deduction appears obvious, but it bears mentioning that decreased germanium content is correlated with decreased germanium ion release (section 5.1). Minimizing germanium content in the glass phase therefore reduces potential risks associated with increased dosage and bioaccumulation.

Secondly, material cost also bears consideration. Germanium dioxide costs $9.12 per gram (CAD) when purchased in 100 gram quantities (Sigma–Aldrich). The other

[2](Oral delivery in a mouse)

two oxides constituting the highest molar fractions: SiO_2 and ZnO are $2.25 per gram and $0.29 per gram (CAD), respectively, when purchased in the same quantity (Sigma–Aldrich). Minimizing germanium content clearly plays an important role in minimizing GPC formulation cost.

Now equipped with greater germanium contextualization, the author suggests an improved optimization approach: the glass phase should be optimized to yield a cement with minimized germanium inclusion (minimized cost) and release (minimized bioaccumulation risk), yet maximized adherence to clinically relevant parameters (working time, setting time, compressive strength). The optimization of this study considered the dissolution of germanium alone. A superior future optimization could be achieved through thoughtful consideration of the beneficial interactions observed for germanium in concert with other oxide components, such as zirconium and sodium.

Chapter 7

Limitations, Conclusions and Future Research Directions

7.1 Limitations

The author acknowledges limitations of this study such that the impact of the discussed data is maximally relevant:

- Inherent material limitations affect the study. Zirconium was accommodated into the glass network by charge composition with sodium in a 1:1 ZrO_2:Na_2O ratio. This material constraint limits independent analysis of the effect of either oxide on material properties. The molar fractions of zinc and strontium were kept constant (0.36 and 0.04, respectively) in all DG glass networks. The author is therefore unable to analyze the property effects these components have individually and in concert with other components.

- The glass compositions considered throughout this work are nominal; empirical compositions have not yet been verified. Some analyses (XRD and TGA) have produced similar data to those for glass melts of the same nominal composition detailed in the literature ([87]), however the author remains unaware of the true empirical compositions.

- Seven ions were surveyed using ICP analysis to produce degradation profiles: Si^{4+}, Ge^{4+}, Na^{+}, Ca^{2+}, Sr^{2+}, Zn^{2+} and Zr^{4+}. Upon degradation, however,

the materials in this thesis may produce moieties that are not amenable to straightforward ICP detection in this manner, thereby leading to a limitation of degradation product results.

- The use of extract ion concentrations as a proxy for concentrations anticipated *in vivo* is limited by the influence of fluctuating environmental conditions within the extracellular milieu of a living organism.

- This study emphasized phase I cytotoxicity evaluation using MTT assays performed with NIH 3T3 mouse fibroblast cells. Although such cell viability testing aligns with international standards for biological materials evaluation and provides valuable screening data, further testing using more representative cells would be beneficial. One such cell line was pursued: human MG–63 osteosarcoma fibroblasts. However, this particular study was limited to analysis of just two DG cement extracts and employed the same basic MTT assay screening method.

- There are intrinsic limitations associated with use of an MTT assay as an indicator of cytocompatibility; section 4.4.2 (page 75) elaborates on this point. In addition to these limitations, and in order to ensure repeatability of cell culture test, it is important that passage number be standardized and confluency be accurately described and measured. It would be further beneficial to normalize to DNA content. Such features would help ensure repeatability for future research.

- The Design of Mixtures (DoM) models have inherent statistical limitations. Multivariate models have been created with 5 or greater estimated coefficients based on only 12 data points strategically selected from the vertices and centroids of compositional ranges. It has been suggested that multivariate models should have 10 to 20 observations for every desired coefficient. Ideally, therefore, models should be created from 120 to 240 observations. However, these studies utilized mutliple centroid runs to validate the responses observed within the design space.

7.2 Conclusions

Current orthopaedic cements fail to offer a balance of biocompatibility and mechanical properties. Although employed readily in dental applications for their unique, advantageous properties, conventional glass polyalkenoate cements have been contraindicated for use in bone augmentation due to aluminum toxicity concerns. In previous work, select compositions from the Dal Glass series of aluminum–free glass polyalkenoate cements have been shown to possess excellent mechanical characteristics and injectability for orthopaedic applications, and for vertebroplasty in particular. These materials had not been analyzed for biological characteristics.

The work of this thesis provided preliminary phase I biological testing for twelve DG glasses and their contiguous polyalkenoate cements through a two–fold analysis: (1) material response under simulated physiological conditions (degradation byproducts) and (2) a preliminary biological response evaluation (cell viabilities). In a preliminary ancillary study, it was discovered that germanium inclusion in DG cement compositions have no statistically significant cytotoxic impact on a human osteosarcoma cell line versus other cement compositions and controls. Ge release from hydrolytically stable bone cements (up to 200ppm) does not cause a cytotoxic effect in cell culture, offering new possibilities for bone cement engineering with respect to aluminum–free GICs.

Design of Mixtures (DoM) was used to model mechanical and biological responses of DG cement candidates, and to trace these back to the components of an optimized vertebroplasty polyalkenoate glass. The optimized glass ($0.36ZnO_2 - 0.04SrO_2 - 0.021SiO_2 - 0.459GeO_2 - 0.0095ZrO_2 - 0.0095Na_2O - 0.101CaO$) was tailored to produce a cement which fit within clinically desirable working time and setting time ranges (360-602 seconds and 900-1200 seconds, respectively) as well as maximized 30 day extract concentration of Ge^{4+}. Minimization of germanium content in the cement matrix was also considered. The terms used in DoM to provide certainty are R^2, $R^2adj.$, R^2pred, p values and F values. All models satisfied statistical validity tests with the exception of 1 and 7 day cell viability models for DG cements; Ca^{2+}, Zn^{2+}, Zr^{4+} degradation product models for DG glasses; and Ca^{2+}, Zn^{2+}, Zr^{4+} and Sr^{2+} degradation product models for DG cements.

7.3 Future Research Directions

Imminently, the author would find it useful to explore potential mutagenic effects of germanium glass and cement extracts given cell viability results that exceed 100 % with respect to a tissue culture water control. Beyond this direction, a host of further potential compositional adjustments and analysis methods continues the orthopaedic bone cement narrative.

7.3.1 Future Compositional Adjustments

Firstly, regression analysis of data collected in this thesis has provided more quantitative tools for understanding and exploring the glass phase of the bone cement platform. Compositional adjustments to the glass phase itself may involve better controlling the germanium release profile by adjusting modifier oxide content, for example.

Secondly, all cements of this study were prepared by mixing the predetermined glass compositions consistently using one polymer molecular weight and one powder:liquid (P:L) ratio. Altering either molecular weight or P:L ratio leads to varying material properties. Some work has already been done in this research area using the glass compositions of this thesis.

Finally, there is the question of bone cement compositional adjustments aimed at combatting metastases of the spine more aggressively. The minimal study previously performed to test the cell viability of MG–63 human osteosarcoma cells in the presence of cement extracts demonstrated that inorganic germanium released by cements of this study likely fails as a cancer antagonist. A fellow student in the lab, Lauren Kiri, has studied the effects of mixing methotrexate – an antimetabolite commonly used in the treatment of cancers – into a glass polyalkenoate cement from the same series studied in this thesis; we eagerly await those results.

Furthermore, now that a substantial complement of mechanical and *in vitro* data have been collected and anlayzed, and taking into consideration the above adjustments, the researchers will be positioned to determine a better optimized glass polyalkenoate cement composition for vertebroplasty.

7.3.2 Future Analysis Methods

Preliminary *in vitro* cell culture studies performed in this thesis form part of the bridge toward more extensive *in vitro* work, and so it is only fitting to pay special consideration to future such work. Biological test method selection becomes more challenging at the *in vivo* level than at the *in vitro* level because the expected benefits of the study must be balanced against a complex interplay of variables including cost, time, animal welfare, and validity of extrapolation to clinical situations. The last of these is arguably the most important for prudent and efficacious medical implant testing.

Lipinski and Hopkins urge that the nature and properties of chemical tools in medicine must be evaluated in their respective proposed living systems for valid consideration [126]. Kirkpatrick and Mittermayer published an article wherein they claim *in vitro* methods are no more than an adjunct to higher levels of biological testing [106]. They cite a number of examples, among them a study testing the performance of a surface-reactive bone bonding ceramic against that of a non-bonding material using both an *in vitro* parameter of foetal rat osteoblast growth and *in vivo* implantation in rat femora. *In vitro*, the bone-bonding material yielded greater growth inhibition than the non-bonding material; *in vivo*, the bone-bonding material showed excellent performance. Had this material been ruled out on the basis of unsatisfactory performance *in vitro*, its benefits *in vivo* may have never been discovered. Bohner and Lemaitre corroborate this idea in their recent article challenging the paradigm that simulated body fluid (SBF) can be used to evaluate the bioactivity of implantable materials *in vitro* [127]. While *in vitro* testing generally is restricted to screening bio-incompatibility, *in vivo* methods provide the necessary direct evidence for biocompatibility and bioactivity. In this same vein, national and international regulatory bodies mandate non-clinical *in vivo* testing of novel materials to justify progression to clinical trials [128, 129]. Small animal models provide accepted rationale for progression of novel implantable materials to larger animal and clinical trials at a later stage.

Considering these arguments, a New Zealand rabbit femur healing model may be proposed for future *in vivo* testing of an optimized glass polyalkenoate cement stemming from the Dal Glass series. Unlike the delayed elution testing common to

preliminary test of this thesis, cements should be mixed and injected during the surgical procedure in order to approximate conditions of the glass polyalkenoate as it would be used in vertebroplasty indications. In particular, the following responses should be assessed for any orthopaedic biomaterial implant: tissue degeneration and necrosis, quantitative extent of fibrous encapsulation, granuloma and bone formation, debris presence, and tissue ingrowth quality and quantity [130]. Special attention must be paid to the bone-implant interface. Responses to the test sample should be compared to responses obtained at the commercial control sample at equivalent locations relative to each implant site according to ISO 10993-6. Of course, any proposed testing protocol must be planned with sensitivity to the 3 Rs of humane animal experimentation: replacement, reduction and refinement [131]. Initially, Wistar rats may be considered for use in a femur healing model investigation, however the rabbit femur may be selected preferentially because it is composed of bony tissue analagous to that of the human vertebrae, and is easily accessible for a surgical procedure. The potential biological study discussed here leaves unanswered the question of mechanical performance *in vivo*: clearly a rabbit femur healing model would not test implant robustness under vertebral compressive forces. To this end, future work is already slated to test the performance of a Dal Glass cement injected into a human cadaver spine and subjected to compressive forces.

Bibliography

1 A. Middleditch and J. Oliver. Functional anatomy of the spine. *Elsevier, Ltd., Philadelphia, PA, Volume 2*, 2005.

2 C. Dickman, M. Fehlings, and N. Gokaslan. Spinal cord and spinal column tumors: principles and practice. *Thieme Medical Publishers, Inc., New York, NY*, page 2, 2006.

3 G. Kayalioglu. The spinal cord: The vertebral column and spinal meninges. *Elsevier Academic Press, London, UK*, pages 17–36, 2009.

4 H. Gray. Gray's anatomy: The unabridged version of the american classic. *Running Press Book Publishers., Philadelphia, PA*, pages 34–54, 1999.

5 S. Standring and H. Gray. Gray's anatomy, 40th edition: Functional anatomy of the muskuloskeletal system. *Elsevier Limited*, 40:81–125, 2008.

6 W. Kahle and M. Frotscher. Color atlas of human anatomy: Nervous system and sensory organs. *Thieme, New York, NY*, 3:37–90, 2003.

7 W. Lewis and H. Gray. Anatomy of the human body. *Bartleby, New York, NY*, 20, 2000.

8 P. Kane and P. Ma. Mimicking the nanostructure of bone matrix to regenerate bone. *Materials Today*, 16(11):418–423, 2013.

9 S. Viguet-Carrin, P. Garnero, and P Delmas. The role of collagen in bone strength. *Osteoporosis International*, 17(3):319–336, 2006.

10 H. Horton. Principles of biochemistry. *Pearson Prentice Hall, Pearson Education, Inc., Upper Saddle River, NJ*, 4, 2006.

11 A. Parra-Torres, M. Valdes-Flores, and L. Orozco. Topics in osteoporosis: Molecular aspects of bone modeling. *InTech, Winchester, UK*, 2013.

12 H. Anderson. Matrix vesicles and calcification. *Current Rheumatology Reports*, 5(3):222–226, 2003.

13 M. Lynch, C. Capparelli, and J. Stein. Apoptosis during bone-like tissue development in vitro. *Journal of Cellular Biochemistry*, 68:31–49, 1998.

14 S. Cowin, L. Moss, and M. Moss. Candidates for the mechanosensory system in bone. *Journal of Biomechanical Engineering*, 113:191–197, 1991.

15 S. Teitelbaum. Bone resorption by osteoclasts. *Science*, 289(5484):1504–1508, 2000.

16 Z. Li, K. Kong, and W. Qi. Osteoclast and its roles in calcium metabolism and bone development and remodeling. *Biochemical and Biophysical Research Communications*, 343:345–350, 2006.

17 G. Mundy. Bone remodelling and its disorders. *Martin Dunitz Ltd., London, UK*, 20, 1999.

18 D. Steele and C. Bramblett. The anatomy and biology of the human skeleton. *Texas A&M University Press, USA*, 1988.

19 WHO. Men ageing and health: Achieving health across the life span. *World Health Organization, Geneva, Switzerland*, 1999.

20 D. Kim and A. Vaccaro. Osteoporotic compression fractures of the spine; current options and considerations for treatment. *The Spine Journal*, 6(5):479–487, 2006.

21 J. Mathis. Percutaneous vertebroplasty: a developing standard of care for vertebral compression fractures. *American Journal of Neuroradiology*, 22(2):373–381, 2001.

22 N. Boos and M. Aebi. Spinal disorders: Fundamentals of diagnosis and treatment. *Springer-Verlag, New York, NY*, pages 925–933, 2008.

23 EPOS. Incidence of vertebral fracture in europe: Results from the european prospective osteoporosis study (epos). *Journal of Bone and Mineral Research*, 17:716–724, 2002.

24 P. Heini. The current treatment - a survey of osteoporotic fracture treatment. *Osteoporosis International*, 16:S85–92, 2005.

25 T. Witham. Surgery insight: current management of epidural spinal cord compression from metastatic spine disease. *Nature Clinical Practice Neurology*, 2(2):87–94, 2006.

26 M. McGirt. Vertebroplasty and kyphoplasty for the treatment of vertebral compression fractures: An evidence-based review of the literature. *The Spine Journal*, 9(6):501–508, 2009.

27 D. Fourney. Percutaneous vertebroplasty and kyphoplasty for painful vertebral body fractures in cancer patients. *Journal of Neurosurgery*, 98(1):21–30, 2003.

28 J. Chevan and P. Clapis. Physical therapy management of low back pain: A case-based approach. *Jones and Bartlett Learning, Burlington, MA*, 2013.

29 M. Farrokhi, E. Alibai, and Z. Maghami. Randomized controlled trial of percutaneous vertebroplasty versus optimal medical management for the relief of pain and disability in acute osteoporotic vertebral compression fractures. *Journal of Neurosurgery: Spine*, 14(5):561–569, 2011.

30 D. Resnik, R. Haid, and J. Wang. Surgical management of low back pain. *Thieme Medical Publishers, Inc., New York, NY*, 2, 2009.

31 R. Hamdy and E. Lewiecki. Osteoporosis. *Oxford University Press, New York, NY*, pages 55–84, 2013.

32 R. McLain. Cancer in the spine: Comprehensive care. *Humana Press, Inc., Totowa, NJ*, pages 7–48, 2008.

33 J. Mathis, H. Daromond, and S. Belkoff. Percutaneous vertebroplasty. *Springer-Verlag New York, Inc. New York, NY*, 2002.

34 G. Lewis. Percutaneous vertebroplasty and kyphoplasty for the stand-alone augmentation of osteoporosis-induced vertebral compression fractures: present status and future directions. *Journal of Biomedical Materials Research. Part B: Applied Biomaterials*, 81(2):371–386, 2007.

35 P. Galibert. Preliminary note on the treatment of vertebral angioma by percutaneous acrylic vertebroplasty. *Neurochirurgie*, 33(2):166–168, 1987.

36 H. Deramond. Percutaneous vertebroplaty with polymethyl methacrylate. technique, indications and results. *Radiologic Clinics of North America*, 36:533–546, 1998.

37 R. Buchbinder. A randomized trial of vertebroplasty for painful osteoporotic vertebral fractures. *The New England Journal of Medicine*, 361:557–568, 2009.

38 D. Kallmes. A randomized trial of vertebroplasty for osteoporotic spinal fractures. *The New England Journal of Medicine*, 361:569–579, 2009.

39 J. Pereira and K. Winstein. Studies find no benefit to popular spine procedure. *The Wall Street Journal*, August 5, 2009.

40 S. Blair. Percutaneous vertebroplasty exposed as ineffective. *The Medical Journal*, August 6, 2009.

41 M. Baerlocher, P. Munk, and D. Liu. Trials of vertebroplasty for vertebral fractures. reply. *The New England Journal of Medicine*, 361(21):2099–2100, 2009.

42 C. Klazen. Vertebroplasty versus conservative treatment in acute osteoporotic vertebral compression fractures, (vertos ii): an open-label randomized trial. *Lancet*, 376(9746):1085–1092, 2010.

43 R. McGuire. Treating spinal compression fractures. *American Academy of Orthopaedic Surgeons*, 2010.

44 F. Miller, D. Kallmes, and R. Buchbinder. Vertebroplasty and the placebo response. *Radiology*, 259(3):621–625, 2011.

45 J. Barr. Position statement on percutaneous vertebral augmentation. *Journal of Vascular and Interventional Radiology*, 25(2):171–181, 2014.

46 T. Predey. Percutaneous vertebroplaty: new treatment for vertebral compression fractures. *American Family Physician*, 66(4):611–616, 2002.

47 S. Kim, B. Son, and S. Lee. Cardiac perforation due to intracardiac bone cement after percutaneous vertebroplasty. *Journal of Cardiac Surgery*, 29(4):499–500, 2014.

48 FDA. Guidelines for industry and fda staff - clinical trial considerations: Vertebral augmentation devices to treat spinal insufficiency fractures. *FDA guidance document: Medical devices and radiation-emitting products*, 2004.

49 M. Baerlocher. Quality improvement guidelines for percutaneous vertebroplasty. *Journal of Vascular Interventional Radiology*, 25:165–170, 2014.

50 G. Lewis. Injectable bone cements for use in vertebroplasty and kyphoplasty: State-of-the-art review. *Journal of biomedical materials research. Part B, Applied biomaterials*, 6(5):456–468, 2005.

51 C. Kelly and R. Wilkins. Treatment of benign bone lesions with an injectable calcium sulphate-based bone graft substitute. *Orthopedics*, 27(Suppl.):S123–S125, 2004.

52 B. Tay, V. Patel, and D. Bradford. Calcium sulphate and calcium phosphate-based bone substitutes. mimicry of the mineral phase of bone. *Orthopedic Clinics of North America*, 30:615–623, 1999.

53 R. O'Hara. Optimization of the mechanical and handling properties of an injectable calcium phosphate cement. *Journal of Materials Science: Materials in Medicine*, 21(8):2299–2305, 2010.

54 T. Duane, E. Jaeger, and W. Tasman. Duane's ophthalmology: Duane's clinical ophthalmology. *Lippincott Williams and Wilkins, Philadelphia*, 6, 2011.

55 T. Kindt-Larson, D. Smith, and J Jensen. Innovations in acrylic bone cement and application equipment. *Journal of Applied Biomaterials*, 6(1):75–83, 1995.

56 J. Palussiere. Clinical results of an open perspective study of a bis-gma composite in percutaneous vertebral augmentation. *European Spine Journal*, 14(10):982–991, 2005.

57 E. Middleton. The safety and efficacy of vertebroplasty using cortoss cement in a newly established vertebroplasty service. *British Journal of Neurosurgery*, 22(2):252–256, 2008.

58 S. Cho and A. Cheng. A review of glass-ionomer restorations in the primary dentition. *Journal of the Canadian Dental Association*, 65(9):491–495, 1999.

59 I. Sherwood. Essentials of operative dentistry. *Jaypee Brothers Medical Publishers, Inc., New Delhi, India*, 2010.

60 Y. Gu. Effects of incorporation of ha/zro_2 into glass ionomer cement (gic). *Biomaterials*, 26:713–720, 2005.

61 P. Hatton and G. Palmer. Drug device combination products - delivery technologies and applications: Glass ionomer cements as drug-device combination products. *Woodhead Publishing, Cambridge, UK*, pages 219–229, 2009.

62 A.D. Wilson and B.E. Kent. The glass-ionomer cement: a new translucent dental filling material. *Journal of Applied Chemistry and Biotechnology*, 21:313, 1972.

63 L. Jonck and C. Grobbelaar. The biocompatibility of glass-ionomer cement in joint replacement: bulk testing. *Clinical Materials*, 4:85–107, 1989.

64 L. Jonck and C. Grobbelaar. Biological evaluation of glass-ionomer cement (ketac-0) as an interface material in total joint replacement. a screening test. *Clinical Materials*, 4:201–224, 1989.

65 L.M. Jonck and C.J. Grobbelaar. Ionos bone cement (glass-ionomer): an experimental and clinical evaluation in joint replacement. *Clinical Materials*, 6(11):323–359, 1990.

66 G. Babigian. Use of a glass ionomer cement in otological surgery. a primary report. *Journal of Laryngology and Otology*, 106(4):954–959, 1992.

67 R.T. Ramsden, R.C.D. Herdman, and R.H. Lye. Ionomeric bone cement in neuro-otologic surgery. *Journal of Laryngology and Otology*, 106(11):949–953, 1992.

68 J. Helms and G. Geyer. Closure of the petrous apex of the temporal bone with ionomeric cement following translabyrinthine removal of an acoustic neuroma. *Journal of Laryngology and Otology*, 108(3):202–205, 1994.

69 H.G. Kempf, P.R. Issing, and T. Lenarz. Ionomeric cement in cochlear implant surgery - application and long-term outcome. *Laryngo-Rhino-Otologie*, 75:388–391, 1996.

70 G. Geyer and J Helms. Ionomer-based cement as a bone substitute in reconstructive middle ear surgery. *Hno*, 45:442–447, 1997.

71 G. Geyer. Ionomer-based cement used as bone substitute in the rabbit's middle ear. *Hno*, 45:222–226, 1997.

72 M.M. Maassen and H.P. Zenner. Tympanoplasty type ii with ionomeric cement and titanium-gold-angle prostheses. *American Journal of Otology*, 19:693–699, 1998.

73 A.D. Kjeldsen and A.M. Grontved. Tympanoplasty with ionomeric cement. *Acta Otolaryngologica*, Suppl. 543:130–131, 2000.

74 D. Kupperman and R.A. Tange. Ionomeric cement in the human middle ear cavity: Long-term results of 23 cases. *Laryngoscope*, 111:306–309, 2001.

75 J.L. Renard, D. Felten, and D. Bequet. Post-otoneurosurgery aluminum encephalopathy [letter]. *Lancet*, 344(8914):63–64, 1994.

76 P. Hantson. Encephalopathy with seizures after use of aluminium-containingbone cement. *The Lancet*, 344(8937):1647, 1994.

77 O. Guillard. Biological levels of aluminium use after aluminium-containing bone cement in post-otoneurosurgery. *Journal of Trace Elements in Medicine*, 11:53–56, 1997.

78 E. Reusche. Subacute fatal aluminum encephalopathy after reconstructive otoneurosurgery: A case report. *Human Pathology*, 32(10):1136–1140, 2001.

79 M. Blades, D. Moore, and P. Revell. In vivo skeletal response and biomechanical assessment of two novel polyalkenoate cements following femoral implantation in the female new zealand white rabbit. *Journal of Materials Science: Materials in Medicine*, 9:701–706, 1998.

80 K. Johal. In vivo response of strontium and zinc-based ionomeric cement implants in bone. *Journal of Materials Science: Materials in Medicine*, 13:375–379, 2002.

81 G. Granstroem, J. Holmquist, and A. Tjellstroem. Facial nerve paralysis following repair of the externalear canal with ionomeric cement. *Ear, Nose and Throat Journal*, 79(7):495–498, 2000.

82 C. Baier, G. Geyer, R. Dieler, and J. Helms. Long-term results after skull base reconstruction with ionomeric cement. *Laryngo-Rhino-Otologie*, 77:467–473, 1998.

83 E. Engelbrecht, G. Foerster, and G. Delling. Ionogran in revision arthroplasty. *The Bone and Joint Journal*, 82(2):192–199, 2000.

84 R. Weber, W. Draf, G. Kahle, and M. Kind. Obliteration of the frontal sinus–state of the art and reflections on new materials. *Rhinology*, 37:1–15, 1999.

85 M. Wolfgang. Biomaterials in skull base surgery. *GMS Current Topics in Otorhinolaryngology, Head and Neck Surgery*, 8:1–14, 2009.

86 P. Heini and U. Berlemann. Bone substitutes in vertebroplasty. *European Spine Journal*, 10:S205–213, 2001.

87 B. Dickey. Novel adaptations to zincsilicate glass polyalkenoate cements: The unexpected influences of germanium based glasses on handling characteristics and mechanical properties. *Journal of the Mechanical Behaviour of Biomedical Materials*, 23:8–21, 2013.

88 J. Nicholson and B. Czarnecka. Role of aluminum in glass-ionomer dental cements and its biological effects. *Journal of Biomaterials Applications*, 24:293–308, 2009.

89 A. Wilson and J. Nicholson. Acid-base cements: their biomedical and industrial applications. *Cambridge University Press, Cambridge, UK*, 1993.

90 D. Boyd and M. Towler. The processing, meachanical properties and bioactivity of zinc based glass ionomer cements. *Journal of Materials Science: Materials M*, 16:843–850, 2005.

91 D. Boyd, O. Clarking, and M. Towler. Zinc-based glass polyalkenoate cements with improved setting times and mechanical properties. *Acta Biomaterialia*, 4(2):425–431, 2008.

92 D. Boyd, M. Towler, and M. Watts. The role of sr2+ on the structure and reactivity of sro-cao-ano-sio2 ionomer glasses. *Journal of Materials Science: Materials in Medicine*, 19:953–957, 2008.

93 A. Wren, D. Boyd, and M. Towler. The processing, mechanical properties and bioactivity of strontium based glass polyalkenoate cements. *Journal of Materials Science: Materials in Medicine*, 19:1737–1743, 2008.

94 O. Clarkin, D. Boyd, and M. Towler. Comparison of an experimental bone cement with a commercial control, hydroset. *Journal of Materials Science: Materials in Medicine*, 20:1563–1570, 2009.

95 O. Clarkin, D. Boyd, and M. Towler. Strontium-based glass polyalkenoate cements for luting applications in the skeleton. *Journal of Biomaterials Applications*, 24:483–502, 2010.

96 A. Wren, R. Laffir, and M. Towler. The structural role of titanium in ca-sr-zn-si/ti glasses for medical applications. *Journal of Non-Crystalline Solids*, 357:1021–1026, 2011.

97 F. Gomes, R. Pires, and R. Reis. Aluminum-free glass-ionomer bone cements with enhanced bioactivity and biodegradability. *Materials Science and Engineering: C*, 33(3):1361–1370, 2013.

98 D. Boyd, B. Dickey, S. Kehoe, and V. Dickinson. Germanium-based glass polyalkenoate cement. *Patent Publication number: WO2013164696 A1*, 2013.

99 S. Tao and P. Bolger. Hazard assessment of germanium supplements. *Regulatory Toxicology and Pharmacology*, 25:211–219, 1997.

100 S. Choi. Synthesis and biological evaluation of water-soluble organogermanium. *European Journal of Medicinal Chemistry*, 45:1654–1656, 2010.

101 K. Yokoi. Dermal absorption of inorganic germanium in rats. *Regulatory Toxicology and Pharmacology*, 52:169–173, 2008.

102 B. Gerber and A. Leonard. Mutagenicity, carcinogenicity and teratogenicity of germanium compounds. *Reviews in Mutation Research*, 387(3):141–146, 1997.

103 P. Farrugia. Research questions, hypotheses, and objectives. *Canadian Journal of Surgery*, 53(4):278–281, 2010.

104 AD. Neve, V. Piddock, and EC. Combe. The effect of glass heat treatment on the properties of a novel polyalkenoate cement. *Clinical Materials*, 12(2):113–115, 1993.

105 International Standards Organization. Biological evaluation of medical devices, part 14: Identification and quantification of degradation products from ceramics. *European Committee for Standardization*, 2009.

106 C. Kirkpatrick and C. Mittermayer. Theoretical and practical aspects of testing potential biomaterials in vitro. *Journal of Materials Science: Materials in Medicine I*, 1(1):9–13, 1990.

107 B. Ratner. Biomaterials science: An introduction to materials in medicine. *Elsevier Academic Press, Inc., London, UK, Second Ed.*, pages 355–359, 2004.

108 Match! phase identification from powder diffraction. *Crystal Impact Gbr*, http://www.crystalimpact.com/match/:1997–2014.

109 International Standards Organization. Biological evaluation of medical devices, part 5: Tests for in vitro cytotoxicity. *European Committee for Standardization*, 2009.

110 P. Whitcomb and M. Anderson. Doe simplified: practical tools for effective experimentation. *Productivity Inc., New York, NY*, 2000.

111 S. Kehoe, N. Kilcup, and D. Boyd. Evaluation of cytotoxicity for novel composite embolic microspheres: Material optimization by response surface methodology. *Materials Letters*, pages 13–17, 2012.

112 P. Richet. Geo2 vs. sio2: Glass transitions and thermodynamic properties of polymorphs. *Physics and Chemistry of Minerals*, 17:79–88, 1990.

113 R. Hill and D. Brauer. Predicting the glass transition temperature of bioactive glasses from their molecular chemical composition. *Acta Biomaterialia*, 7:3601–3605, 2011.

114 A. Paul. Chemistry of glasses. *Chapman and Hall, New York, NY*, 1982.

115 M. Weidenbruch. Compounds containing silicon, germanium, and tin polyhedra: The first octahedral tin cluster. *Angewandte Chemie*, 32(4):545–546, 2003.

116 R. Jugdaohsingh. Germanium-based glass polyalkenoate cement. *The Journal of Nutrition Health and Aging*, 11(2):99–110, 2013.

117 Fisher. Materials safety data sheet: Germanium (iv) oxide. *Acros Organics*, 2012.

118 Fisher. Materials safety data sheet: Arsenic oxide. *Acros Organics*, 2011.

119 E. Jallot, H. Benhayoune, and G. Balossier. An original method to assess short-term physicochemical reactions at the periphery of bioactive glass particles in biological fluids. *American Chemical Society: Langmuir*, 17(15):4467–4470, 2001.

120 A. Tilocca. Sodium migration pathways in multicomponent silicate glasses: Carparrinello molecular dynamics simulations. *The Journal of Chemical Physics*, 133(014701):1–10, 2010.

121 F. Angeli, T. Charpentier, and D. Ligny. Boron speciation in soda-lime borosilicate glasses containing zirconium. *Journal of the American Ceramic Society*, 93:2693–2704, 2010.

122 J. van Meerloo, G. Kaspers, and J. Cloos. Cell sensitivity assays: the mtt assay. *Methods of Molecular Biology*, 731:237–245, 2011.

123 E. Place, N. Evans, and M. Stevens. Complexity in biomaterials for tissue engineering. *Nature Materials*, 8:457–470, 2009.

124 L. Zhuravlev. The surface chemistry of amorphous silica. zhuravlev model. *Colloids and Surfaces A: Physicochemical and Engineering Aspects*, 173:1–38, 2000.

125 R. Brill. Glass chemistry. *General Books Llc.*, 2011.

126 C. Lipinski and A. Hopkins. Navigating chemical space for biology and medicine. *Nature*, 432:855–861, 2004.

127 M. Bohner and J. Lemaitre. Can bioactivity be tested in vitro with sbf solution? *Biomaterials*, 30:2175–2179, 2009.

128 ISO. Biological evaluation of medical devices, part 1: Evaluation and testing. *European Committee for Standardization*, 2003.

129 FDA. Medical devices guidance document: Use of international standard iso 10993 - biological evaluation of medical devices part 1: Evaluation and testing. *US Food and Drug Administration*, 1995.

130 ISO. Biological evaluation of medical devices, part 6: Tests for local effects after implantation. *ISO; European Committee for Standardization*, 2007.

131 A. Goldberg. The principles of humane experimental technique: Is it relevant today? Published Plenary Lecture, 2010.

Appendix A

Degradation Product Maxima

Glasses:

The maximum mean Ca^{2+}, Ge^{4+}, Si^{4+}, Na^{+}, Sr^{2+}, and Zn^{2+}, Zr^{4+} release concentration expressed as Mean±SD

	Germanate glasses				Silicate glasses				Mix Glasses			
	Maximum mean ± SD (ppm)											
	gDG1	gDG2	gDG3	gDG4	gDS1	gDS2	gDS3	gDS4	gDM1	gDM2	gDM3	gDM4
Ca^{2+}	0.79±0.08	0.5±0.5	1.2±0.9	1.6±0.9	1.5±0.4	1.49±0.05	1.78±0.03	2.0±0.2	2±1	6±3	2.6±0.2	1.9±0.1
Ge^{4+}	102±6	370±10	90±30	132±8	NA				34±9	50±10	34±3	37±2
Si^{4+}	NA				2±2	3.5±0.1	3.3±0.1	2.2±0.4	9±5	11.7±0.5	7.8±0.7	10.1±0.2
Na^{+}	NA	110±4	10±10	104±5	NA	0.71±0.02	0.27±0.04	0.4±0.1	20±10	11.6±0.7	5.8±0.6	5.9±0.9
Zr^{4+}	NA	0.09±0.01	0.07±0	0.07±0	NA	0.07±0	0.07±0	0.070±0.004	0.07±0.004	0.07±0	0.07±0	0.07±0
Zn^{2+}	0.03±0.01	0.2±0.1	0.05±0.03	0.018±0.004	1.0±0.8	0.59±0.04	1.1±0.2	0.7±0.2	0.08±0.05	0.09±0.05	0.25±0.05	0.6±0.2
Sr^{2+}	20±2	4.7±0.7	11±8	8±1	1.4±0.2	2.10±0.03	2.1±0.1	1.7±0.2	4±3	18±3	9±1	11.7±0.3

Cements:

The maximum mean Ca^{2+}, Ge^{4+}, Si^{4+}, Na^{+}, Sr^{2+}, and Zn^{2+}, Zr^{4+} release concentration expressed as Mean±SD (ppm)

	Germanate glasses				Silicate glasses				Mix Glasses			
	Maximum mean ± SD (ppm)											
	cDG1	cDG2	cDG3	cDG4	cDS1	cDS2	cDS3	cDS4	cDM1	cDM2	cDM3	cDM4
Ca^{2+}	1.9±0.5	0.1±0.1	0.01±0.01	0.2±0.2	1.7±0.1	1.1±0.2	0.05±0.09	1.0±0.5	0±0	0.04±0.07	0.03±0.03	0.02±0.04
Ge^{4+}	200±60	160±10	160±40	80±10	NA				66±7	43±4	49±5	89±7
Si^{4+}	NA				45±7	40.6±0.9	27±2	31±3	15±2	15±2	14±4	23.4±0.2
Na^{+}	NA	14±3	19±5	17±3	NA	32±4	7.0±0.1	15±4	15±3	11±1	11±3	10.1±0.7
Zr^{4+}	NA	0.090±0.008	0.12±0.03	0.08±0	NA	0.17±0.02	0.14±0.01	0.20±0.02	0.11±0.01	0.11±0.01	0.12±0.01	0.140±0.004
Zn^{2+}	0.148±0.004	1±1	0.10±0.08	0.1±0.1	0.91±0.07	58±9	0.3±0.5	5±3	0.05±0.01	0.2±0.2	0.06±0.02	0.2±0.2
Sr^{2+}	2.3±0.6	0.1±0.1	0.04±0.02	0.1±0.1	2.0±0.2	5±1	0.04±0.04	0.6±0.3	0.013±0.009	0.03±0.03	0.018±0.008	0.05±0.05

Appendix B

Degradation Product Statistical Analyses for Relevant Ions

DG Glasses: Si^{4+}**,** Ge^{4+}**,** Ca^{2+} **and** Sr^{2+}

Statistical analyses of silicon, germanium, sodium and strontium dissolution data for DG glasses is provided in B.1, B.2, B.3, and B.4, respectively.

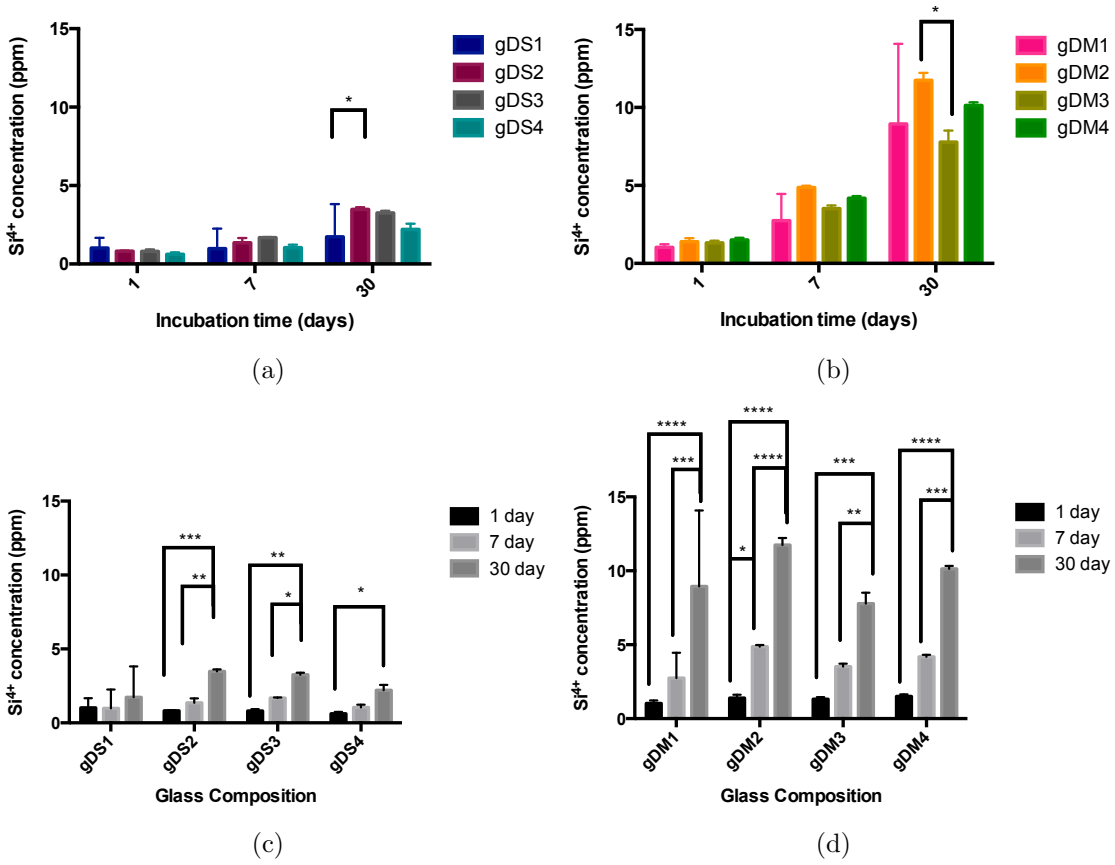

(a) (b) (c) (d)

Figure B.1: Two-way ANOVA test results for the Si^{4+} ion release of the 8 DG silicon containing glasses: silicate (a) and mixed (b) glasses with respect to each other; and silicate (c) and mixed (d) glasses over time

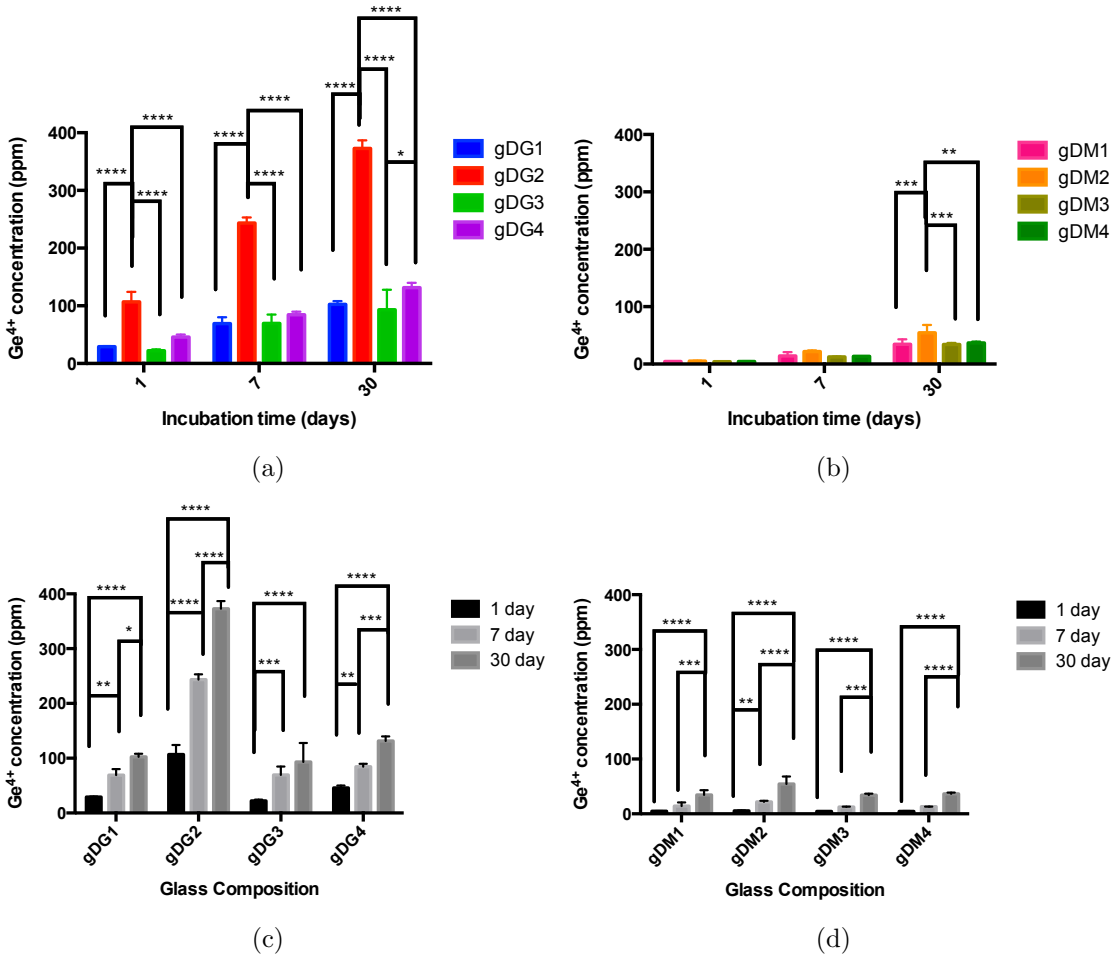

Figure B.2: Two-way ANOVA test results for the Ge^{4+} ion release of the 8 DG germanium containing glasses: germanate (a) and mixed (b) glasses with respect to each other; and germanate (c) and mixed (d) glasses over time

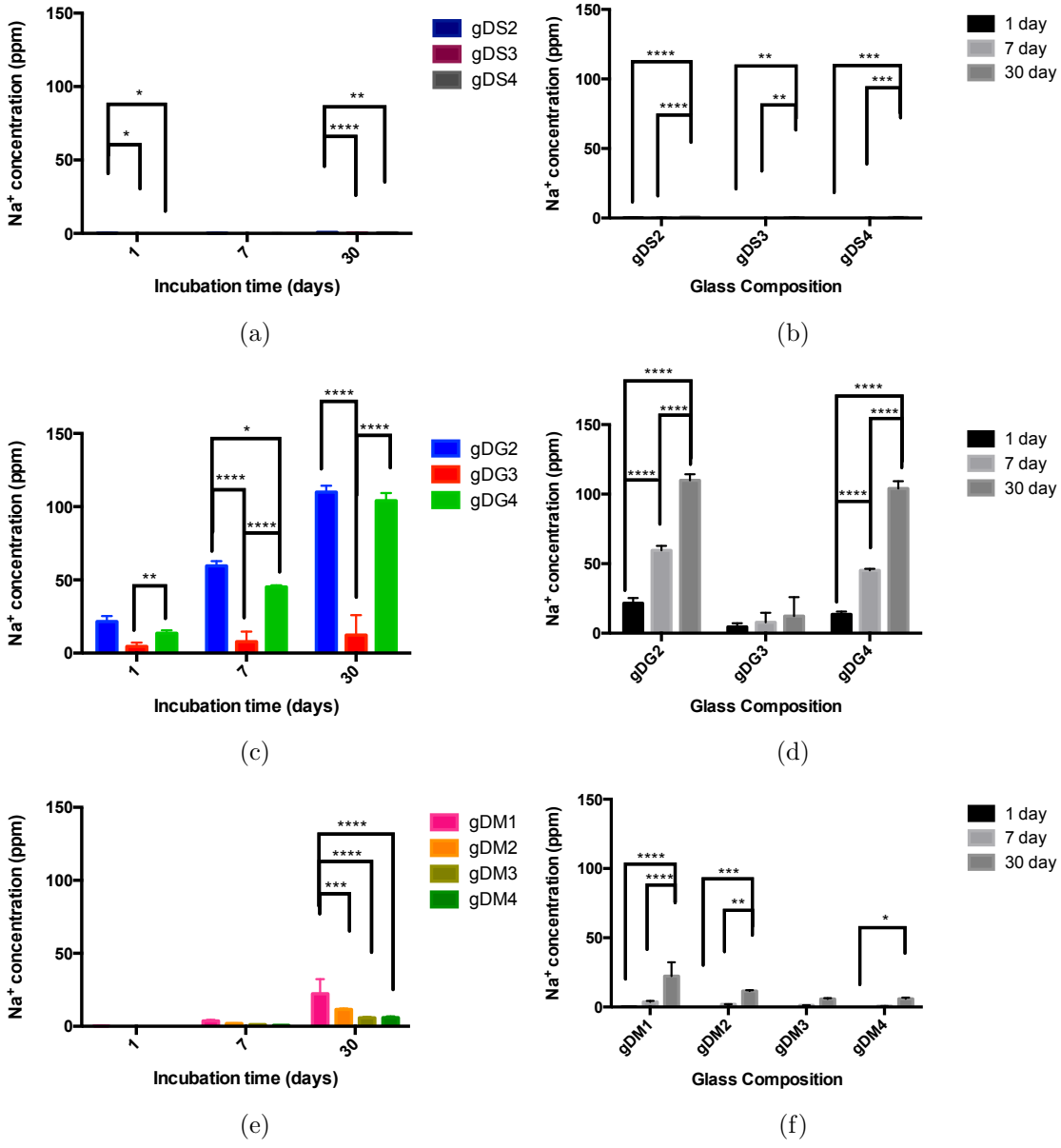

Figure B.3: Two-way ANOVA test results for the Na^+ ion release of DG glasses: silicate cements compared with each other (a) and over time (b); germanate cements compared with each other (c) and over time (d); and mixed cements compared with each other (e) and over time (f)

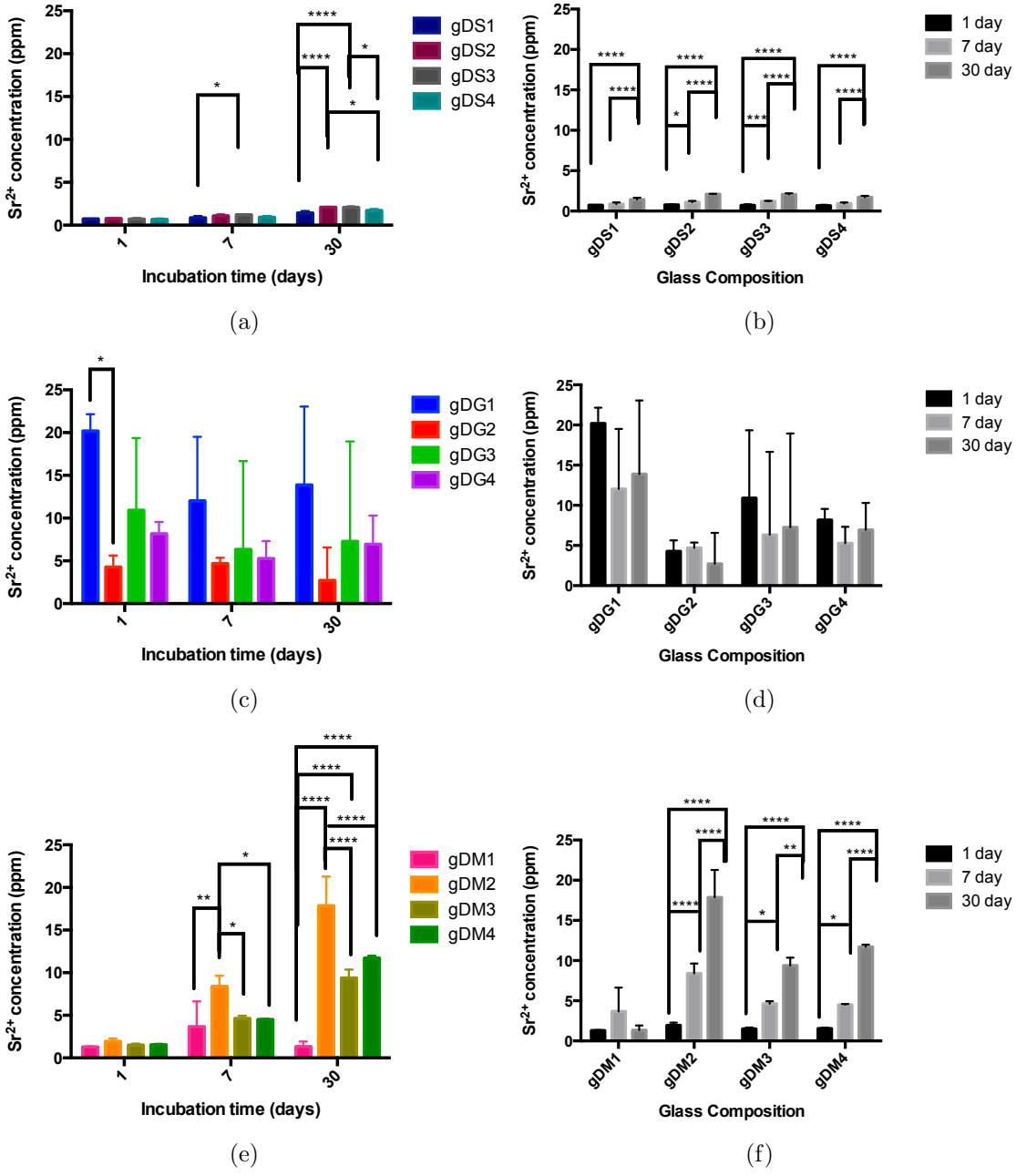

Figure B.4: Two-way ANOVA test results for the Sr^{2+} ion release of DG glasses: silicate cements compared with each other (a) and over time (b); germanate cements compared with each other (c) and over time (d); and mixed cements compared with each other (e) and over time (f)

DG Cements: Si^{4+}, Ge^{4+} and Na^{2+}

Statistical analysis of silicon dissolution data is provided in B.5.

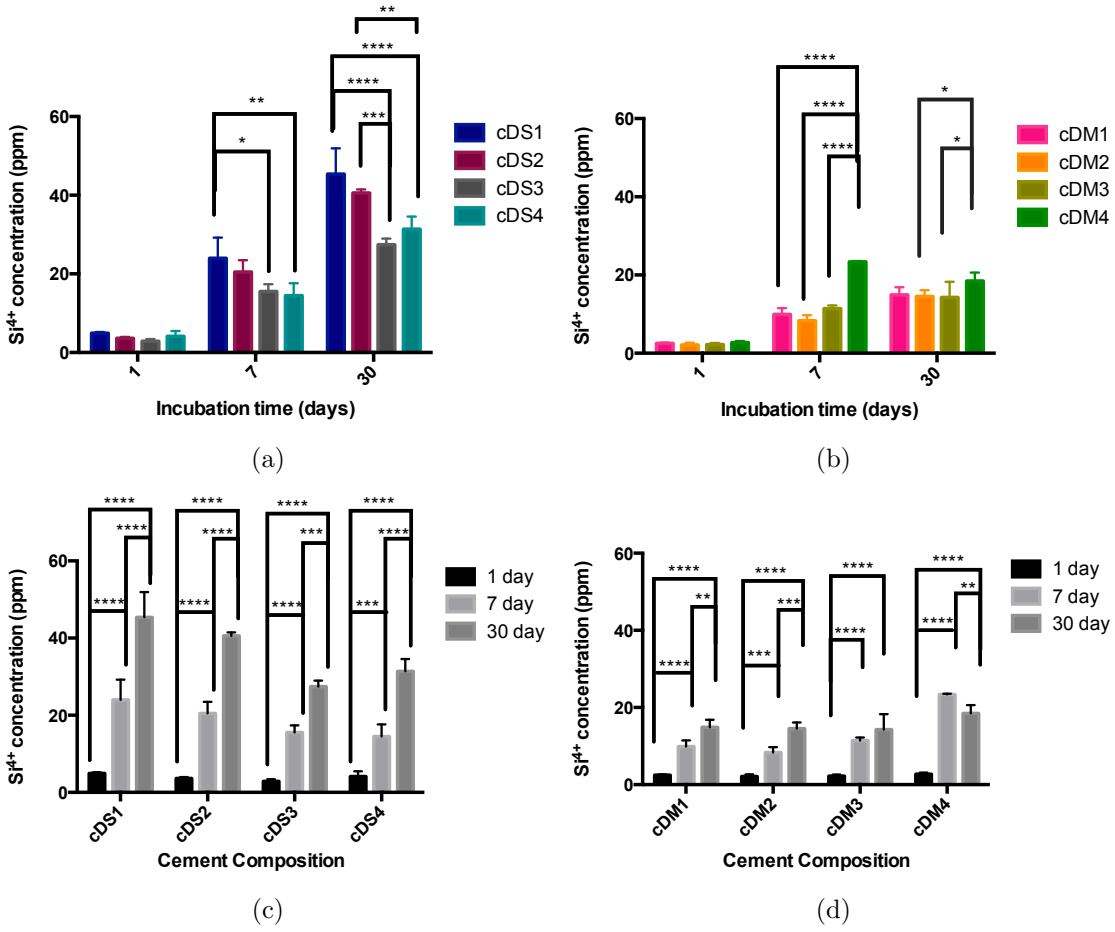

Figure B.5: Two-way ANOVA test results for the Si^{4+} ion release of the 8 DG silicon containing cements: silicate cements compared with each other (a) and over time (c); and mixed cements compared with each other (b) and over time (d)

Statistical analysis of germanium dissolution data is provided in B.6.

Statistical analysis of sodium dissolution data is provided in B.7.

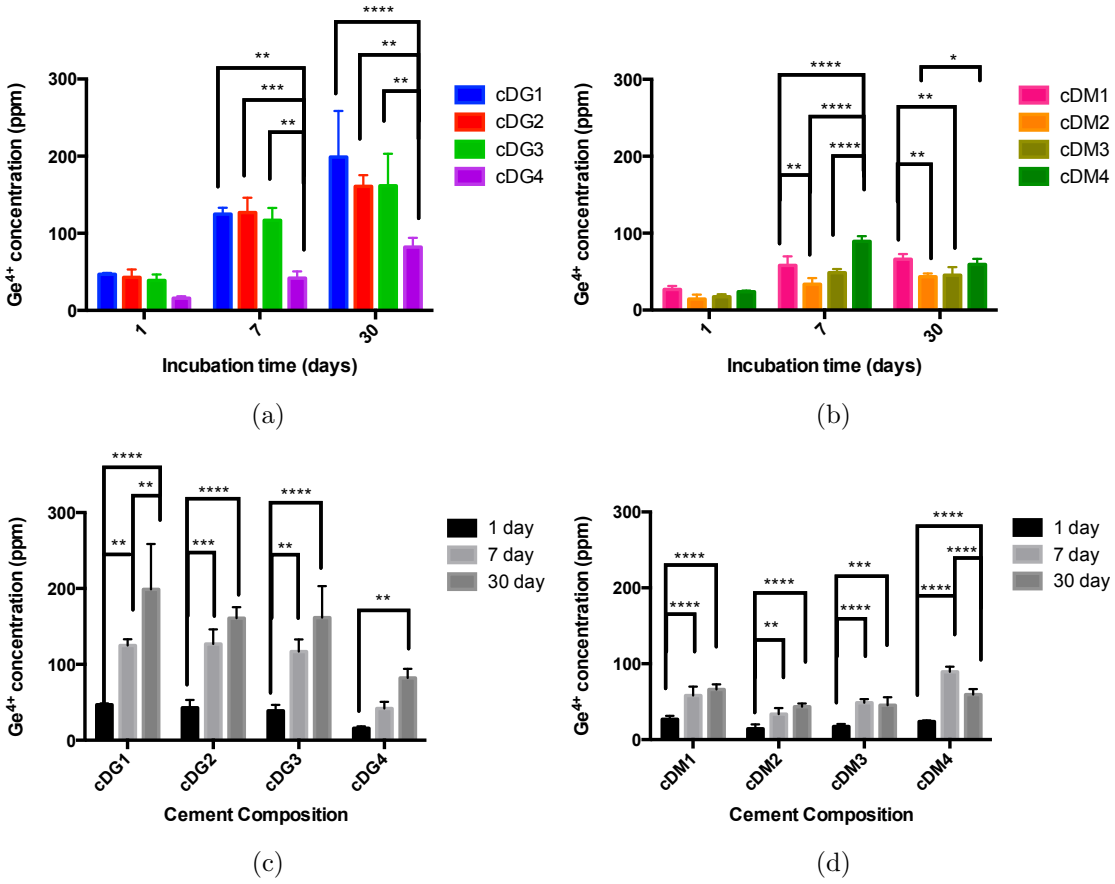

Figure B.6: Two-way ANOVA test results for the Ge^{4+} ion release of the 8 DG germanium containing cements: germanate cements compared with each other (a) and over time (c); and mixed cements compared with each other (b) and over time (d)

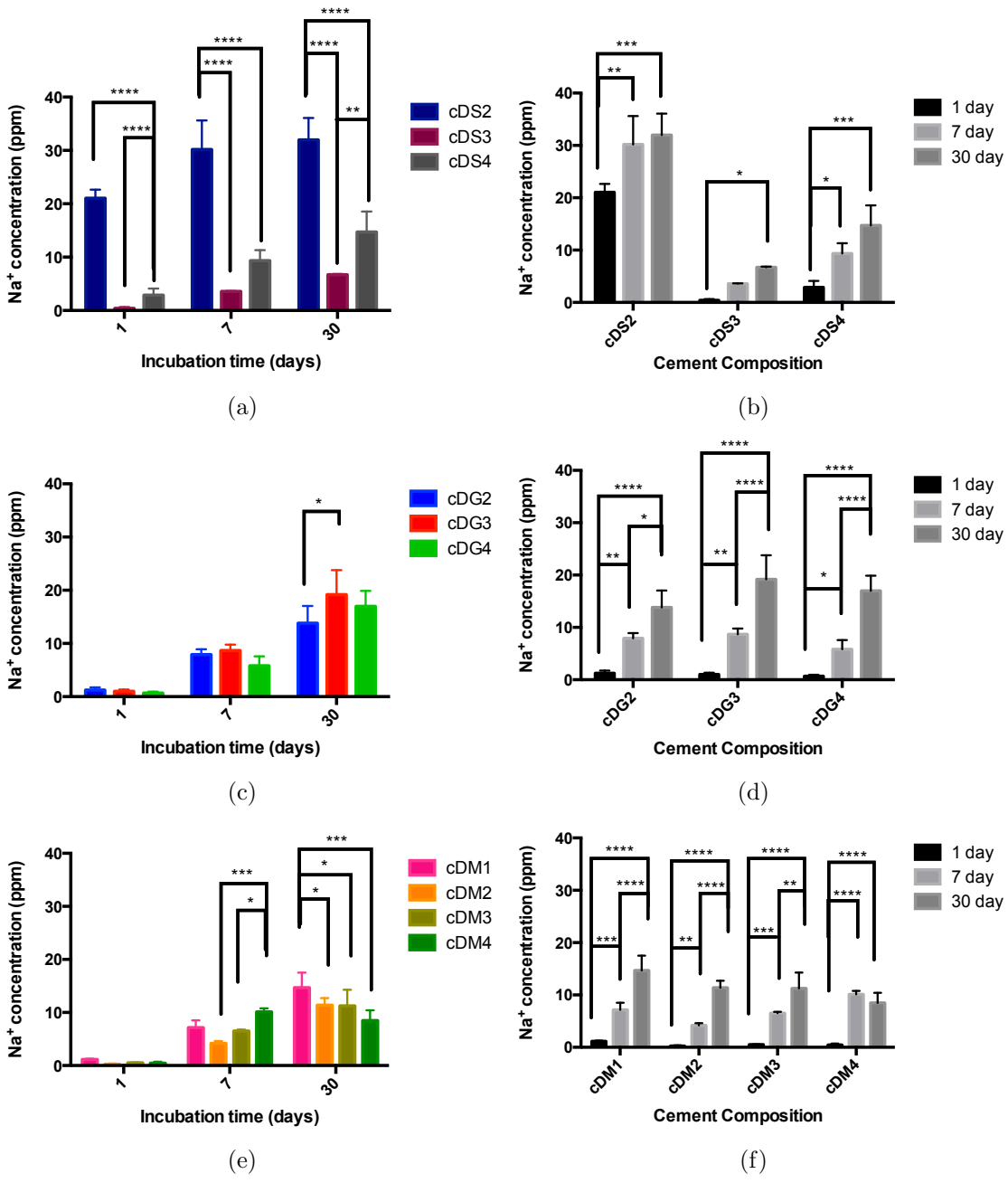

Figure B.7: Two-way ANOVA test results for the Na^+ ion release of DG cements: silicate cements compared with each other (a) and over time (b); germanate cements compared with each other (c) and over time (d); and mixed cements compared with each other (e) and over time (f)

Appendix C

Data for Low Release Ions

DG Glasses: Ca^{2+}, Zn^{2+} **and** Zr^{4+}

The Ca^{2+} ion release levels for each calcium containing glass composition (after incubation at 1, 7 and 30 days) are shown in figure C.1.

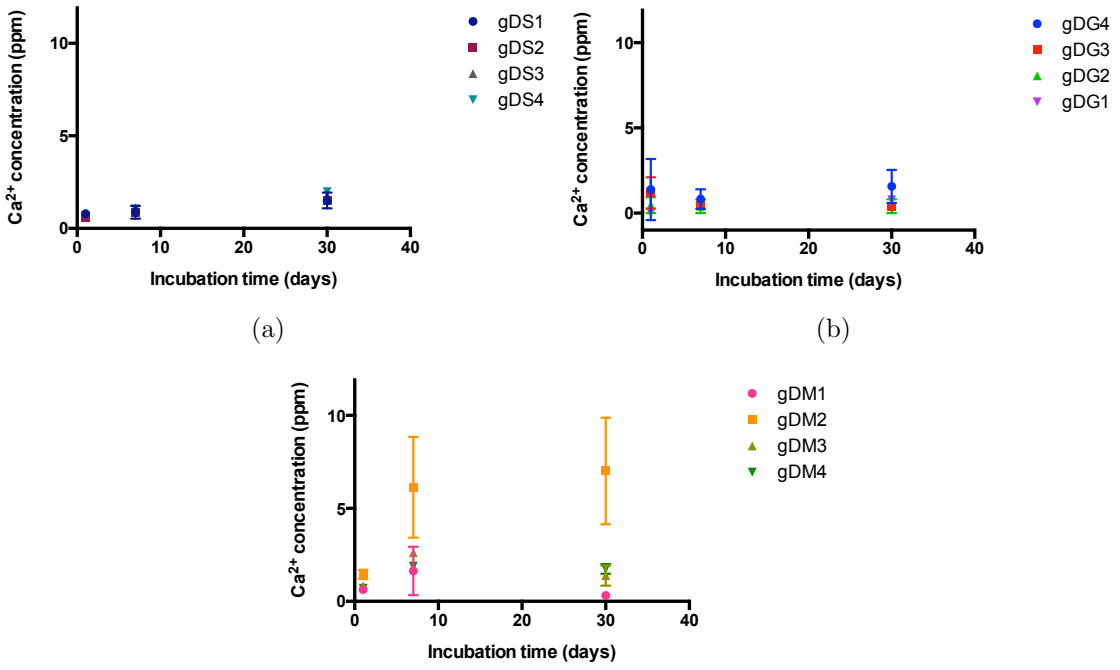

Figure C.1: The Ca^{2+} ion release levels of DG glasses with time dependency: (a) silicate glasses, (b) germanate glasses, and (c) mixed former glasses over 1, 7 and 30 day incubation periods.

The Zn^{2+} ion release levels for each zinc containing glass composition (after incubation at 1, 7 and 30 days) are shown in figure C.2.

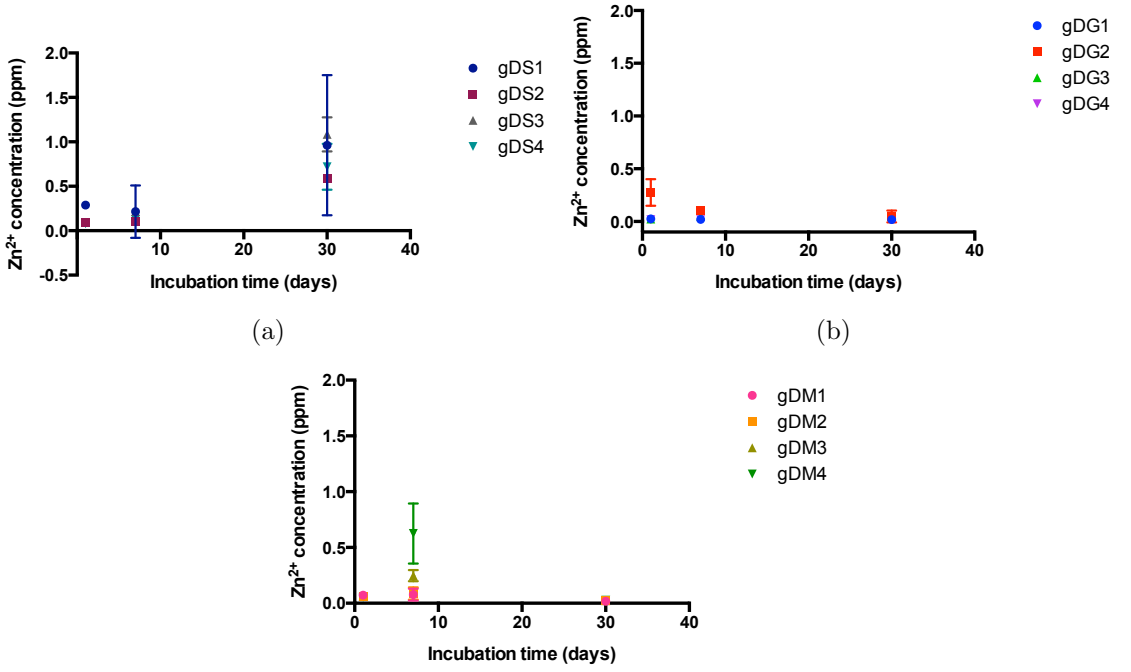

Figure C.2: The Zn^{2+} ion release levels of DG glasses with time dependency: (a) silicate glasses, (b) germanate glasses, and (c) mixed former glasses over 1, 7 and 30 day incubation periods.

The Zr^{4+} ion release levels for each zirconium containing glass composition (after incubation at 1, 7 and 30 days) are shown in figure C.3.

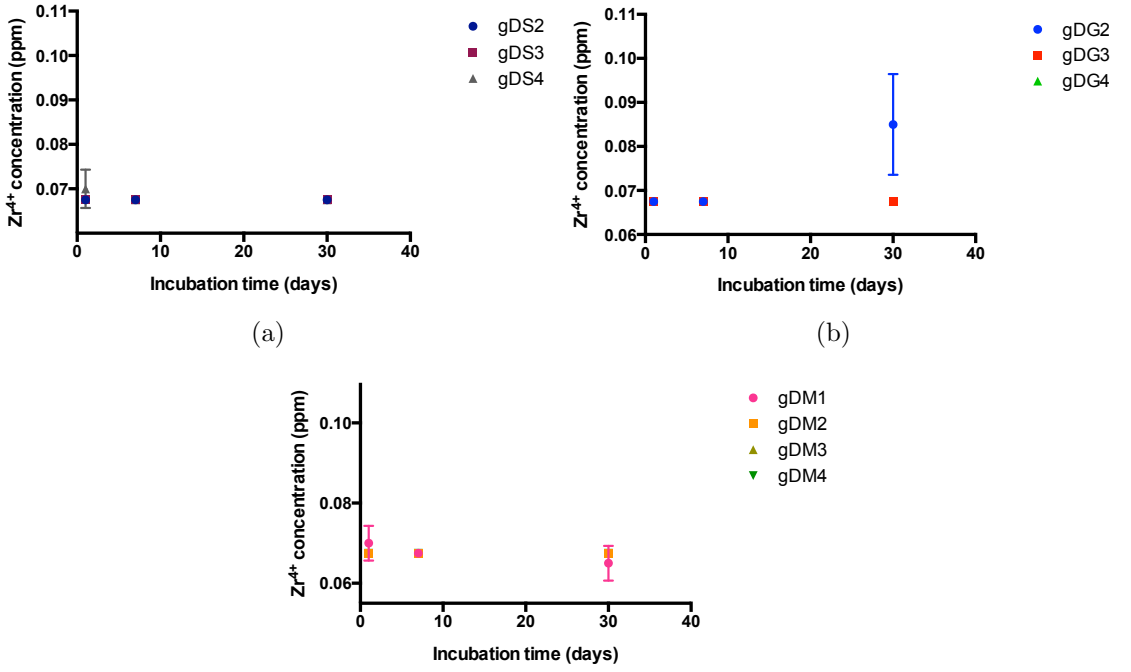

Figure C.3: The Zr^{4+} ion release levels of DG glasses with time dependency: (a) silicate glasses, (b) germanate glasses, and (c) mixed former glasses over 1, 7 and 30 day incubation periods.

DG Cements: Ca^{2+}, Sr^{2+}, Zn^{2+}, Zr^{4+}

The Ca^{2+} ion release levels for each calcium containing cement composition (after incubation at 1, 7 and 30 days) are shown in figure C.4.

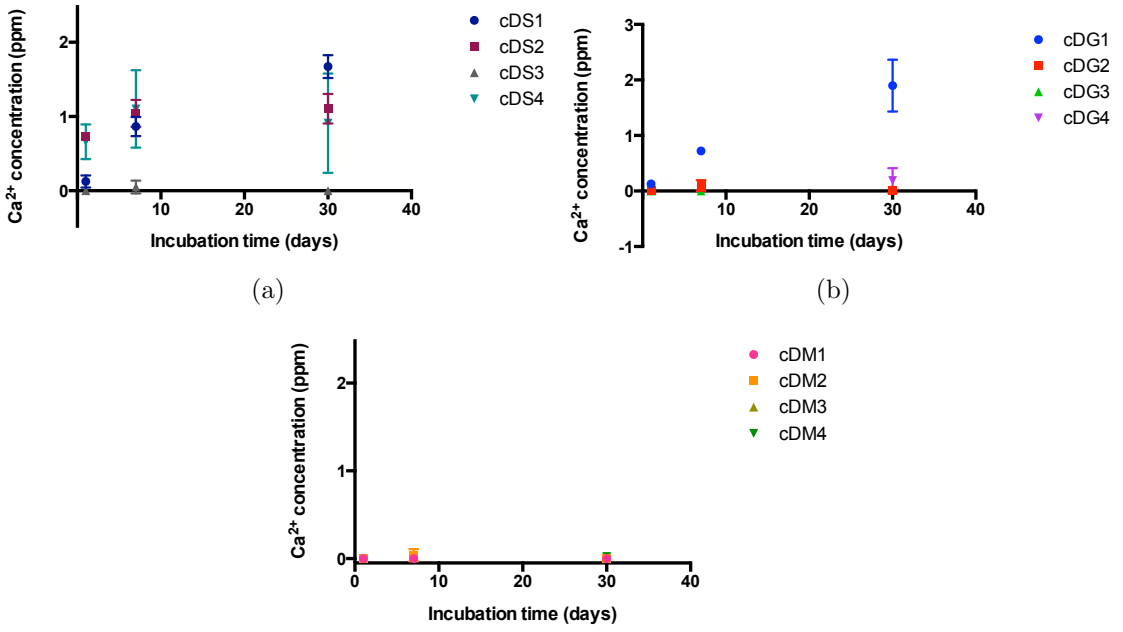

Figure C.4: The Ca^{2+} ion release levels of DG cements with time dependency: (a) silicate cements, (b) germanate cements, and (c) mixed former cements over 1, 7 and 30 day incubation periods.

The Sr^{2+} ion release levels for each strontium containing cement composition (after incubation at 1, 7 and 30 days) are shown in figure C.5.

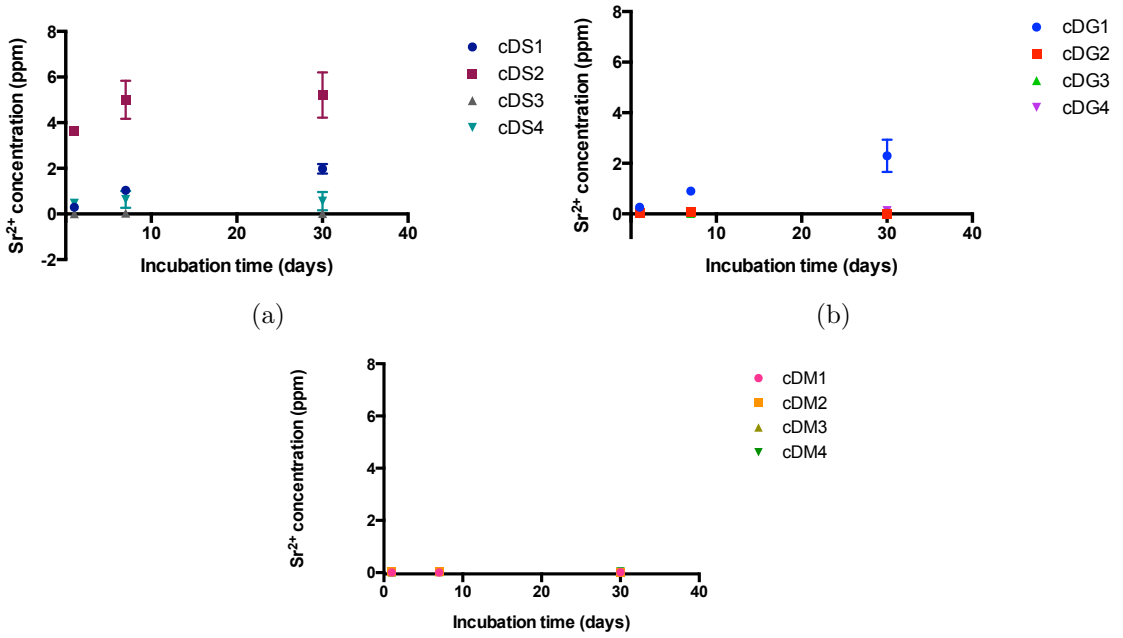

Figure C.5: The Sr^{2+} ion release levels of DG cements with time dependency: (a) silicate cements, (b) germanate cements, and (c) mixed former cements over 1, 7 and 30 day incubation periods.

The Zn^{2+} ion release levels for each zinc containing cement composition (after incubation at 1, 7 and 30 days) are shown in figure C.6. (cDS2 was a cement that never set as a hydrolytically stable mass.)

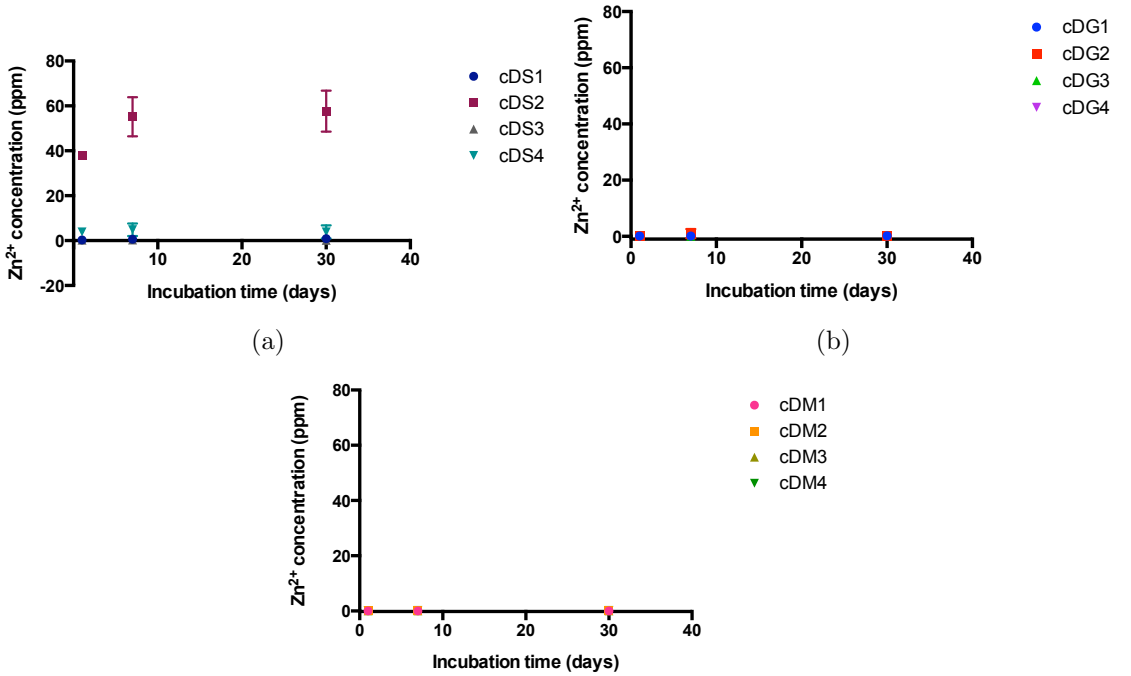

Figure C.6: The Zn^{2+} ion release levels of DG cements with time dependency: (a) silicate cements, (b) germanate cements, and (c) mixed former cements over 1, 7 and 30 day incubation periods.

The Zr^{4+} ion release levels for each zirconium containing cement composition (after incubation at 1, 7 and 30 days) are shown in figure C.7.

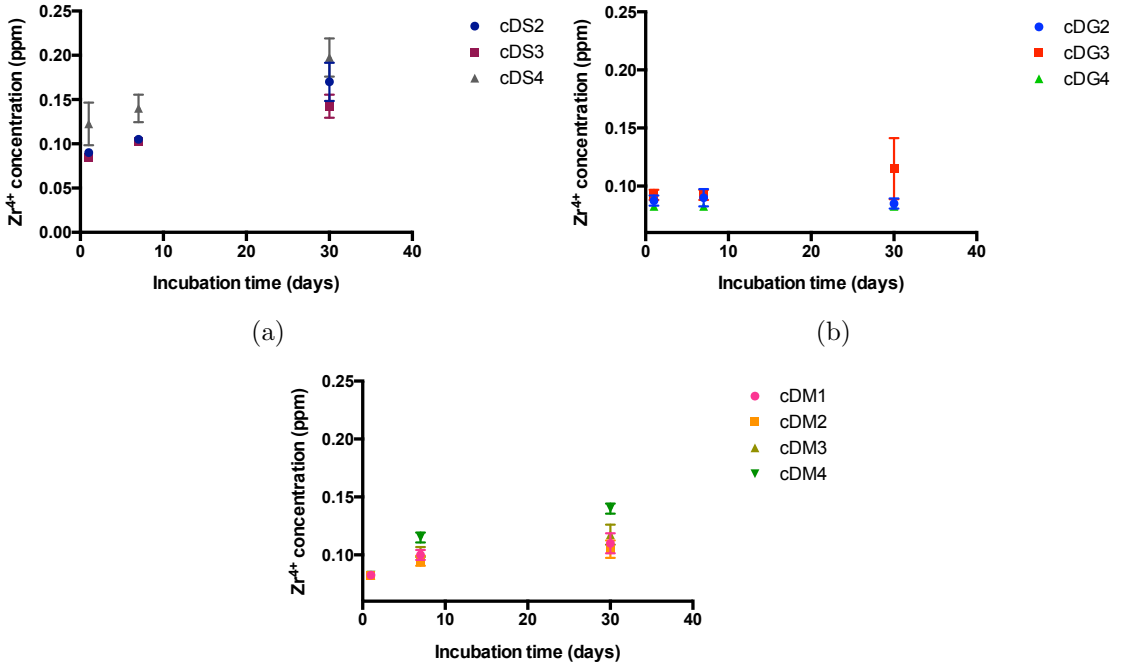

Figure C.7: The Zr^{4+} ion release levels of DG cements with time dependency: (a) silicate cements, (b) germanate cements, and (c) mixed former cements over 1, 7 and 30 day incubation periods.

Appendix D

Modeling the Cement Parameters (Chapter 6)

D.0.3 Mechanical Outputs of DG Cements

A clinically relevant cement would be workable for 6 to 10 minutes[1], set in 15 to 20 minutes, and have a uniaxal compression strength >30 MPa [87]. During the modeling process, it was discovered that compression strength could not be modeled successfully. Importantly, 1d compression data for all tested DG cements showed strength values greater than 30 MPa. Since this output cannot be modeled properly, the optimized cement must be validated for adequate compression strength.

D.0.4 Biological and Degradation Outputs of DG Cements

Cell viability tests have been performed on 1, 7 and 30 day cement extracts using NIH 3T3 mouse fibroblast cells, and extracts have been analyzed for elemental degradation products. It is clear from statistical one-way ANOVA analysis that cell viability does not vary significantly with glass composition. Furthermore, all setting cements demonstrated high cell viability (section 5.2, page 91). This biological output (cell viability) will therefore be ignored in DoM consideration.

ICP analysis yielded the 1, 7 and 30 day extract concentrations of potential therapeutic ions (Zn^{2+}, Ge^{4+}, Zr^{2+}, Sr^{2+}) for each cement composition (figure D.1). It is important to consider these results before constructing the DoM parameters.

[1] A permissable working time range of 5 to 10 minutes is indicated earlier in this work; the range 6 to 10 minutes has been selected deliberately for optimization purposes

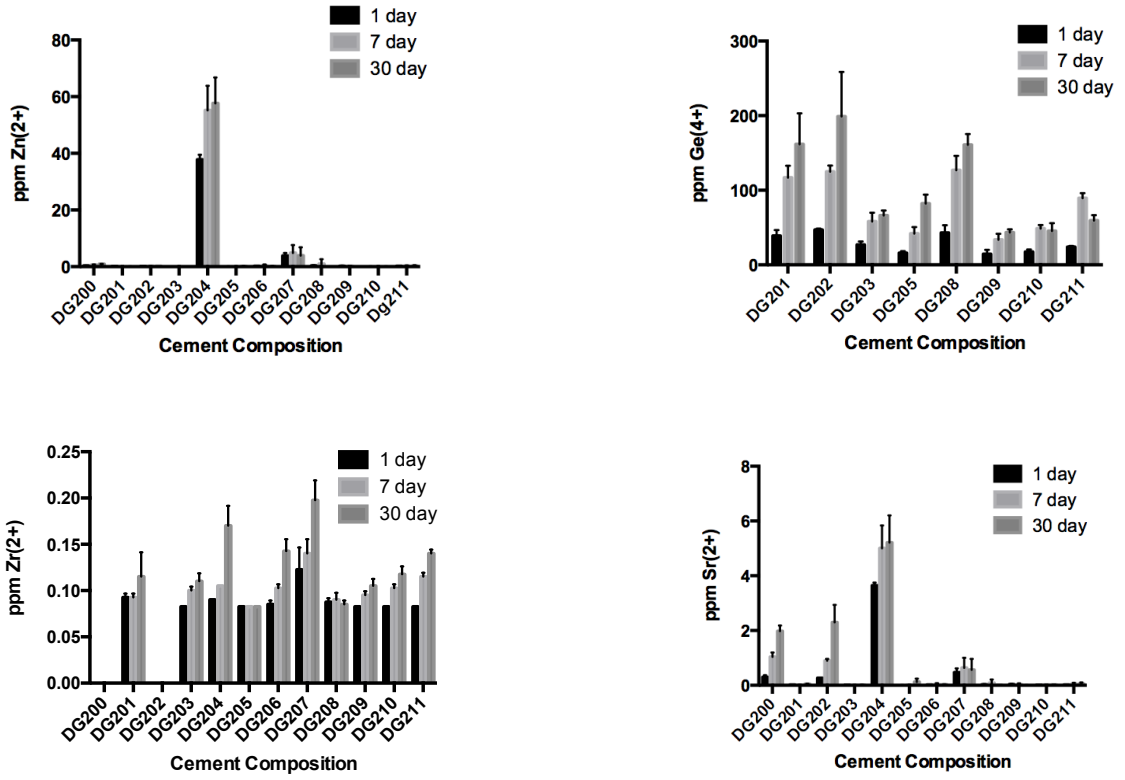

Figure D.1: Zn^{2+}, Ge^{4+}, Zr^{2+}, Sr^{2+} ion release at 1, 7 and 30 days

Zn^{2+}, Zr^{2+} and Sr^{2+} show concentration levels below (and often far below) 4, 0.25, and 6 ppm, respectively, over all time periods. The DG204 cement is an exception to this trend; extract Zn^{2+} concentrations were found to reach 58 ppm. This cement never set, however, and should be excluded from degradation product consideration. These three ions (Zn^{2+}, Zr^{2+} and Sr^{2+}) are released at very low concentrations over all time periods, and so it would be prudent to focus on the degradation byproduct released at significantly higher levels: Ge^{4+}. The 30 day Ge^{4+} extract concentration is used in the optimization modeling.

D.1 Modeling the Cement Parameters

The author modeled the responses using Scheffé multiple comparisons equations: quadratically (working time and $[Ge^{4+}]$) and cubically (setting time). The general forms of the polynomials are shown below in D.1 and D.2 .

$$Output_Q = \sum_{i=1}^{q} \beta_i \chi_i + \sum_{i=1}^{q-1} \sum_{j=i+1}^{q} \beta_{ij} \chi_i \chi_j + e \tag{D.1}$$

where χ_i correspond to i^{th} compositional factors, q=4, β_i correspond to the effects of individual χ_i, β_{ij} represent the effect of two-way interactions between χ_i and e is the residual.

$$\begin{aligned} Output_C = & \sum_{i=1}^{q} \beta_i \chi_i + \sum_{i=1}^{q-1} \sum_{j=i+1}^{q} \beta_{ij} \chi_i \chi_j \\ & + \sum_{i=1}^{q-1} \sum_{j=i+1}^{q} \gamma_{ij} \chi_i \chi_j (\chi_i - \chi_j) + \sum_{i=1}^{q-2} \sum_{j=i+1}^{q-1} \sum_{k=j+1}^{q} \beta_{ijk} \chi_i \chi_j \chi_k + e \end{aligned} \tag{D.2}$$

where γ_{ij} represent the coefficients of the cubic blending of binaries $(\chi_i \chi_j (\chi_i - \chi_j))$, and β_{ijk} represent the coefficients of the cubic blending of ternaries $(\chi_i \chi_j \chi_k)$.

Regression Models

Backward regression modeling yielded equations in table D.1 in terms of L-pseudo components.

Table D.1: Regression Outputs

Output	Regression Equations	R^2	R^2 adj.	R^2 pred.	p
Working time (quadratic)	$+386.56 * SiO_2$ $+589.09 * GeO_2$ $+627.88 * ZrO_2/Na_2O$ $+7462.16 * CaO$ $+1196.78 * SiO_2 * GeO_2$ $-10890.71 * SiO_2 * CaO$ $-9956.51 * GeO_2 * CaO$ $-13144.13 * ZrO_2/Na_2O * CaO$	0.9872	0.9648	0.9240	0.0013
Setting time (cubic)	$+1568.67 * SiO_2$ $+2569.36 * GeO_2$ $+146.00 * ZrO_2/Na_2O$ $-6774.50 * CaO$ $+2.797E5 * SiO_2 * GeO_2 * ZrO_2/Na_2O$ $-1.262E5 * SiO_2 * GeO_2 * CaO$	0.9168	0.8337	0.8056	0.0099
30d extract [Ge^{4+}] (quadratic)	$-108.27 * SiO_2$ $+203.79 * GeO_2$ $+506.08 * ZrO_2/Na_2O$ $-2428.04 * CaO$ $-185.28 * SiO_2 * GeO_2$ $+3536.84 * SiO_2 * CaO$ $-654.33 * GeO_2 * ZrO_2/Na_2O$ $+3152.02 * GeO_2 * CaO$	0.9948	0.9858	0.9115	0.0002